Neutron Induced Cross Section and Fission Yield Measurements for Thorium and Uranium

By

Sadhana Mukerji

PHYS01200804023

Bhabha Atomic Research Centre
Mumbai-400085

A thesis submitted to the

Board of Studies in Physical Sciences

In partial fulfillment of requirements

for the Degree of

DOCTOR OF PHILOSOPHY

of

HOMI BHABHA NATIONAL INSTITUTE

August 2015

Version approved during the meeting of Standing Committee of Deans held during 29-30 Nov 201

Homi Bhabha National Institute

Recommendations of the Viva Voce Board

As members of the Viva Voce Board, we certify that we have read the dissertation prepared by **Sadhana Mukerji** entitled **"Neutron Induced Cross Section and Fission yield Measurements for Thorium and Uranium"** and recommend that it may be accepted as fulfilling the dissertation requirement for the Degree of Doctor of Philosophy.

_____ **Date: 18/01/2017**

Chairman- **Prof. S.B.Degweker**

_____ **Date: 18/01/2017**

Guide / Convener- **Prof. B.N.Jagatap**

_____ **Date: 18/01/2017**

Co-Guide- **Prof. S.Ganesan**

_____ **Date: 18/01/2017**

Member 1- **Prof. S.K.Agarawal**

प्रोफेसर सैबल बसु / Prof. Saibal Basu
डीन -शैक्षणिक / Dean - Academic
भौतिक एवं गणितीय विज्ञान/Physical & Mathematical Sciences
होमी भाभा राष्ट्रीय संस्थान /Homi Bhabha National Institute
भा.प.अ.कें. / Bhabha Atomic Research Centre
मुंबई / Mumbai - 400 085.

_____ **Date: 18/01/2017**

Member 2- **Dr. H.Naik (Technical Advisor)**

_____ **Date: 18/01/2017**

External Examiner- **Prof. V. Kumar**

Final approval and acceptance of this dissertation is contingent upon the candidate's submission of the final copies of the dissertation to HBNI. 18/01/2017

I hereby certify that I have read this dissertation prepared under my direction and recommend that it may be accepted as fulfilling the dissertation requirement.

Date: 18/01/2017

Place: Mumbai

Prof. S. Ganesan 18/01/2017

(Co-Guide)

Prof. B.N.Jagatap

(Guide)

STATEMENT BY AUTHOR

This dissertation has been submitted in partial fulfillment of requirements for an advanced degree at Homi Bhabha National Institute (HBNI) and is deposited in the library to be made available to borrowers under rules of the HBNI.

Brief quotations from this dissertation are allowable without special permission, provided that accurate acknowledgement of source is made. Requests for permission for extended quotation from or reproduction of this manuscript in whole or in part may be granted by the Competent Authority of HBNI when in his or her judgment the proposed use of the material is in the interests of scholarship. In all other instances, however, permission must be obtained from the author.

Sadhana Mukerji

Sadhana Mukerji

DECLARATION

I, hereby declare that the investigation presented in the thesis has been carried out by me. The work is original and has not been submitted earlier as a whole or in part for a degree / diploma at this or any other Institution / University.

Sadhana Mukerji

Sadhana Mukerji

Version approved during the meeting of Standing Committee of Deans held during 29-30 Nov 2013

Dedicated to ……

My late Parents

Publications by the Candidate in support of this thesis

Publications in Refereed Journals

A. Journal Publications: 6

1. "Measurement of ^{232}Th(n, γ) and ^{232}Th(n, 2n) cross-section at neutron energies of 13.5, 15.5 and 17.28 MeV," using neutron activation techniques," Sadhana Mukerji, H. Naik, S. V. Suryanarayana, S. Chachara, B. S. Shivsankar, Sudipta Samanta, B. K. Nayak, A. Saxena, S. C. Sharma, V. Bhagwat, K .K. Rashid, R .N. Jindal, S. Ganesan, A .K. Mohanty, A. Goswami and P. D. Krishnani, Pramana, 79, 249-262 (2012), EXFOR Entry No. 33044.

2. "Application of Neutron Activation Techniques for the Measurement of ^{238}U(n, γ) and ^{238}U(n, 2n) Cross Section at Neutron Energies of 13.5 and 17.28 MeV," Sadhana Mukerji, H. Naik, S. V. Surayanarayana, B. S. Shivashankar, V. K. Mulik, Sachin Chachara, Sudipta Samanta, A. Goswami and P .D. Krishnani, Journal of Basic and Applied Physics, 2, 104-113 (2013).

3 "Measurements of Fission Product Yield in the neutron-induced fission of ^{238}U with average energies of 9.35 and 12.52 MeV," Sadhana Mukerji, P. D. Krishnani, B. S. Shivsankar, V. K. Mulik, S .V. Suryanarayana, H. Naik and A. Goswami, Journal of Korean Physical Society, 65, 18-24 (2014).

4. "Measurement of the neutron capture cross-section of ^{238}U at neutron energies of 5.9 ± 0.5 and 15.5 ± 0.7 MeV, by using the neutron activation technique," V .K. Mulik, S. V. Surayanarayana, H. Naik, Sadhana Mukerji, B. S. Shivsankar, P .M. Prajapati, S .D. Dhole, V. N. Bhoraskar, S. Ganesan and A. Goswami, Annals of Nuclear Energy, 63, 233–240 (2014).

5. “Measurement of fission product yields in the quasi-mono-energetic neutron-induced fission of ^{238}U,” H. Naik, Sadhana Mukerji, Rita Crasta, S.V. Suryanarayana, S.C. Sharma and A. Goswami, Nuclear Phys. A 941 (2015) 16–37.

6. “Measurement of fission products yields in the quasi-mono-energetic neutron-induced fission of ^{232}Th.” H. Naik, Sadhana Mukherji, S.V. Suryanarayana, K.C. Jagadeesan, S.V. Thakare and S.C. Sharma, Nucl. Phys. A 652 (2016) 100-120.

C. International Conference: 1

“Fission Product Yield in the neutron-induced fission of ^{238}U with average energies of 11.85 MeV,” Sadhana Mukerji, H. Naik, S. V. Suryanarayan, B. S. Shivshankar, V. Mullik, A. Goswami and P. D. Krishnani, Proceedings of International Symposium on Nuclear Physics, 58, 368-369 (2013).

D. National Conferences: 9

1. “Neutron Capture Cross Section Measurement for ^{232}Th at E_n= 2.8 MeV,” Sadhana Mukerji, H. Naik, S. V. Suryanarayana, A. Goswami, National Conference on Power from Thorium: Present Status and Future Directions December 22-24, 2014, BARC, Mumbai..

2. ”Fisson Product Yield In Neutron Induced Fission of ^{232}Th Using Neutron Source from ^{7}Li(p, n)^{7}Be Reaction at Incident Proton Energy of 20 MeV,” Sadhana Mukerji, H. Naik, S. V. Suryanarayan, Proceedings of the DAE Symposium on Nuclear Physics, 59, 426-427 (2014).

3. “Measurement of fission product yield in the neutron-induced fission of ^{232}Th with average energies of 11.85 MeV”, Sadhana Mukerji, H. Naik, S.V. Suryanarayan, B. S. Shivshankar, V. Mullik, A. Goswami and P .D. Krishnani, Fission-75, May 8-10, 2014, BARC, Mumbai..

4. “Measurement of ^{232}Th(n, γ)^{233}Th and ^{238}U(n, γ)^{239}U reaction cross sections at E_n= 3.12 MeV,” Sadhana Mukerji, H. Naik, S. V. Suryanarayan, B. S. Shivshankar, V. K. Mullik, A. Goswami and P. D. Krishnani, Eleventh Biennial DAE-BRNS Symposium on Nuclear and Radiochemistry (NUCAR-2013), February 19-23, 2013, Government Model Science College, Jabalpur, M.P.

5. “^{238}U(n, γ)^{239}U and ^{238}U(n, 2n)^{237}U reaction cross section measurement at E_n=13.5 MeV,” Sadhana Mukerji, H. Naik, S. V. Suryanarayan, A. Saxena, B. S. Shivshankar, V. Mullik, A. Goswami and P .D. Krishnani, National Symposium on Radiation Physics (NSRP-19), December 14-16, 2012, IGCAR.

6. “Measurement of ^{232}Th(n, γ) cross section at E_n = 13.5 MeV,” Sadhana Mukerji, H. Naik, S. V. Suryanarayan, S. Chachara, B. S. Shivsankar, Sudipta Samanta, K K. Rashid, R .N. Jindal, S. Ganesan, A. Goswami and P .D. Krishnani, National Symposium on Radiation Physics (NSRP-19), December 14-16, 2012, IGCAR.

7. “^{238}U(n, γ)^{239}U and ^{238}U(n, 2n)^{237}U reaction cross section measurement at E_n=17.28 MeV,” Sadhana Mukerji, H. Naik, S. V. Suryanarayana, B. S. Shivashankar,V. Mulik, A. Goswami and P. D. Krishnani, Proceedings of the DAE Symposium on Nuclear Physics, 57, 542-543 (2012).

8. “The (n, γ) and (n, 2n) cross sections for ^{238}U at neutron energy of 15.5 MeV”, S. V. Suryanarayana, V. K. Mulik, Sadhana Mukerji, H. Naik, P .M. Prajapati, B. S.

Sivashankar, A. K. Mohanty, A. Goswami, S. D. Dhole, V .N. Bhoraskar, Proceedings of the DAE Symposium on Nuclear Physics, 57, 566-567 (2012).

9. “Measurement ^{232}Th(n, γ) reaction cross-section at En=17.28 MeV”, Sadhana Mukerji, H. Naik, S. V. Suryanarayana, B. S. Shivashankar, V. K. Mulik, B .K. Nayak, A. Saxena, S .C. Sharma, P. V. Bhagwat, S. Ganesan, A. Goswami and P .D. Krishani, Proceedings of the DAE Symposium on Nuclear Physics, 56, 626-627 (2011).

Acknowledgements

It is great pleasure to express my gratitude to all the personal directly or indirectly contributed to the work presented in this thesis.

I am greatly indebted to my guide, Prof. B.N. Jagatap, Director, Chemistry Group, BARC, for his active support during the research work presented in this thesis.

I am grateful to Prof. S. Ganesan, who was my guide during initial days of Ph.D. registration, for his guidance and initiating a fruitful collaboration with Dr. H. Naik. Thanks to Dr. Naik.

My sincere gratitude to all the members of Doctoral Committee, specially to Prof. S.B. Degwekar, who is chairman of the doctoral committee, and acted promptly as and when required. I am also thankful to Prof. S.K. Aggarawal for his cooperation.

There are many people without whom this work would not have been possible. My sincere thanks to Pelletron accelerator support crew for their hard work to keep the pelletron operational during the experiments. Thanks to Prof. A. Goswami, for allowing me to work at RCD lab at TIFR.

Many of my colleagues and seniors in BARC deserve special mention i.e. Prof. A. Saxena, Prof. A .Chatterjee, Prof. S. Kailas, Prof. V.N. Datar, Prof. H.P.Gupta, Prof. R.S..Modak. Prof. B.K. Nayak, Prof. Sangeetha, Dr. S. V. Suryanarayanan, Shri. S.K. Singh, Shri R.N. Jindal, Shri K.K. Rasheed, Dr. Superna, for their cooperation.

I am grateful to authorities of Bhabha Atomic Research Centre, for their cooperation and support during the course of the work presented here. Special thanks to Prof. D. Saha and Prof. R. Srivenkatesan, Prof. P.D. Krishnani.

I am thankful to authorities of Homi Bhabha National Institute, BARC. Special thanks to Prof. S. Banerjee, Prof. R.B. Grover and Prof. B.K.D utta, Prof. A.P. Tiwari and Prof. Saibal Basu. Many thanks to all members of RPDD.

SADHANA MUKERJI

Table of Contents

Synopsis 1

List of Table 8
List of Figures 9

Chapter-1

1.0Introduction 13

1.1 Need for Nuclear Data Measurements 16

1.1.1 Neutron Induced Reaction 17

1.1.2 Need for reaction cross section Measurements 18

1.2 Neutron Induced Fission Product Mass yield 20

1.2.1 Definitions of Fission Yield 21

1.2.2 Need for Fission Product Yield Measurements 23

1.3 Basics of Neutron Activation Technique 25

1.4 Neutron Sources 29

Chapter-2

2.0 Experimental setup details 34
2.1 14 UD Pelletron Accelerator at TIFR 34

2.2 Target Fabrication 35
2.3 Gamma ray Spectroscopy 37
2.4 Experimental Details 45

Part- I

Reaction Cross Section Measurements

Chapter-3 Measurements of the (n, γ) and (n, 2n) reaction 50

Cross-section of ^{238}U

3.1 Mechanism of Nuclear Reactions 50
3.2 Cross section of a Nuclear Reaction 51
3.3 Nuclear model computer code Talys 52
3.4 Practical applications of the Cross Section Measurements 54
3.5 Experimental Procedure 57
3.6 Calculation of the neutron energy (<E>) 62
3.7 Determination of ^{238}U (n, γ) ^{239}U and ^{238}U(n, 2n)^{237}U 65
reaction cross-sections
3.8 Uncertainty associated with the measurements 68
3.9 Results and Discussions 68
3.10 Summary and Conclusions 75

Chapter-4 Measurements of the (n, γ) and (n, 2n) reaction 78
Cross-section of ^{232}Th
4.1 Motivation behind the reaction cross section Measurement for ^{232}Th 78
4.2 Description of the experiment 83
4.3 Data analysis 84
4.4 Determination of ^{232} Th(n, γ) ^{233} Th and ^{232}Th(n, 2n)^{231} Th reaction cross 87
sections and their results.
4.5 Uncertainties associated with the measurements. 89
4.6 Results and Discussions 90
4.7 Conclusions 94
Part- II
Fission Studies

Chapter-5 Measurement of mass yield distribution of twelve fission products nuclides from neutron induced fission of ^{238}U at incident neutron energies of 9.35 and 12.52 MeV. 97

5.1 Outline of the present investigation 97

5.2 Fission product mass distribution 99

5.3 Utility of fission product mass distribution in nuclear energy 100

5.4 Description of experimental set-up 102

5.5 Calculation of effective average neutron energy 103

5.6 Calculation of fission product yield 104

5.7 Results and Discussions 105

5.8 Conclusions 110

Chapter-6 Measurement of mass yield distribution of twelve fission products nuclides from neutron induced fission of ^{232}Th at incident neutron energies of 9.35 and 12.52 MeV. 112

6.1 A brief description of the systems in which ^{232}Th-^{233}U is the source for power production. 114

6.2 Experimental set-up for fission studies 117

6.3 Data analysis and mass yield distribution calculations 118

6.4 Results and Discussions 121

6.5 Uncertainties in the results 122

6.6 Conclusions 122

7.0 Summary and Conclusions 126

References 131

SYNOPSIS

Thesis presents the original contribution from the author towards the measurements of basic nuclear data related to neutron induced reaction cross sections and fission fragment yields for ^{232}Th and 99.3% ^{238}U. Experiments were carried out with the quasi-mono-energetic neutrons of 2.18-17.28 MeV from the ^{7}Li(p,n) reaction. The neutron beam was produced by using the 5-20 MeV proton beam from main line at 6 meter height irradiation set up at the 14UD BARC-TIFR Pelletron facility at TIFR, Mumbai, India. The measurements reported here for the 2.18, 3.15, 13.5, 15.5 and 17.24 MeV neutron energies are done for the first time. Neutron energies above 3.15 MeV reported in the thesis correspond to the average neutron flux weighted energy in ^{7}Li(p,,n) reaction. Nuclear data, especially neutron induced reactions and fission, have become important in the low to high energy range. They are necessary for (i) development of new concepts of nuclear energy systems, (ii) design of reactors and accelerators, (iii) production and transmutation of radioactive waste with the use of accelerators and fast reactors, (iv) shielding design, (v) dosimetry and applications in nuclear astrophysics. They are also necessary for the calculations of the neutron production in the spallation target, for developing models of nuclear interactions, nuclear structure and to validate the reaction models codes as well as for the system based on high-current accelerator i. e., Accelerator Driven Sub-critical System (ADSs). ADSs is important for transmutation of long-lived radioactive waste beside nuclear energy production. The precision

measurements of nuclear data are thus needed for both basic research and applications in many branches of science and technology.

The availability of high resolution gamma ray spectrometer makes these measurements possible from the analysis of fission and reaction products. We have used this technique for the measurement of fission product yield and activation cross section of ^{232}Th and ^{238}U at various neutron energies.

In the present work, measurements of neutron induced reactions are reported for neutrons energy range of 2.18-17.28 MeV. Gamma ray spectroscopy was carried out for a range of fission and reaction products in the neutron induced fission reactions of ^{232}Th and ^{238}U. Contemporary higher multi-group analyses of current reactors, GEN-IV reactors and ADSs demand improvements of the nuclear data for ^{238}U and ^{232}Th and especially precision measurements at higher neutron energies. Cross sections for transmutation and target design for ADSs also demand measurements for reaction cross sections for incident neutron energies in the range 10-20 MeV.

The problems investigated in this thesis are broadly classified into two parts:

A. Measurement of reaction cross section

As mentioned before, neutron capture cross sections of Thorium and Uranium are important for the research, design and development of innovative nuclear reactors, the fast reactor and ADSs. Although there are numerous measurements available in the literature, markable differences between the sets of measured data and differences in various evaluations and libraries are frequently pointed out. With the availability of a new neutron irradiation set up at 6 meter height off main line at TIFR Pelletron, it is now possible to measure the reaction cross sections at relatively higher neutron energy, due to

availability of higher neutron flux. Our measurements are slightly different from the conventional measurements which are based on the neutron flux monitor using the ^{197}Au (n, γ)^{198}Au reactions. The capture cross section for gold is less at higher neutron energies compared to thermal neutrons by a factor of 2.5. So using gold as flux monitor at high energy incident neutrons is not as ideal as it is for thermal neutrons. We use ^{115}In (n, n')^{115m}In reaction as the flux monitor up to neutron energy of 5 MeV and fission product yields at higher neutron energies. The experiments were carried out at TIFR-BARC Pelletron facility at the 6 meter height irradiation set up of main line. A stack of Ta-Li-Ta was made for the production of neutron beam using the ^{7}Li(p, n) reaction. About 1.0 cm^2 of ^{232}Th and ^{238}U metal foils with thickness 344.1-634.2 mg/cm^2 doubly wrapped with 0.025 mm thick Al foil was mounted at zero degree with respect to the beam direction at a distance of 2.1 cm from the location of the Ta-Li-Ta stack. The ^{232}Th and ^{238}U metal foils were irradiated for 9-12 hours with 2.18-17.28 MeV quasi-mono-energetic neutrons generated from the ^{7}Li(p, n) reaction using the 5-20 MeV proton beam. The proton current during the irradiations was around 100-200 nA. After irradiation, the samples were cooled for one hour. Then the irradiated target of ^{232}Th and ^{238}U along with Al wrapper was mounted on Perspex plate and taken for γ-ray spectrometry. The γ-rays of reaction/fission products from the irradiated ^{232}Th and ^{238}U sample were counted in energy and efficiency calibrated 80 c.c. HPGe detector coupled to a PC-based 4K channel analyzer. The counting dead time was kept always less than 5 % by placing the irradiated ^{232}Th and ^{238}U sample at a suitable distance from the detector to avoid pileup effects. The gamma ray counting of the irradiated sample was carried out in live time mode and was followed as a function of time. The ^{238}U(n,γ)^{239}U reaction cross-section at

the average neutron energies of 3.15, 13.5, 15.5 and 17.28 MeV and $^{238}U(n, 2n)^{237}U$ reaction cross-section at the average neutron energies of 13.5, 15.5 and 17.28 MeV have been determined using activation and off-line γ-ray spectrometric technique. Since the neutrons are not mono-energetic, appropriate corrections to the cross sections are incorporated. The experimentally determined $^{238}U(n, \gamma)^{239}U$ and $^{238}U(n, 2n)^{237}U$ reaction cross-sections from present work were compared with the evaluated data of ENDF/B-VII.1(Evaluated Nuclear Data File), JENDL-4.0(Japanese Evaluated Nuclear Data Library), JEFF-3.1(Joint Evaluated Fission and Fusion File) and CENDL-3.1(Chinese Evaluated Nuclear Data Library) nuclear data library. The experimental values were found to be in general agreement with the evaluated values of ENDF/B-VII.1 and JENDL-4.0 but different from the values of JEFF-3.1 and CENDL-3.1. It is observed that, the $^{238}U(n, \gamma)$ reaction cross-section decreases in the energy range of 100 keV to 8 MeV with a dip at 6-8 MeV. It then increases above the neutron energy of 8.0 MeV and thereafter remains constant up to the neutron energy of 14 MeV. However, the $^{238}U(n,2n)$ reaction cross-section increases from its threshold to 8MeV. There after remains almost constant up to 14 MeV. Beyond 14 MeV both $^{238}U(n, \gamma)$ and $^{238}U(n, 2n)$ reaction cross-sections show decreasing trend due to opening of (n, 3n) and (n, 2nf) reaction channels. The present data along with literature data in a wide range of neutron energies were interpreted in terms of competition between $^{238}U(n, \gamma)$, (n, f), (n, nf) and (n, xn) reactions channels. The $^{238}U(n, \gamma)$ and $^{238}U(n, 2n)$ reaction cross-sections were also compared with theoretical results of TALYS computer code. The TALYS results for $^{238}U(n, \gamma)$ reaction cross-section over predict the experimental data within the neutron energy of 1 keV to 3 MeV and thereafter it is in agreement with the experimental data. However, the TALYS

results for ^{238}U(n, 2n) reaction cross-sections are in good agreement with the experimental data up to 8 MeV. Above 8 MeV, the ^{238}U(n, 2n) reaction cross-sections remain constant up to 14 MeV. There after it shows decreasing trend due to opening of (n, 3n) and (n, 2nf) reaction channels. These cross-sections have been determined for the first time using activation and off-line γ -ray spectrometric technique. The ^{232}Th(n, 2n) cross section for 17.28 MeV has also been determined using the same technique. The experimentally determined ^{232}Th(n, γ) and ^{232}Th(n, 2n) reaction cross-sections from the present work were compared with the evaluated data of ENDF/B-VII.1 and JENDL-4.0 and were found to be in good agreement. The present data along with literature data in a wide range of neutron energies were interpreted in terms of competition between ^{232}Th(n, γ), (n, f), (n, nf) and (n, xn) reactions channels. The ^{232}Th(n, γ) and ^{232}Th(n, 2n) reaction cross-sections were also calculated theoretically using the TALYS computer code and were found to be in good agreement with the experimental data of present work but are slightly higher than the literature data at lower neutron energies. The ^{232}Th(n, γ) reaction cross section shows decreasing trend up to the neutron energy of 6-8 MeV. then increasing and remaining constant up to 14 MeV. The ^{232}Th(n,2n) reaction cross section increases from its threshold energy to 8 MeV and then remains constant up to 14 MeV. After 14 MeV both ^{232}Th(n, γ) and ^{232}Th(n,2n) reaction cross sections decrease with neutron energy due to opening of (n, 3n) and (n, 2nf) reaction channels.

B. Measurement of Fission Product Yield data

In addition to neutron capture and (n, 2n) cross sections discussed above, nuclear data of fission cross section, fission product yields and decay data including half-lives, decay energies, branching ratios are required for many reactor physics calculations. At

present, the available experimental data of fission product yields at different incident neutron energies is insufficient for the development of fission systematics, whereas the theoretical models of fission are still not well understood. Therefore, measurements are needed for high energy neutron-induced fission of ^{232}Th and ^{238}U. Further, not many experimental data of fission product yields are available in the neutron energies range of 16-20 MeV. In the present study, fission product yield measurement has been carried out by neutron irradiation at 9.32 MeV and 12.52 MeV energies on ^{232}Th and ^{238}U targets by using off-line gamma ray spectroscopy. Activated targets are counted in highly shielded HPGe detectors over a period of several weeks to identify decaying fission products. The fission yields values are reported for twelve fission products. The results obtained from present work at 12.53 MeV have been compared with the similar data of mono-energetic neutrons of comparable energy of 14.1 MeV from literature and are found to be in good agreement. The fission products yields data at the neutron energy of 9.25 MeV from the present work are determined for the first time. There are no data available in literature around the neutron energy of 9.25 MeV to compare with the data of present work. The mass yield distribution in the symmetric valley region shows the presence of a third peak. Thus the mass yield curve in ^{232}Th(n, f) is triple humped unlike in ^{238}U(n, f), where it is double humped.

Thesis is organized in seven chapters as mentioned below:

Chapter-1 includes the introduction and importance of nuclear data such as reaction and fission product yield measurements. Here practical application and relevance of nuclear data measurements for the design, safety and operations of conventional reactor i.e., Pressurized Water Reactor (PWR), Pressurized Heavy Water Reactor (PHWR) and

thorium based systems i.e., Advanced Heavy Water Reactor (AHWR) and ADSS are discussed. Also the concepts used in the subsequent chapters are discussed in detail. Chapter-2 is devoted to the description of the experimental set-up used in the thesis work. Chapter-3 includes the measurement of neutron induced reaction cross sections for ^{238}U. Chapter-4 describes the ^{232}Th(n, γ) and ^{232}Th(n, 2n) reaction cross-sections measurement at average neutron energies of 2.18, 3.15, 13.5, 15.5 and 17.28 MeV from the ^{7}Li(p, n) reaction. Chapter-5 discusses the measurement of fission product yields in the neutron induced fission of ^{238}U at two different energies (9.25 and 12.35 MeV). Chapter-6 reports the measurement of fission product yields in the neutron induced fission of ^{232}Th at incident neutron energies of 9.25 and 12.53 MeV. Finally the important conclusions arriving from the present study and its future prospects are discussed in Chapter-7.

List-of-Tables

Table 2.1	Gamma ray energies of the radionuclide used for HPGe detector calibration.	42
Table 3.1	Nuclear spectroscopic data used in the reaction cross section and flux calculations.	65
Table 3.2	Neutron induced reaction cross section measured values for ^{238}Ucompared to ENDF/B-VII and JENDL-4.0.	76
Table 4.1	Nuclear Spectroscopic data used for ^{232}Th data analysis.	88
Table 4.2	Neutron induced reaction cross section measured values of ^{232}Th compared to ENDF/BVII and JENDL-4.0.	92
Table 5.1	Yields of fission products in the neutron induced fission of ^{238}U at E_n = 9.35 MeV relative to ^{97}Zr fission yield at E_n = 11.3 MeV as reference.	108
Table 5.2	Yields of fission products in the neutron induced fission of ^{238}U at E_n = 12.35 MeV relative to ^{97}Zr fission yield at E_n=14 MeV.	109
Table 6.1	Nuclear spectroscopic data and yields of fission products in the neutron induced fission of ^{232}Th at E_n = 9.35 MeV relative to ^{97}Zr fission yield at E_n = 14.0 MeV.	123
Table 6.2	Nuclear spectroscopic data and yields of fission products in the neutron induced fission of ^{232}Th(n,f) at neutron energy of 12.52 MeV relative to ^{97}Zr fission yield at E_n =14. 0 MeV [40].	124

List of Figures

Figure 1.1 Status of reaction cross section for ^{238}U in the literature 18

Figure 1.2 Status of reaction cross section for ^{232}Th in the literature 19

Figure 1.3 A schematic view of the fission process 24

Figure 1.4 Schematic representations of the double humped fission barrier 25

Figure 1.5 Neutron Activation Process 26

Figure 1.6 Principle scheme of the spallation reaction 33

Figure 2.1 BARC-TIFR Pelletron Facility 35

Figure 2.2 HPGe Detector with PC based 4K analyzer 37

Figure 2.3 The linear attenuation coefficient of Germanium and its component parts 39

Figure 2.4 Measured gamma -ray spectrum from a calibrated ^{152}Eu reference source. The energies of the detected photo peaks and their corresponding branching ratios. 44

Figure 2.5 Detector efficiency(%) as a function of gamma energy (keV) 46

Figure 2.6 Set up for Sample Holder at 6 meter height at BARC-TIFR Pelletron facility 47

Figure 2.7 Schematic diagram showing the arrangement 48

used for neutron irradiation

Figure 3.1 Schematic diagram of (n, γ) and (n, 2n) reaction of ^{238}U followed by beta decay in the U-Pu fuel cycle 54

Figure 3.2 Gamma-ray Spectrum of for $^{238}U(n, \gamma)^{239}U$ and $^{238}U(n, 2n)^{237}U$ reactions 59

Figure 3.3 Typical gamma-ray spectrum of Indium Foil 62

Figure 3.4 Neutron spectrum from $^{7}Li(p, n)$ reaction at E_p=16.0 MeV calculated using results of Meadows and Smith 63

Figure 3.5 Neutron spectrum from $^{7}Li(p, n)$ reaction at Ep=20.0 MeV calculated using results of Meadows and Smith 64

Figure 3.6 Plot of experimental and evaluated $^{238}U(n, \gamma)^{239}U$ reaction cross-section as a function of neutron energy (E_n) from 1 keV to 5 MeV. Experimental reaction cross-section at E_n= 3.12 MeV is indicated 71

Figure 3.7 Plot of experimental and evaluated $^{238}U(n, \gamma)^{239}U$ reaction cross-section as a function of neutron energy from 1 keV to 20 MeV. Experimental values from present work and from Refs. [36-56] are in different symbols, where as the evaluated and theoretical values from TALYS are in solid line of different color 72

Figure 3.8 Plot of experimental and evaluated $^{238}U(n, 2n)^{237}U$ reaction cross-section as a function of neutron energy from 5 MeV to 25 MeV. Experimental values from 77

present work and from Refs. [56-61] are in different symbols, whereas the evaluated and theoretical values from TALYS are in solid lines with different colors

Figure 4.1 Schematic diagram of the Th–U fuel cycle 81

Figure 4.2 A typical γ -ray spectrum from the irradiated ^{232}Th sample showing the γ –rays of ^{233}Th and ^{233}Pa from ^{232}Th(n,γ) reaction 85

Figure 4.3 A typical γ -ray spectrum from the irradiated ^{232}Th sample showing the γ –rays of ^{231}Th from ^{232}Th(n,2n) reaction 85

Figure 4.4 ^{232}Th(n,γ) ^{233}Th reaction cross sections at incident neutron energies of 2.8 MeV and 3.12 MeV 94

Figure 4.5 Variation of capture cross section of ^{232}Th as a function of neutron energy 95

Figure 4.6 Variation of (n, 2n) cross section of ^{232}Th as a function of neutron energy 95

Figure.5.1 Neutron spectrum from ^{7}Li(p, n) reaction at E_p=16.0 MeV calculated using the results of Meadows and Smith 105

Figure 5.2 Neutron spectrum from ^{7}Li(p, n) reaction at E_p=20.0 MeV calculated using the results of Meadows and Smith. 107

Figure 5.3 Decay schemes of ^{129}Sb, ^{131}Xe, ^{115}Cd, ^{143}Ce, ^{97}Zr, ^{95}Zr, ^{105}Ru, ^{132}Te, ^{139}Ba, ^{133}I, ^{91}Sr, ^{92}Sr 107

Figure 5.4 Fission yield of fission products for E_n = 9.35 MeV 110

Compared to 11.3 MeV values taken from literature.

Figure 5.5	Fission yield of fission products for $^{238}U(n, f)$ at E_n = 12.52 MeV compared to 14 1 MeV values taken from literature	111
Figure 6.1	Schematics of Advanced Heavy Water Reactor	115
Figure 6.2	Schematics of Molten Salt Reactor	117
Figure 6.3	ADS System Basic Concept	118
Figure 6.4	Fission product yield for $^{232}Th(n, f)$ reaction at incident neutron energy of 9.32 MeV compared to the literature values at 14 MeV.	124
Figure 6.5	Fission product yield for $^{232}Th(n, f)$ reaction at incident neutron energy of 12.52 MeV compared to the literature values at 14 MeV.	126

CHAPTER 1

1.0 Introduction

Nuclear cross section data are essential for the design and analysis of nuclear energy systems, such as reactor cores layout, fuel elements, and stored mixtures of nuclear waste with other materials, burned fuel elements. Data of neutron induced reactions with Thorium and Uranium [1] at energies from several keV to tens of MeV are also required for nuclear physics applications. More nuclear cross section data measurements for Uranium and Thorium are necessary for the design of fast reactors [2], Accelerator Driven Sub-critical System (ADSs) [3] and Advanced Heavy Water Reactor AHWR [4], energy amplifiers [5], future fusion reactors [6], and GEN-IV [7] reactor design. Due to lower priority in some countries where data have been generated, availability of experimental information regarding nuclear data for thorium fuel cycle is limited.

One of the established methodologies for nuclear fission for energy production is mixing of thorium with a starter of uranium isotopes to kick off chain reactions as is the case in molten salt reactors (MSRs) and pebble bed reactors (PBRs) [7]. Sometimes, preference is given in putting thorium into conventional reactors. Some reports suggest that alternative reactors like MSRs, PBRs and another type called a fast reactor could offer significant advantages over conventional reactors. In addition, thorium reactors could theoretically be used to burn up the dangerous plutonium stored in existing nuclear

waste stockpiles.

Another approach suggested by Carlo Rubbia [5] would be to use thorium in sub-critical accelerator-driven reactors. Nuclear fission using thorium is within our reach, and, can be similar to the conventional nuclear energy and the risks are considerably lower. There are some drawbacks to thorium fuel cycles, but they are highly technical. For instance, thorium reactors have been criticized as potentially having more neutron leak compared with conventional reactors. More neutron leak means more shielding and other radiation protection is needed for workers at the power plant [6].

In this thesis, two most important nuclear cross section data i.e. reaction cross sections of (n,γ) and (n,2n) have been measured for the first time at energies 2.18,3.12,13.5,15.5 and 17.28 MeV and fission product mass distribution for ^{238}U and ^{232}Th at energies 9.35 and 12.52MeV. Although, nuclear data measurements is a part of basic research, the accuracy of measurement of cross sections and fission product mass yield distribution would provide important input for the development of Nuclear Technology. In the present thesis, experiments have been carried out with the quasi-mono-energetic neutrons in the energy range of 2.18-17.28 MeV produced in the ^{7}Li(p,n) reaction. The neutron beam was produced by using the 5-20 MeV proton beam from main line at 6 meter height irradiation set up at the 14UD BARC-TIFR Pelletron facility at TIFR, Mumbai, India. The measurements reported are the original contributions by the author. The details about the experimental set ups and measurements covering the sample preparation, performed experiments are described in Chapter 2. In Chapter 3 we describes the reaction cross section measurements for ^{238}U, data analysis and comparison

with the theoretically obtained results using reaction model computer code TALYS (8,9) and different evaluated nuclear data ENDF/B-VII [10], JEFF3.1 [11], JENDL-4.0 [12], CENDL-3.1[13]. Chapter 4 describes reaction cross section measurements for ^{232}Th, data analysis and comparison with the theoretical and evaluated data. It is seen that up to incident neutron energy of 5 MeV the reaction cross sections are matching with all the four evaluated data ENDF-B/VII, JEND-4.0, JEFF-3.1 and CENDL-3.1. At higher neutron energies >10 MeV the reaction cross sections are matching with ENDF-B/VII, JENDL-4.0 and JEFF-3.1 but differs from CENDL results. Chapter 5 describes about the results on fission product mass distribution for the ^{238}U(n,f) at incident neutron energies of 9.35 MeV and 12.52 MeV respectively. The results obtained were compared with the literature values and found to be within the acceptable limits. Chapter 6 is devoted to fission product mass distribution for the ^{232}Th (n,f) at incident neutron energies of 9.35 MeV and 12.52 MeV, the results obtained were compared with the literature values. This chapter also covers brief description of nuclear energy systems using ^{232}Th(n,f) as the source of energy production. The fission product mass yield distribution becomes more symmetric with increasing incident neutron energy. The probability of symmetric fission increases with increase in neutron energy. The increase in the symmetric fission component with the increase in the incident neutron energy is more prominent in the case of thorium compared to uranium. This fact could be seen from peak to valley (P/V) ratio. In the case of ^{232}Th(n, f) third peak in the mass distribution is observed. This is because of second dip at the outer fission barrier called the thorium anomaly. The yield of fission products at mass numbers 133-135, 145-146 and their complementary parts are higher because of presence of 82n shells and deformed 88n shells at mass numbers 133-135 and

144-145 because of closure of shells. Higher yield at certain mass numbers are because of even-odd effect which indicates role of structural effect. Finally, chapter 7 presents a conclusion.

The basic properties and concepts used for neutron induced cross section and fission yield measurements are described in the following sections.

1.1 Need for nuclear data measurements

Based upon the current status of nuclear theory and available models, predictions could be made about the probability (likelihood) that a specific nuclear process will occur under certain conditions (e.g. incident energy, angle of observation). The quantitative measure of this prediction is the cross section of the process. That is, nuclear theory is used to predict the specific cross section of a process. These cross sections are measured in laboratory. Present thesis deals with one of these types of measurements. Comparison between theoretical predictions and measurement is used to evaluate the nuclear models and validation of the nuclear theory.

Sometimes, large difference between the experimental and the evaluated cross sections are observed. The expression for the cross sections involves, among others, transmission coefficients and level densities [14]. Much work has been done to develop models, codes and optical potential parameters recommendations for use in Hauser-Feshbach calculations [14]. However, a given set of cross section data can often be reproduced by several parameter combinations. This ambiguity reflects our insufficient knowledge of the underlying nuclear structure properties at the energies relevant to compound-nuclear reactions. Consequently, for cases where there is little or no data to

constrain the structure models and cross sections, we opt for more cross section measurements.

1.1.1Neutron induced reaction

When a collision occurs between the incident particle and a target nucleus, the neutron can cause different type of interactions. The neutron may simply scatter off the nucleus. The scattering could be elastic or inelastic. Neutron may actually be absorbed in the nucleus. If the neutron is absorbed in the nucleus, it may result in the emission of gamma rays and subatomic particle or it may cause the nucleus to fission. A nuclear reaction is described by identifying the incident particle, target nucleus, and reaction products. The investigation of the fundamental constituents of matter and their interactions comes from the experimental and theoretical analysis of nuclear reactions. These reactions can be scattering experiments with or without production of particles, and decays of the unstable particles produced in these reactions. When the incident particles are neutrons, it is called neutron induced reaction. Due to electrical neutrality the neutron is able to interact with a nucleus at close distance at all energies.

A neutron induced reaction is denoted by A (n, Y) B, when a neutron (denoted by n) comes significantly close to the target nucleus A, i.e. closer than the range of the nuclear forces (10^{-15} m). A particle Y is then emitted, leaving a residual nucleus B, which can be either stable, radioactive or an isomer. The interaction of the projectile with the target nucleus is generally described in terms of the cross section $\sigma_{(n,Y),}$ which is a measure of probability for a reaction to occur. The cross section is usually given in barns (1 barn = 10^{-28} m^2) and it is a function of energy of the incident particle. One of the important characteristics of neutron induced reactions is its total cross section which is relatively

well defined. It is the sum of elastic scattering and reaction cross section. Cross sections are estimated using nuclear reaction models (TALYS). Comparing the measured and calculated values of the cross sections for many reactions validates the assumptions of the nuclear model.

1.1.2 Need for reaction cross section measurement

As seen from Fig. 1.1, sufficient measured reaction cross sections for ^{238}U are available in the low incident neutron energy region. At incident neutron energies in the range 7-14MeV, quite a few measured $^{238}U(n, \gamma)^{239}U$ are reported by Daniels (1982) [15] ,and one measurement has been reported by by Vuong et al., in 1996 [16] . These measurements are following the trend of evaluation and model calculation. Whereas measurements beyond 14 MeV carried out by by Panitkin [17,18] and Ding [19] are totally different from the evaluations and model calculations. To check this fact we have carried out measurements at incident neutron energies of 13.5 and 17.28 MeV.

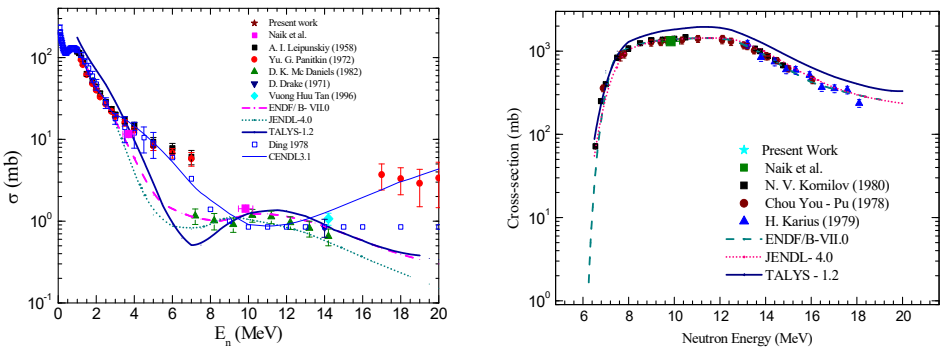

Fig. 1.1 Status of reaction cross section measurements for ^{238}U in the literature

Th-cycle did not receive sufficient attention in the past. Most of the available experimental data are those generated two to three decades ago. In addition, generally, these experimental data are of poor quality and very limited. In recent years there has

been a renewed interest in the thorium cycle in connection with transmutation of waste and accelerator driven systems (ADS). The concept of the energy amplifier (EA), for example, combines the two in a hybrid system based on the thorium fuel cycle and a spallation neutron source. Successful development and implementation of these concepts depends on the availability of accurate neutron-induced reaction data. A comparison of the different neutron data available however shows that, large discrepancies exist for some of the cross sections, even in the well studied region of neutron energies 0-20 MeV which is the range of of interest for conventional nuclear technologies.

A careful look at the nuclear cross-section data, available in the existing cross-section libraries shows that, ^{232}Th(n, γ) reaction cross-section within neutron energies of thermal to 2.73 MeV which are based on direct measurements [20,21] and activation technique [22,23,24]. As it is seen in Fig. 1.2, sufficient measured reaction cross sections and n,2n capture cross sections for ^{232}Th are available in the low incident neutron energy region.

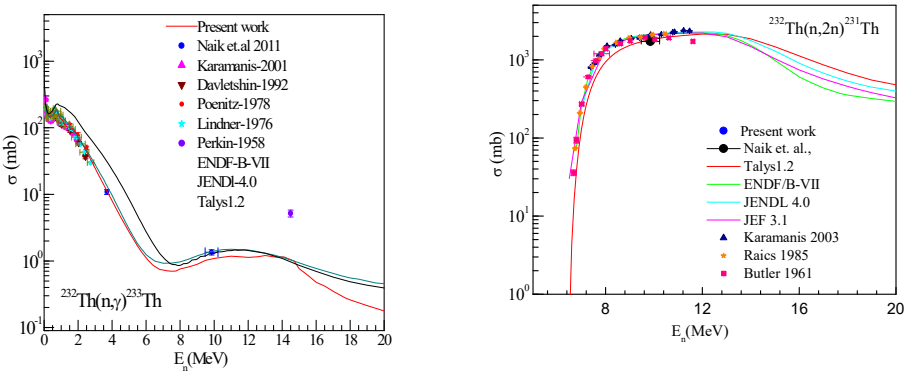

Fig. 1.2 Status of reaction cross section measurements for ^{232}Th in the literature.

Beyond these there are only two measurements carried out by H.Nail et at.,[24] and at 14.5 MeV (Perkin *et al.,* [25]) using the activation technique. Therefore we have carried out measurements at 13.5, 15.5 and 17.28 MeV.

1.2 Neutron induced fission product mass yield

Knowledge of fission [26] and its consequences is important for the nuclear power industry and the related field of nuclear waste management and environment clean-up. From the point of view of basic research, fission is interesting in its own right as a large scale collective motion of the nucleus, as an important exit channel for many nuclear reactions, and as a source of neutron rich nuclei for nuclear structure studies and use as radioactive beams. In Figure 1.3 a schematic view of the fission process has been shown. A nucleus with some equilibrium deformation absorbs energy, becoming excited and deforms to a configuration known as the "transition state" or "saddle point" configuration. As it deforms, the nuclear coulomb energy decreases (as the average distance between the nuclear proton increases) while the nuclear surface energy increases (as the nuclear surface area increases). At the saddle point, the rate of change of Coulomb energy is equal to the rate of change of the nuclear surface energy. If the nucleus deforms beyond this point it is irretrievably committed to fission. When this happens, then in a very short time, the neck between the nascent fragments disappears and the nucleus divides into two fragments at the "scission point". At the scission point, one has two highly charged, deformed fragments in contact with each other. The large coulomb repulsion between the two fragments accelerates them to 90% of their final kinetic energy.

The daughter nuclei showing up right at scission of a fissioning mother nucleus are called primary fission “fragments”. In the large majority of the cases, the fragments will be sufficiently excited to evaporate neutrons in times less than 10^{-15} s. This means that the nuclei detected in experiments are not the primary fragments, but instead secondary fragments having lost a varying number of neutrons. The secondary fragments are called the fission products (i.e. fission fragments after prompt neutron evaporation).

A fission product is denoted symbolically by the notation (A, Z, I) where A and Z are respectively the mass number and the atomic number, and I indicates the isomeric state (I = 0 for the ground state, I = 1, 2 . . . for the 1st, 2nd , . . . isomeric states) [26]. If a fission product has no isomers, or if one is referring to the sum of yields of all its isomers, the notation (A, Z) is used. Using this terminology, the following fission yield definitions are given.

1.2.1 Definitions of fission yield

In nuclear fission a heavy nuclide splits into two light nuclides, which are called fission products. In fission process, the probability of measuring the production of an isotope or a nuclide is generally expressed as yield (given in units of production per unit fission or in percentage). Yield is defined in three ways as

1. Independent Yield IND (A,Z,I)

2. Cumulative Yield Y (A, Z, I) is the total yield of an individual fission product nuclide as sum of its independent yield and of its formation by decay of its chain precursor.

3.Chain Yield Ch (A) gives the yield of nuclei of given mass number regardless of atomic number. This is known as “Chain Yield” because it represents a decay chain of beta decay.

Independent fission yield, IND (A, Z, I)

The independent fission yield, IND (A, Z, I), is the number of atoms of a specific nuclide produced directly (after emission of prompt neutrons but excluding radioactive decay) per 100 fission reactions.

Cumulative fission yield, Cumulative (A, Z, I)

The cumulative fission yield, Cumulative (A, Z, I), is the number of atoms of a specific nuclide produced directly and via decay of precursors per 100 fission reactions. The cumulative yield is very nearly equal to the amount produced at a time short compared to its half-life but long compared to the half-life of its precursors. However, for a radioactive nuclide for which this is not the case, some atoms will have decayed before all have been produced. In such a case, at no time will there actually be present the reported cumulative yield of atoms per fission present. In the present investigation the cumulative yield of fission products in the neutron induced fission of ^{238}U and ^{232}Th(n,f) are measured at average incident neutron energies of 9.35 MeV and 12.52 MeV respectively. These measurements are done for the first time at these energies.

Chain yield, Y (A)

The chain yield is the number of isobars of a specific mass, produced in 100 fission reactions. In other words, the chain yield Y (A) is equal to the sum of all stable or long-lived cumulative yields for a given mass chain. The cumulative yield of the last (stable or long-lived) chain member is generally identical to the chain yield. These chain yields apply to fission products after emission of prompt neutrons that takes place in a time of 10^{-16} s after scission [Fig. 1.3].

1.2.2 **Need for fission product yield measurements**

From EXFOR compilation [27], it can be seen that sufficient data on fission product yields are available in the reactor neutron [28,29] energy range. Beyond this very limited data are available in the energy range 8 to 14 MeV except few measurements carried out using quasi mono energetic neutrons [30-53]. It has been also seen that mass yield curve for neutron induced fission are asymmetric for ^{232}Th(n,f) with a triple humped distribution. To studies the effect of excitation energy on the mass yield curve there is a need for more experimental data at different energies. The yield of fission products are higher around mass number (A) 133-134,138-140 and 143-145 and their complementary products. Nuclear structure effects disappear at higher excitation energy. Keeping these in mind two mass yield measurements were carried out at energies 9.35 MeV. and 12.52 MeV. No measured data are available at these energies in the literature.

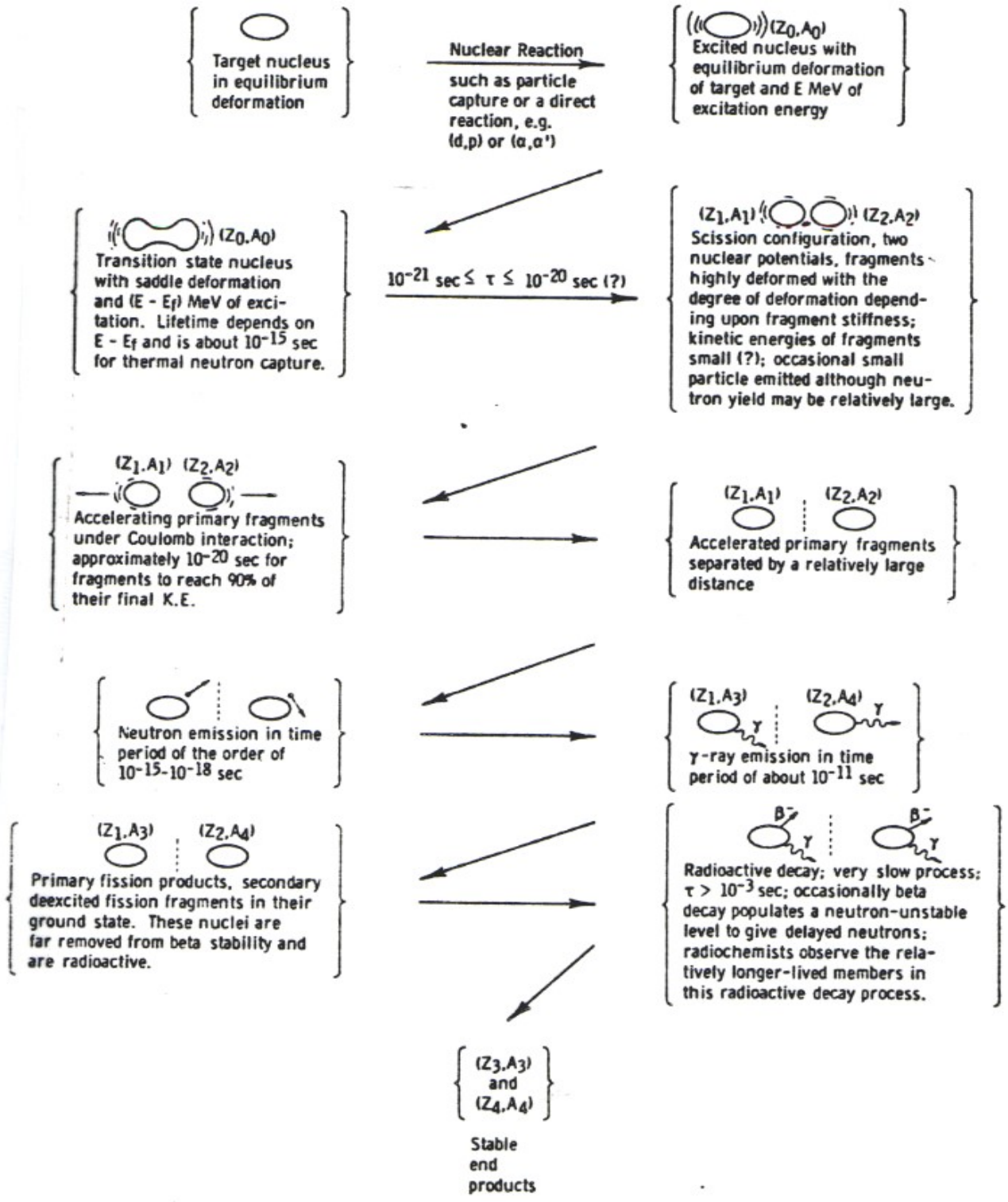

Fig 1.3 A schematic view of the fission process [26].

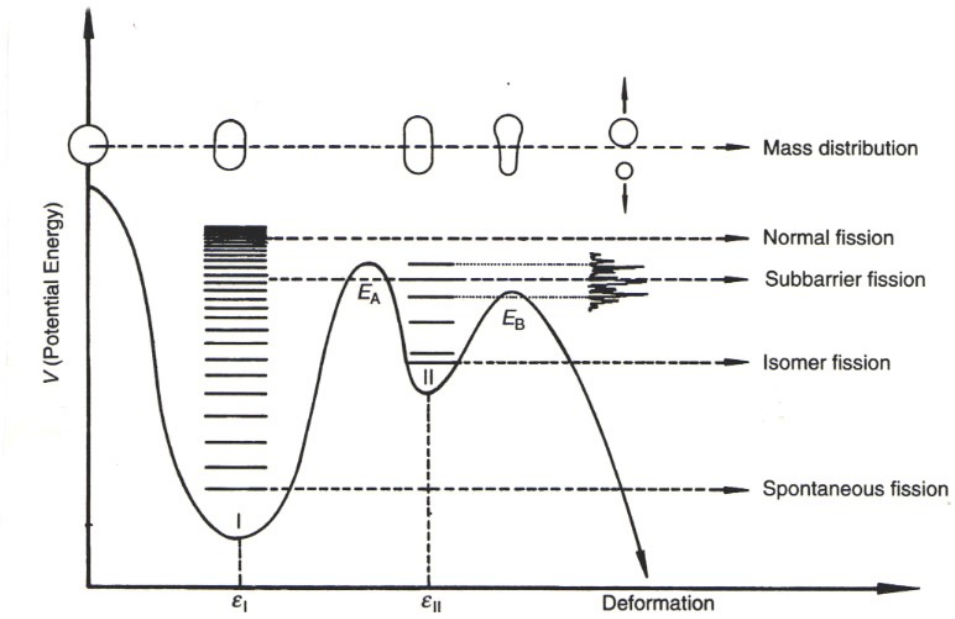

Fig. 1.4 Schematic representation of a double humped fission barrier. Intrinsic excitations in the first and second minimum are shown along with the path of fission from isomeric states and ground state spontaneous fission.

1.3 Basics of neutron activation technique

The principle of neutron activation analysis is that a particle (neutron) induces a nuclear reaction in a nucleus of a target element. The product of the reaction is detected by its decay properties. Other neutron reactions used in Activation Analysis are induced fission, (n, f), for fissionable elements (U, Pu, Th) and inelastic neutron scattering, (n, n' γ), in which a radioactive isomeric state of the target nuclide is measured.

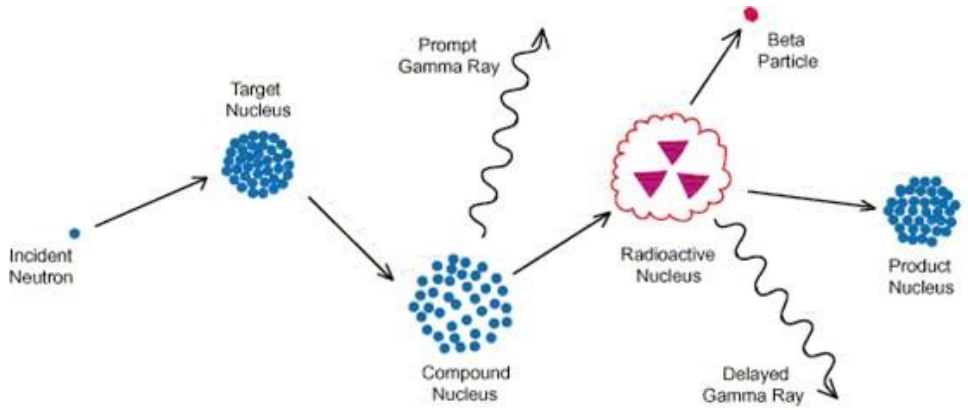

Fig. 1.5 Neutron Activation Process

The most common type of reaction used for neutron activation analysis is the (n, γ) reaction, also threshold reactions like (n,p), (n,xn), (n,α). A schematic of neutron activation is shown in the Fig. 1.5. Neutron activation analysis falls into two categories (i) prompt gamma ray neutron analysis where measurements take place during irradiation (2) delayed gamma ray neutron activation analysis, where the measurements follow radioactive decay. The second method is more common, thus, when one mentions neutron activation analysis, it is generally assumed that measurement of the delayed gamma rays is intended. The quantitative characteristics are the energy of the emitted gamma ray and the half life of the nuclide.

The probability of a neutron interacting with a nucleus is a function of energy and is a characteristic of the nuclide. This probability is called the cross section, and each nuclide has its own neutron energy capture cross section [54]. The activity of a particular nuclide, at a time t during irradiation, can be calculated from the equation mentioned below:

Activation Equation

Activation of a sample by neutrons is the first stage in Neutron Activation Analysis. The reaction rate R per nucleus capturing a neutron per unit of time is given by:

$$R = \int n(v) v\, \sigma(v) dv$$

Where v stands for neutron velocity

n(v) stands for number density at velocity v

σ(v) stands for reaction cross section

Production of radioactive nuclei is described by

$$dN/dt = RN_0 - \lambda N \qquad (1.2)$$

The disintegration rate of produced radionuclide at the end of irradiation time (t_{irr}) is given by

$$A(t_{irr}) = N(t_{irr})\, \lambda = N_0 R\, [\, 1 - \exp(-\lambda t_{irr})\,] \qquad (1.3)$$

This equation can be written in more simplified form as:

$$A = N\, \sigma\, \varphi\, [\, 1 - \exp(-\lambda t_{irr})\,] \qquad (1.4)$$

After a delay of time t_d

$$A = N\, \sigma\, \varphi\, [\, 1 - \exp(-\lambda t_{irr})\,] \exp(-\lambda t_d) \qquad (1.5)$$

For a counting time of t_c

$$A = N\, \sigma\, \varphi\, [1 - \exp(-\lambda t_{irr})] \exp(-\lambda t_d)\, [1 - \exp(-\lambda t_c)] \qquad (1.6)$$

A = number of decays per second (Activity) .

N_0 = number of atoms of the target isotope at time t=0

N = number of atoms of the target isotope.

λ = decay constant = $0.693/t_{1/2}$

$t_{1/2}$ = Half-life of the isotope

φ = neutron flux $n.cm^{-2}.sec^{-1}$

σ = activation cross-section $10^{-24}cm^2$

t_{irr} = irradiation time

The cross-section and neutron flux density are neutron energy dependent.

From this equation we can see that the total activity for a particular nuclide is a function of the activation cross-section, the neutron flux, the number of parent nuclei, and the irradiation time. It can be seen from Eq. 1.2 that, for any particular radioactive nuclide, radioactive decay is also occurring during irradiation; hence the total activity is determined by the rate of production minus the rate of decay. If the irradiation time is much longer than the half-life of the nuclide, saturation is achieved. What this means is that the rate of production and decay is now in equilibrium and further irradiation will not lead to an increase in activity.

After the sample has been activated, the resulting gamma ray energies and intensities are determined using a High Purity Germanium Detector (HPGe) in off-line. Given the differences in half-lives for various nuclides, there are optimum times to count an activated sample. In general nuclides with relatively short half-lives, of the order of

hours to days, are counted within the first week of irradiation. This cooling of 4 to 8 weeks after irradiation is meant for the short- and medium-lived nuclides to decay, so that the gamma peaks from short lived nuclides will not cause any overlap with the peaks of long lived nuclides of interest and the activity measurements will become better. Hence, activated samples are counted several times up to a long period after irradiation.

1.4 Neutron sources

Proper neutron sources are necessary for the determination of neutron reaction cross sections. There are different methods of producing neutrons, such as in a research reactor [55], with spallation sources or by methods of nuclear reactions. Few of the methods for generation of neutrons are mentioned here in details.

1.4.1 The d-d reaction

The reaction $^{2}H+^{2}H \rightarrow ^{3}He+n+3.3$ MeV (the D-D reaction) [56] was historically the first reaction to serve as a source of mono energetic fast neutrons. Its usefulness as a source of mono energetic neutrons is limited to neutron energies below about 8 MeV, since at bombarding energies above 4.5 MeV the deuterons break up and produce a continuum of much lower energy neutrons.

1.4.2 The d-t reaction

The reaction $^{3}H + D = {}^{4}He + n + 17.6$ MeV (the D-T reaction) [56] is of interest as an accelerator-based source for the same reason that it is the most promising reaction for a fusion reactor, i.e. it has a very large cross section at low bombarding energies.

1.4.3 Protons on lithium and beryllium

Here neutrons are generated by a threshold reaction. The neutron spectra from the proton bombardment of thick Li [57] and Be targets are quasi-mono energetic. At neutron energies above 5 MeV there is a broad maximum for neutrons emitted in the forward direction. The intensity of the energetic neutrons decreases rapidly with emission angle[57]. Present experiment uses this type of neutron source. Neutrons are generated from ^{7}Li(p, n)^{7}Be reaction.

1.4.4 Spontaneous fission

Certain isotopes undergo spontaneous fission with emission of neutrons. The most commonly used spontaneous fission source is the radioactive isotope ^{252}Cf [58]. When purchased new a typical ^{252}Cf neutron source emits between 1×10^{7} to 1×10^{9} neutrons per second but, with a half-life of 2.6 years, this neutron output rate drops to half of this original value in 2.6 years. Other spontaneous fission neutron sources are produced by irradiating uranium or another transuranic element in a nuclear reactor.

1.4.5 Radioisotopes which decay with alpha particles packed in a low-Z elemental matrix

Neutrons are produced when alpha particles impinge upon any of several low atomic weight isotopes including isotopes of beryllium, carbon and oxygen. This nuclear reaction can be used to construct a neutron source by inter mixing a radioisotope that emits alpha particles such as radium or polonium with a low atomic weight isotope, usually in the form of a mixture of powders of the two materials. Typical emission rates for alpha reaction neutron sources range from 1×10^{6} to 1×10^{8} neutrons per second. Usual

combinations of materials are plutonium-beryllium (Pu-Be), americium-beryllium (Am-Be), or americium-lithium (Am-Li) [59].

1.4.6 Radioisotopes which decay with high energy photons co located with beryllium or deuterium

Gamma radiation with an energy exceeding the neutron binding energy of a nucleus can eject a neutron. Two examples and their decay products:

^{9}Be + >1.7 MeV photon → 1 neutron + 2 ^{4}He

^{2}H (deuterium) + >2.26 MeV photon → 1 neutron + ^{1}H [60].

1.4.7 High energy photo-neutron / photo-fission systems

Photo neutrons are produced when sufficiently energetic photons interact with a nucleus causing it to undergo excitation. The nucleus decays by neutron emission (photo neutron reaction) or undergoes fission (photo-fission) releasing neutrons in the process. Typically photons begin to produce neutrons on interaction with normal matter at energies of about 7 to 40 MeV. The photons may be produced by bombardment of electrons of energy of about 50 MeV on a heavy target. These photons induce giant dipole resonance in target nuclides by a mechanism which is the inverse of internal conversion and decay by neutrons emission by a mechanism similar to that of photo-neutrons [61].

1.4.8 Nuclear fission reactors

In a reactor, when a heavy atomic nucleus such as ^{235}U absorbs a neutron, it undergoes nuclear fission. Nuclear fission is the process in which a large nucleus splits into two smaller nuclei with the release of energy. Nuclear fission reactors produce power as well as a very large number of neutrons and can be used for a variety of purposes.

Some of the reactors used as neutron source are: Swimming Pool Type reactors, Heavy water moderated and Natural Uranium Fuel Research Reactors, Miniature Neutron Source Reactor (MNSR) and Multipurpose research reactor[55].

1.4.9 Nuclear fusion system

Nuclear fusion [62], the combining of the heavy isotopes of hydrogen, also has the potential to produces large quantities of neutrons. Small scale fusion systems exist for research purposes at many universities and laboratories around the world. A small number of large scale nuclear fusion systems also exist including the National Ignition Facility in the USA, JET in the UK, and the recently started ITER experiment in France.

1.4.10 High energy particle accelerators

A spallation source is a high-flux source in which protons that have been accelerated to high energies hit a target material, prompting the emission of neutrons [63]. Spallation reactions are processes where a relatively light accelerated ion such as proton impinges on a massive heavy metal target, which results in a breakup of the heavy nucleus. This leads to a production of different particles with relatively high energies and mainly neutrons with a wide range of different energies. A schematic of spallation reaction is shown in Fig. 1.4. For example a spallation process starts when a proton interacts with the target nucleus (e.g. lead) and gives its energy to the nucleons of the nuclei. This stage is known as an intra-nuclear cascade. The target nucleus is in a highly excited state after the intra-nuclear cascade and evaporates particles and photons to lower its energy. After this emission the nucleus further remains in an excited state and can split or emit neutrons and mainly gamma photons to lower its excitation energy. Neutrons

which result from a spallation reaction have a wide range of energies. The highest energy of the resulting neutrons can reach up to the energy of the incident beam particles.

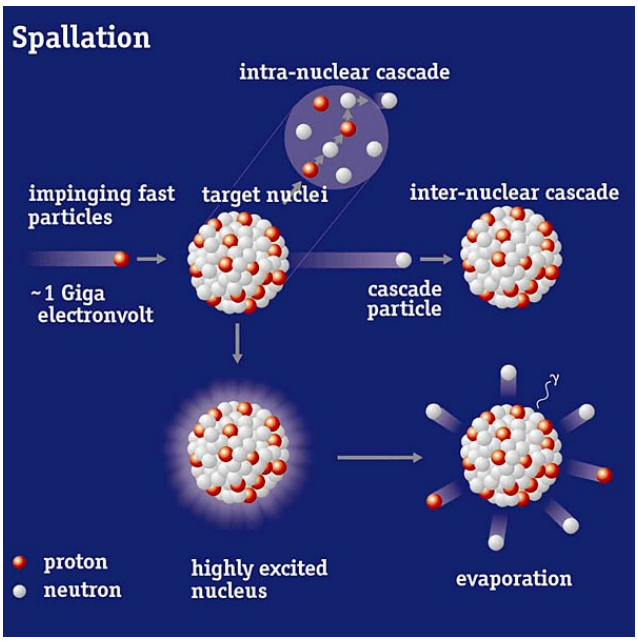

Fig. 1.6 Schematics of principle of the spallation reaction [63]

.

CHAPTER 2

Experimental setup

2.0 Experimental setup details

This chapter provides details of the experimental setup, measurements, detectors and electronics used in the present study. Present thesis is mainly focused on the measurement of reaction cross sections and fission product mass yield distribution in the neutron induced fission of ^{232}Th and 99.3% ^{238}U. Brief description of the accelerator facility used in the experiment is given. The target fabrication techniques are described followed by the description of the detector and nuclear data measurement setup.

2.1 14UD Pelletron accelerator at TIFR

14UD Pelletron accelerator is a medium energy heavy ion accelerator facility jointly set up by Bhabha Atomic Research Centre (BARC) and Tata Institute of Fundamental Research (TIFR) at TIFR campus for research in the field of nuclear physics, atomic physics, condensed matter physics and several other areas. This facility is based on a 14 MV tandem, Van-de-Graaff accelerator which is a 14UD Pelletron [64, 65] accelerator using the pellet charging chain system. It can deliver heavy ion beams of energies (q+1)V, where V is the terminal voltage and q is the charge state of the ions after passing through the stripper foil located in the high voltage terminal. At present 14 UD BARC-TIFR Pelletron accelerator at TIFR, is capable of accelerating ions, except inert gases, from proton to nikel up to energy of about 5-8 MeV/A depending upon the ions. The accelerator is installed in vertical configuration in an insulating tank of length 26.5 m and diameter 5.5 m, filled with SF_6 gas. The schematic diagram of the accelerator is shown in Fig. 2.1.

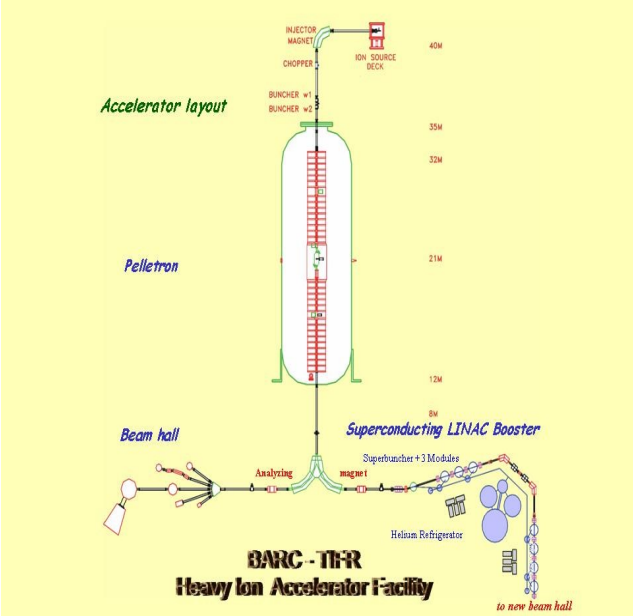

Fig. 2.1 BARC-TIFR Pelletron Facility.

2.2 Target fabrication

Preparation of thin target is an important and challenging task in any nuclear reaction experiment. Study of reaction cross sections and fission product mass distributions for ^{232}Th and ^{238}U require very thin targets. Accurate experimental nuclear data, demand a careful attention to sample preparation. For each experiment two type of samples were prepared such as:

1. Samples were prepared for Lithium targets for neutron generation using ^{7}Li(p,n)^{7}Be reaction.

2. ^{232}Th and ^{238}U samples for nuclear data experimentation.

1. Here neutrons are generated using ^{7}Li(p,n)^{7}Be reaction. If the lithium targets used are thick then, the incident beam and the reaction products loose energy as they pass through the target material. This energy loss will alter the energy definition of the incident beams as well as the resolution of the energy spectra of the reaction products. If the target is

sufficiently thick the low energy reaction products like evaporation residues and even high energy fission fragments, will be stopped inside the target itself. Hence, in an ideal case we prefer self-supporting targets or targets with very thin backing material. Targets were prepared using the rolling techniques at BARC-TIFR target preparation lab at TIFR. Stainless steel plates are generally used for rolling the samples. Different precautions were taken for different target materials i.e. lithium sticks with stainless steel plates so oil was used between the plate and the target material while rolling. At times this process created hole in the lithium foil, subsequently teflon plates were used to cover lithium foils while rolling. A small piece of natural lithium (^{6}Li - 7.42 % and ^{7}Li - 92.58 %) was soaked in paraffin or kerosene first before use. Lithium was first covered with a tissue paper and then was placed between two teflon plates of dimensions 50 mm × 50 mm and thickness 0.7 mm/0.8 mm. The lithium foil was rolled along with the teflon sheets. This rolling was done in all the directions so that lithium thickness is uniform. Finally a rectangular piece of lithium was cut and its weight was measured. This method gives an idea of the thickness of the lithium foil measuring its weight and dimension.

2. An intensive efforts were made to prepare 0.27-0.28 mm thick ^{232}Th and 0.18-0.33 mm thick 99.3% ^{238}U targets. The samples were prepared using the rolling techniques at BARC-TIFR target preparation lab at TIFR. Stainless steel plates are generally used for rolling the samples. Total thirteen targets were prepared. Seven targets were made of thorium, out of these five were used for reaction cross section measurement and two were used for fission product mass distribution studies. Six targets were prepared of uranium, out of which four were used for reaction cross section measurements and two were used for fission product mass distribution studies.

2.3 Gamma ray spectroscopy

2.3.1 HPGe detector set-up

Gamma spectroscopy is the quantitative study of energy spectra of gamma-ray sources. A typical gamma-ray spectrometry system is comprised of a detector (HPGe) with a shielding mainly lead, to reduce the background, high voltage power supply, electronics for signal processing (preamplifier, amplifier, multi channel analyzer); computer and dedicated validated software package for collecting, storing and analyzing the gamma ray spectrum. The block diagram of a typical HPGe setup is shown in Fig. 2.2.

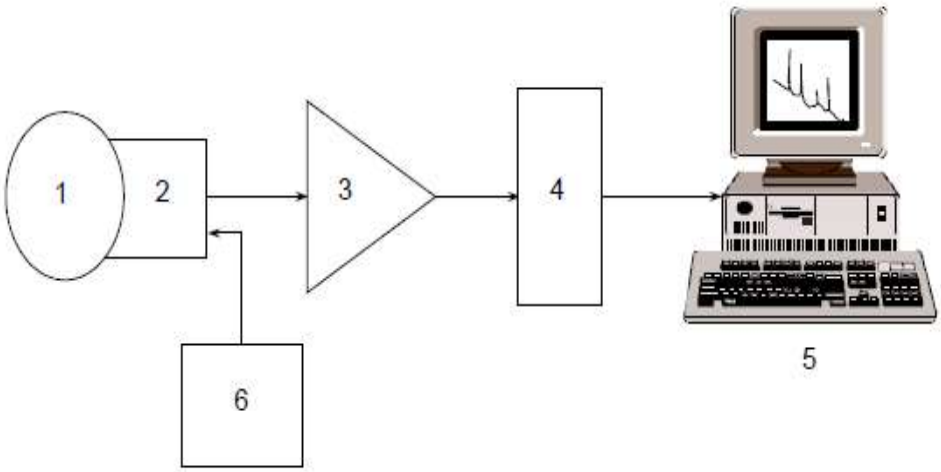

Fig. 2.2. HPGe Detector setup with PC based MCA for Gamma Spectroscopic Studies

1.0 High Purity Co-axial Germanium Detector

2.0 Preamplifier

3.0 Amplifier

4.0 Multichannel Analyzer

5.0 Computer

6.0 Bias Supply

A high purity germanium semiconductor detector (HPGe) is used here for better energy resolution which is very important for identification of radioactive isotopes during gamma activation analysis. The high resolution HPGe detectors are suitable for samples containing many radio nuclides (e.g. from the natural radioactive series), when the gamma-ray spectrum presents a large number of peaks to be resolved. The detector is cooled with liquid nitrogen to a temperature of 77 K to reduce dark current and detector noise. The detector produces a signal which is proportional to the energy of the gamma rays of the incoming radiation. Gamma rays passing through the detector generate free electron and hole pair. The number of electrons (current) is related to the energy of the gamma ray. There are three processes by which gamma ray interaction occur in the detector such as Compton scattering, photoelectric effect and production of electron-positron pairs. The relative magnitudes due to these effects are shown in Fig. 2.3 for a germanium detector. In Fig. 2.3, it can be seen that photo electronic interactions are dominant at low energies, pair production at high energies and Compton scattering is the most important interaction in the mid-energy range.

The γ-ray counting of the samples were done in the live time mode. Modern multi-channel analyser (MCA) have inbuilt feature of dead time correction by counting in live time mode. As the dead time in the analogue to digital converter (ADC) increases, the real (clock) time increases proportionally so as to keep fixed live time. To minimise dead time and the pile up effect, the sample was placed at a suitable distance from the detector. The details of these components have been discussed in the following section.

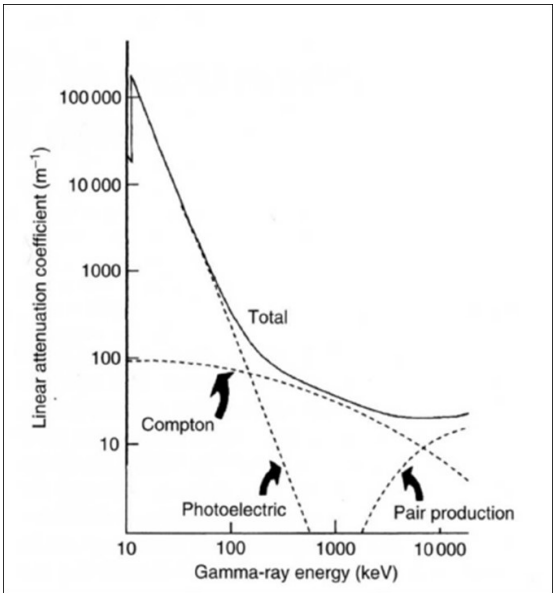

Fig. 2.3 The linear attenuation coefficient of Germanium and its component parts [66].

2.3.1.1 High Voltage Bias Supply

In order to collect the charge formed in the detector, a bias voltage must be placed across the detector. The optimum bias voltage is up to 5000 V for a large detector. The voltage is chosen low enough to avoid break down, but otherwise high enough for charge collection. The bias voltage is maintained at a stable value.

2.3.1.2 Preamplifier

This comes as an integral part of the detector assembly. In order to minimize the electronic noise, the input stage of the preamplifier is cooled in the same manner as the detector. Preamplifier has two functions in the circuit, (i) it converts low amplitude, short duration current pulse from the detector into a voltage pulse whose amplitude is proportional to the energy deposited by the gamma ray in the detector, (ii) It maximizes the signal to noise ratio of the output pulse and preserves the gamma ray energy information.

2.3.1.3 Amplifier

The purpose of amplifier is to amplify the pulse from the preamplifier into a linear voltage pulse in the range of 0 to 10 V. The amplifier also shapes the pulse to meet the requirements of the pulse height analysis instrumentation. This is important since the analyzer measures the input pulse amplitude relative to a reference voltage so that the output pulse from the amplifier should return as fast as possible to stable voltage.

2.3.1.4 Multichannel analyser

The multichannel analyzer (MCA) performs the function of collecting the data, providing a visual monitor of the pulse height spectrum produced by the detector. An analog-to-digital converter (ADC) converts the analog voltage pulse from the amplifier into a binary output. The ADC sorts the pulses into a large number of channels according to the height of the voltage pulse and since the height is proportional to the energy of the gamma ray, the relationship between the channel number and energy is nearly linear.

2.3.2 HPGe detector specification

Experiments were carried out using an 80 c.c. HPGe detector. The detector efficiency was 20 % at 1332.5 keV relative to 3" diameter × 3" length NaI (Tl) detector. The uncertainty in the efficiency was 2-3 %. The resolution of the detector system had a FWHM of 1.8 keV at 1332.5 keV γ -line of ^{60}Co. HPGe detector has low band gap of 0.67 ev at 300 K, so it can generate current (called leakage current) at room temperature. Therefore HPGe detector is operated at 77 K.

2.3.3 Detector Parameters

Resolution

The resolution of a detector is its ability to resolve two near by peaks. It is specified as full width at half maximum (FWHM), detector resolution depends upon statistics of charge creation, charge collection and electronic noise. FWHM is expressed as,

FWHM= $2\sigma\ (2\ln 2)^{1/2}$

The (%) resolution at a given energy E is given by

R = (FWHM / E)*100

Smaller is the R, better is the resolution of the detector. Resolution is generally expressed in terms of FWHM at 1332 keV or at 122 keV for low energy.

Detector Efficiency:

The efficiency is the most important parameter since it goes as input in estimating the flux and cross sections as per Eq. (3.7). For conversion of the measured count rate to the disintegration rate (disintegration per second) of the radionuclide monitored, it is important to calibrate the system for efficiency. Calibration was carried out using different standard gamma sources such as ^{133}Ba and ^{152}Eu for various gamma energies .The results are shown in Fig. 2.5. The uncertainty in the efficiency was estimated to be about 2-3 %. The results are fitted to a suitable function so that efficiency can be obtained at γ-ray energies other than the ones at which measurements are carried out. The detector efficiency (ε) for the γ-ray energy at a fixed geometry was calculated as follows:

$$Log\ \varepsilon_i = \Sigma a_j\ (Log\ E_i)^j$$

Where a_j represent the fitting parameters and E_i is the γ-ray energy which ranges from 89.85 to 1408.0 keV for ^{133}Ba and ^{152}Eu standard sources.Several fitting functions are available. Often two functions are used, one for lower energy (up to 200 keV) and other for higher energy range (above 200 keV). Generally a fourth order polynomial (j) function is sufficient to fit the whole energy range from 80 keV to 2 MeV.

2.3.4 Calibration of the HPGe detector

For gamma ray spectrometric analysis, the counting was done using a 80 cm^3 high purity germanium detector (HPGe) detector connected to a PC based 4094 channel analyzer. The resolution of the detector was 2.0 keV at the 1332.0 keV of ^{60}Co. Before using the detector and analyzer set up, a proper energy calibration was carried out to identify the energies of the gamma ray emission spectrum, i.e. the gamma-ray emitter radio nuclides contained in the sample. The quantitative analysis, i.e. the activity (Curies) and its standard uncertainty determination for each radionuclide present in the sample, requires a full-energy peak (FEP) efficiency calibration. For both calibrations, various radioactive standard sources with certified activity were used. The energy calibration of the detector system was done by using a multi gamma ray standard source such as ^{152}Eu having the gamma lines from 89.85 keV to 1408.0 keV. The efficiency calibration of the HPGe detector system within 5-1500 keV was carried out using a set of mono energetic standard sources such as ^{241}Am, ^{137}Cs, ^{54}Mn and ^{60}Co to avoid co-incidence summation error. These sources can be used for efficiency calibration at a distance closer to the detector. For a distance greater than 5 cm, the multi gamma ray sources such as ^{152}Eu (13.5 y) and ^{133}Ba (10.5 y) were used for efficiency calibration. These two different types of efficiency calibration were done to avoid coincidence summing error. The gamma ray

energies and abundances along with the half-lives of these radio nuclides are given in Table 2.1.

Table 2.1 Gamma ray Energies of the Radionuclide used for HPGe Detector Calibration

Nuclide	Gamma Lines (keV)	γ ray abundance (%)
Eu-152 ($T_{1/2}$=13.54 Yrs)	89.85	69.95
	121.78	25.6
	244.70	7.6
	344.26	26.5
	411.12	2.2
	443.96	3.1
	488.60	0.4
	563.0	0.5
	678.0	2.0
	688.67	0.9
	778.9	12.9
	867.0	4.2
	964.0	14.6
	1085.0	10.2
	1089.0	1.7
	1112.1	13.6
	1212.95	1.4
	1299.0	1.6
	1408.0	21.0
Ba-133 ($T_{1/2}$=10.5Yrs)	80.997	34.10
	276.4	17.80
	302.9	18.33
	356.02	69 00
	356.01	62.05
Co-60 ($T_{½}$=5.26 Yrs)	1173.23	100.00
	1333.50	100.00
Mn-54 ($T_{½}$=0.856 Yrs)	835.0	99.98
Cs-137 ($T_{½}$=30 Yrs)	661.66	85.00
Am-241 ($T_{½}$= 458 Yrs)	59.54	36 00

However, the availability of mono energetic primary standards is a constraint. So in most of the cases multi-gamma ray sources like ^{152}Eu (13.5 y), ^{133}Ba (10.5 y), were used for the efficiency calibration as they cover a wide energy range and are long-lived.

Because there can be hundreds to thousands of gamma ray interactions per second with the detector, an important criteria in system design is the response time of the detector to gamma ray interactions (as measured by the dead time).

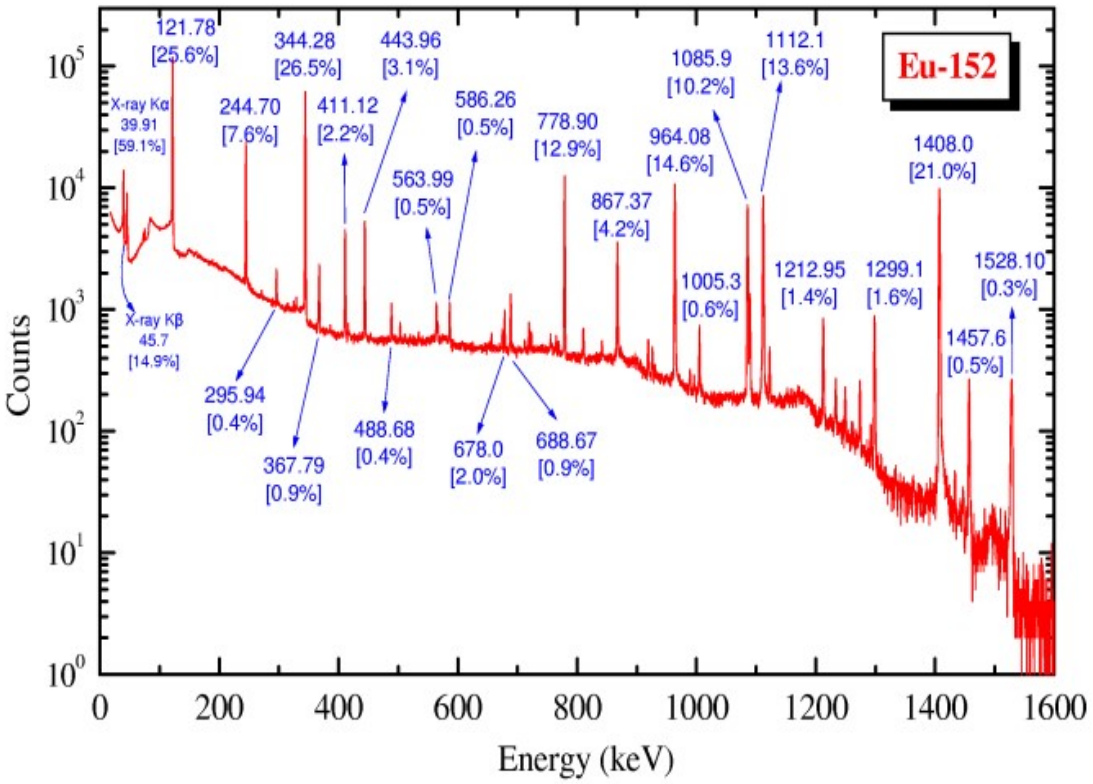

Fig. 2.4 Measured gamma-ray spectrum from a calibrated ^{152}Eu reference source.

The counting dead time was kept always less than 5 % by placing the sample at a suitable distance from the detector to avoid coincidence summation (pileup) effects. The energy and efficiency calibration of the detector system was done by counting the γ-ray

of standard sources having energies in the keV region and keeping the same geometry, where the summation error was negligible. The gamma lines of a typical ^{152}Eu sources which is used for detector calibration are shown in Fig 2.4 and the detector efficiency calibration is shown in Fig. 2.5.

2.3.5 Efficiency calibration

The efficiency values are calculated using known activity sources for the HpGe detector using the following equation [66,67,68]

$$\varepsilon = A_{obs} / (\varepsilon_g \cdot t \cdot \Lambda \cdot p) \qquad (2.1)$$

where: ε = is the detector efficiency

A_{obs} = is the peak area in number of counts at that energy

Λ = is the absolute activity of the standard [Bq]

t = is the measurement time

p = is the probability of disintegration of the particular radionuclide

ε_g = is the geometric efficiency. This is independent of the gamma ray energy and d**2.4**

2.4 Experimental details

2.4.1 Sample mounting and irradiation facility

Quasi-mono-energetic [30] and fast neutrons were produced in ^{7}Li(p, n) reactions as neutron source for this experiment at the BARC-TIFR Pelletron-Linac accelerator Facility (PLF Fig. 2.1). epends upon the solid angle subtended by the source on the detector. Present experiments require the neutron yield to be as high as 10^{7}-10^{9} n/s. In the experimental setup drift space above analyzing magnet is modified to accommodate a proton beam irradiation setup at 6 meter level at this facility (see Fig. 2.6).

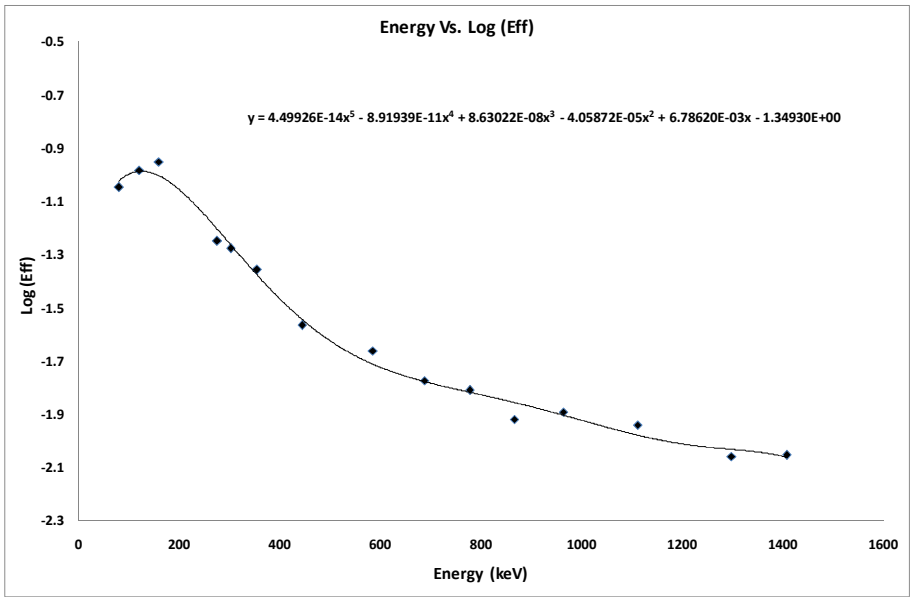

Fig 2.5 Plot of Log (E_{ff}) as a function of gamma-ray energy (keV)

This setup is capable of delivering proton beam in the energy range of 2 MeV to 26 MeV and current up to μA range. The shielding at this level is such that radiation is within permissible limit when proton beam with high energy and high current is accelerated. This setup can provide high neutron yields, produced by bombarding Lithium targets with protons of a few MeV. Handling these targets pose specific hazards. Lithium is flammable when exposed to air. Specific assemblies have been designed and being used to handle such targets which can be directly installed at the 6 meter experimental port without exposing the hazardous materials to the users. The sample mounting set up is shown in Fig. 2.6 (in this thesis the experiments were carried out at incident proton energies of 4.7, 5.1, 16, 18 and 20 MeV) with a 100-400 nA beam current.

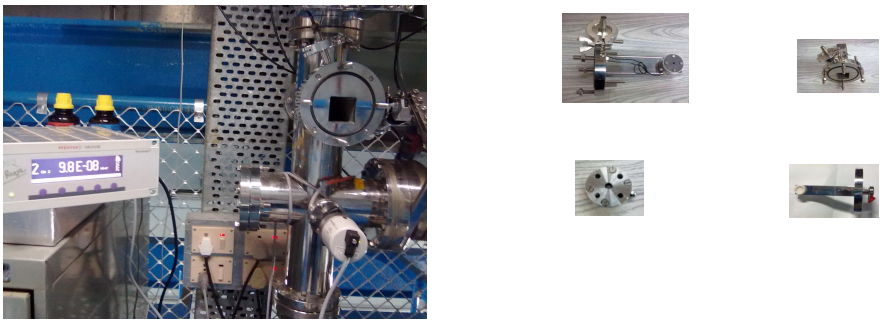

Fig. 2.6 Set up for Sample Holder at 6 mete

2.4.2 Nuclear data measurement set-up

The experiments were carried out using the 14UD BARC-TIFR Pelletron facility at Mumbai, India. The neutron beam was obtained from the ^{7}Li(p, n) reaction by using the proton beam in the main line at 6 m height above the analysing magnet of the Pelletron facility to utilize the maximum proton current from the accelerator. Furthermore, ^{7}Li(p,n) reaction-based setup has less radiation hazards compared to other neutron sources because it uses a non-radioactive target to produce neutrons. The geometry of the ^{7}Li(p,n) reaction-based setup is shown in Fig. 2.6 The energy spread for proton at 6 meter height was maximum 50-90 KeV. At this port, the terminal voltage was regulated by GVM mode using terminal potential stabilizer. Further, we used a collimator of 6 mm diameter before the target. The lithium foils were made up of natural lithium with thickness 3.7 mg/cm^2, sandwiched between two tantalum foils of different thickness. The front tantalum foil facing the proton beam was the thinner, with thickness of 3.9 mg/cm^2, in which degradation of proton energy was only 30 keV. On the other hand, the back tantalum foil was the thicker (0.025 mm), which was sufficient to stop the proton beam.

The Ta-Li-Ta stack is shown in Fig. 2.7. For each experiment fresh lithium foils were used.

This thesis is mainly focusing around the nuclear cross section and fission yield measurements for ^{238}U and ^{232}Th. All the samples comprising of natural ^{238}U or ^{232}Th metal foils were individually wrapped with 0.025 mm thick aluminium foil during irradiation and counting. The aluminium wrapper was used to stop and collect the fission products recoiling out from the surface. The sample foil wrapped with aluminium was mounted at zero degree with respect to the beam direction at a distance of 2.1 cm from the location of the Ta-Li-Ta stack. A schematic diagram of Ta-Li-Ta stack and foils is shown in Fig. 2.7. Different sets of samples were made for different irradiations at various neutron energies for Th and U target materials.

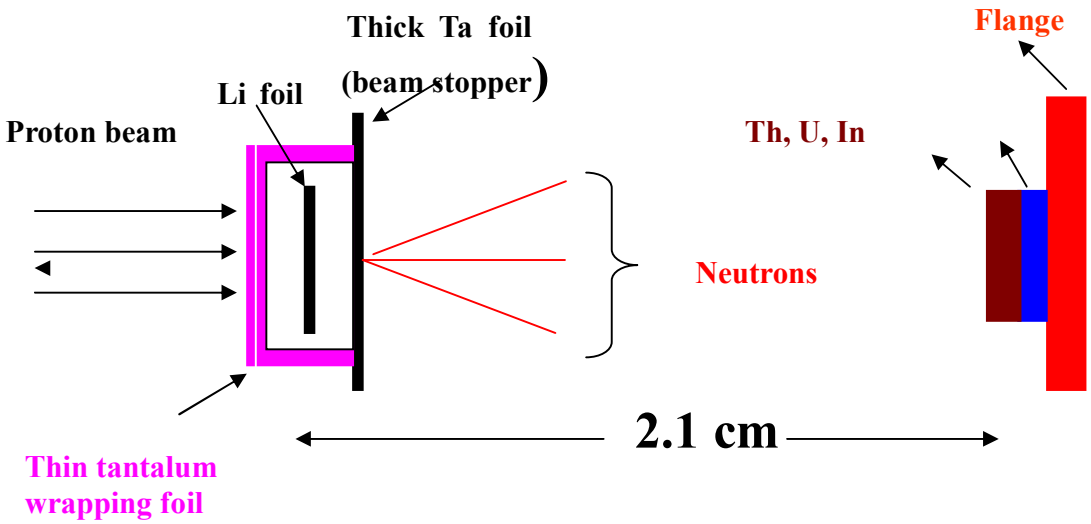

Fig. 2.7 Schematic diagram showing the arrangement used for neutron irradiation

Reaction Cross Section Measurements

CHAPTER 3

Measurements of $^{238}U(n, \gamma)^{239}U$ and $^{238}U(n, 2n)^{237}U$ reaction cross-sections at the spectrum averaged neutron energies (<E>) of 13.5 and 17.28 MeV

In this chapter we present the measurements of the (n, γ) and (n, 2n) reaction cross-section of ^{238}U at the spectrum averaged neutron energies of 3.12, 13.5 and 17.28 MeV. Neutrons are generated using ^{7}Li (p, n)^{7}Be reaction. Cross sections have been determined adopting activation and off-line γ–ray spectrometric technique. The experimentally determined $^{238}U(n, \gamma)^{239}U$ and $^{238}U(n,2n)^{237}U$ reaction cross-sections from present work have been compared with the evaluated data of ENDF/BVII.0 and JENDL-4.0, JEFF-3.1/A and CENDL-3.1. The experimental values were found to be in general agreement with the evaluated values obtained using ENDF/BVII.0, JENDL-4.0 and JEFF-3.1/A and CENDL-3.1 values at average incident neutron energy of 3.13 MeV but it differs from the values obtained using CENDL-3.1 at 13.5 MeV and 17.28 MeV. The present data along with literature data in a wide range of neutron energies were interpreted in terms of competition between $^{238}U(n, \gamma)$, (n, f), (n, nf) and (n, xn) reactions channels. The $^{238}U(n, \gamma)$ and $^{238}U(n, 2n)$ reaction cross-sections were also theoretically calculated using the TALYS [8,9] computer code and were found to be in general agreement with the present experimental data.

3.1 Mechanism of nuclear reactions

3.1.a Compound nuclear reaction

This reaction can be treated as a two-step process. In the first step, the incident

particle which stays in the nucleus for a relative long time (10^{-15} s) delivers its energy to many nucleons in the target nucleus, and this energy is rapidly distributed throughout the nucleus. The incident particle itself becomes indistinguishable from other nucleons in the compound nucleus, and we can say that the compound nucleus 'forgets' the way in which it was formed. Due to this forgetfulness of the compound nucleus, the second step is independent and unrelated to the first step. The excitation energy of the compound nucleus is equal to the kinetic energy introduced by the incident particle plus its binding energy. This energy is statistically distributed among the nucleons, and each nucleon is rapidly colliding with the others and changing its energy.

3.1.b Pre-compound reaction:

With increasing projectile energy (above 10 MeV) sometimes a particle emission can occur even before the whole energy could distribute evenly among the nucleons of the compound nucleus.

3.1.c Direct Reactions:

This process becomes probable when the projectile spends less time in the vicinity of the target nucleus (10^{-22} s). The interaction between the incident particle and the target nucleus takes place usually close to the surface of the nucleus. Only a few nucleons of the target nucleus take part in this process.

3.2 Cross-section of a nuclear reaction

A nuclear reaction A(x, y) B occurs, when a projectile x comes sufficiently close to the target nucleus A, i.e. closer than the range of the nuclear forces (10^{-15} m). A particle y is then emitted, leaving a residual nucleus B, which can be either stable, radioactive or an isomer. The interaction of the projectile with the target nucleus is generally described in

terms of the cross section σ(x, y), which is a measure of the probability for a reaction to occur. The cross section is usually given in barns (1b $=10^{-28}m^2$) and is a function of the energy of the incident particle.

3.3 Nuclear model computer code TALYS

TALYS is a versatile and user friendly computer code to simulate nuclear reactions. Many nuclear models are included to cover all main reaction mechanisms encountered in light particle-induced nuclear reactions. It also provides a complete description of all reaction channels and observables in a nuclear reaction. The basic objective here is the simulation of nuclear reactions that involve projectiles like photons, neutrons, protons, deuterons, tritons, ^{3}He- and α-particles. TALYS covers nuclear reactions for the incident neutrons of energy range 1 keV - 200 MeV and for target mass numbers between 12 and 239. It can incorporates modern nuclear models for the optical model, level densities, direct reactions, compound reactions, pre-equilibrium reactions, fission reactions, and a large nuclear structure database. It can calculate total and partial cross sections, energy spectrum angular distributions, double-differential spectra, residual production cross sections and recoils. The proof that **TALYS** is able to produce physical meaningful results, comparisons of calculated results with experimental data are generally done, there are two different options to use TALYS. A very detailed calculation with various adjusted parameters and choices for nuclear models, so that specific experimental data are reproduced. In second option, a large scale, default calculations for many nuclides, in which case adjustment to experimental data is impossible.

These two approaches are strongly linked. Since nuclear model calculations and fits to experimental data generally require many adjustable parameters, it is important that

these parameters all remain within physically acceptable boundaries. Reliability of the code is reasonably high because the default calculations produce results that are not too far from the measurement. Starting from these default parameters, usually only one or a few parameters need to be adjusted to obtain the best possible result, after which we can be pretty confident that we did not end up in some strange corner of parameter space. TALYS output are usually compared automatically with available EXFOR database.

3.4 Practical importance of ^{238}U reaction cross section measurements

One of the major components of the nuclear waste comprises of long-lived minor actinides such as ^{237}Np, ^{240}Pu, ^{241}Am, ^{243}Am and ^{244}Cm. Almost all the minor actinides are generated due to capture (n, γ) and (n, 2n) reactions of ^{238}U and ^{239}Pu followed by beta decay. For electricity generation, Light Water Reactors (PWR & BWR) or Heavy Water Reactors (HWR) is primary reactor of choice for many decades. In these reactors appreciable amount of ^{237}Np is produced by (n, 2n) reaction of ^{238}U followed by beta decay. The fuels used in these reactors are mainly based on enriched or natural uranium. ^{237}Np is one of the most problematic minor actinides generated in these reactors. After million of years, ^{237}Np dominates in terms of radio-toxicity to the population because of the leakage of the actinide from the disposal site. In order to avoid this, the concept of advanced heavy water reactor AHWR) [4] have been proposed in the recent past to generate nuclear power. In AHWR, ^{232}Th-^{233}U in the oxide form is used as the primary fuel, where the production of long lived minor actinides such as (^{237}Np, ^{237}Np, ^{240}Pu, ^{241}Am, ^{243}Am and ^{244}Cm) can be avoided. Significant effort has also been made to develop fast reactors [3-7] to fulfill the increased demand of power production. In the fast reactor ^{238}U-^{239}Pu in the form of carbide is used as the primary fuel. Since the fast reactor

has a fast neutron spectrum, the production of long-lived minor actinides can be suppressed. The ^{239}Pu used in the fast reactor is first generated in a research reactor from ^{238}U(n, γ)^{239}U reaction followed by successive two beta decays. A schematic diagram of (n, γ) and (n, 2n) reaction of ^{238}U followed beta decay in the U-Pu fuel cycle is shown below.

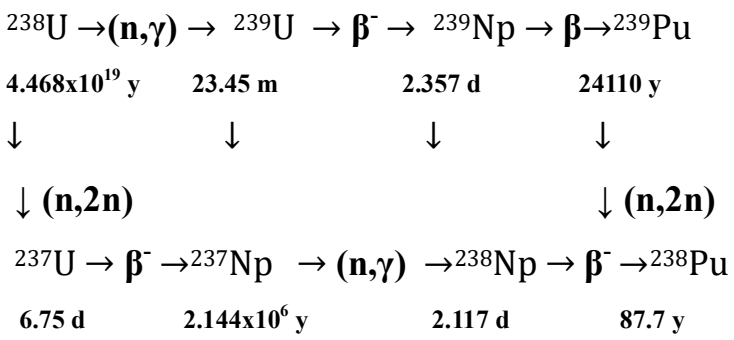

Fig. 3.1 A schematic diagram of (n, γ) and (n, 2n) reaction of ^{238}U followed beta decay in the U-Pu fuel cycle

In the fast reactor, ^{238}U is used as the breeding material to regenerate the fissile material ^{239}Pu. Thus the production of fissile nucleus ^{239}Pu depends on the ^{238}U(n, γ)^{239}U reaction cross-section, which is required with an accuracy of 1-2 % for predicting the dynamical behavior of complex arrangements in fast reactors [2] safely. In fusion-fission hybrid systems, a sensitivity study has shown that the production rate of ^{239}Pu can be predicted within 1 %, provided that the ^{238}U(n, γ)^{239}U cross-section between 3 keV and 3 MeV is known within 2 % [69]. In fast breeder reactors the most important region for neutron capture of ^{238}U lies between 10 keV to 100 keV [70]. At neutron energy of 100 keV, the ^{238}U(n, γ)^{239}U reaction cross-section shows a sharp increasing trend due to resonance neutron capture. Thereafter it decreases up to 6-7 MeV, where the ^{238}U(n,

2n)^{237}U reaction cross-section starts. The fast reactor has harder neutron spectrum with neutron energy up to 15 MeV, whereas the ^{238}U(n, 2n)^{237}U reaction cross-section has threshold energy of 6.18 MeV. Thus above the neutron energy of 6.18 MeV, the ^{238}U(n, 2n)^{237}U reaction is one of the reaction channel besides (n, f) and (n, γ) reactions of ^{238}U. Above neutron energy of 6.18 MeV, the ^{238}U(n, 2n)^{237}U reaction cross-section increases rapidly. Thus the ^{238}U(n, γ)^{239}U and ^{238}U(n, 2n)^{237}U reactions cross-sections at higher neutron energy have a strong impact on the performance and safety assessment for fast reactor [71].

^{237}Np itself is generated from ^{238}U(n, 2n)^{237}U reaction followed by beta decay. Thus at various neutron energies, it is necessary to have knowledge about the ^{238}U(n, 2n)^{237}U reaction cross-section besides the ^{238}U(n, γ)^{239}U reaction cross-section. The ^{238}U(n, γ)^{239}U reaction cross-section data are available in the literature over a wide range of neutron energies from thermal to 18 MeV based on direct measurements [72-81] and activation technique [81-89]. Similarly, sufficient data on ^{238}U(n, 2n)^{237}U reaction cross-section is also available in a wide range of neutron energy above 6 MeV from off-line γ-ray spectrometry and neutron activation methods [88-102].

From the literature data [73-91], it can be seen that the ^{238}U(n, γ)^{239}U reaction has numerous resonance cross-section from thermal energy to 0.1 MeV. However, above neutron energy of 0.1 MeV the ^{238}U(n, γ)^{239}U reaction cross-section decreases up to 6-7 MeV [15, 82,84]. Above neutron energy of 7 MeV, the ^{238}U(n, γ)^{239}U reaction cross-section data of D. K. Mc Daniels *et al.* [15] decreases sharply and remain almost constant up to14 MeV. At neutron energy of 9.85 MeV, the data of H. Naik *et al.* [88] is comparable to the data of D. K. Daniels *et al.* [83]. At neutron energy of 17 MeV, the

^{238}U(n, γ)^{239}U reaction cross-section data of Yu. G. Panitkin *et al.* [16, 17] and V. A. Tolstikov *et al.* [103] increase sharply and thereafter remain constant up to 20 MeV. Within neutron energy of 6.18-20 MeV, the ^{238}U(n, 2n)^{237}U reaction become the predominant mode besides (n, γ) and (n, f) reaction of ^{238}U. It can be seen from Refs. [88-93] that the increase of ^{238}U(n, 2n)^{237}U reaction cross-section is very sharp from the neutron energy of 6.18 MeV to 7-8 MeV and then remains constant up to 13-14 MeV. Thereafter, it decreases with increase of neutron energy due to opening of other channels such as (n, 2nf) and (n, xn) reactions.

From the above observations it is clear that there are three different trends in the ^{238}U(n, γ)^{239}U and ^{238}U(n, 2n)^{237}U reaction cross-sections data within the neutron energy of 0.1-20 MeV [37-71 75-106]. However, for ^{238}U(n, 2n)^{237}U reaction, the cross-sections data [88-101] follow a smooth trend without the break up. On the other hand, the ^{238}U(n, γ)^{239}U reaction cross-section data [67-88] have a sharp fall around neutron energy of 7 MeV and sudden rise around neutron energy of 16 MeV. In order to examine this aspect, it is important to determine the ^{238}U(n, γ)^{239}U reaction cross-section around these energies regions in spite of the availability of sufficient data in the literature [67-88]. In view of the above facts, in the present work we have experimentally determined the ^{238}U(n, γ)^{239}U and U^{238}U(n, 2n)^{237}U reaction cross-section at average neutron energies of 13.5 and 17.28 MeV using the neutron beam in ^{7}Li(p, n) reaction and by activation technique followed by off-line γ-ray spectrometry.

3.5 Experimental procedure

3.5.1 Description of the experiment

The 14UD BARC-TIFR Pelletron facility at Mumbai, India [55] was used to carry out the

present experiment. The proton beam main line at 6 m height above the analyzing magnet of the Pelletron facility was utilize to obtained the neutron beam by using the $^{7}Li(p, n)^{7}Be$ reaction. The proton energies of the experiment were 16 and 20 MeV, respectively. The energy spread for proton beam was maximum 50-90 keV. A collimator of 6 mm diameter was used before the Li target to avoid the energy spread of the proton beam. The lithium foil used for neutron production was made up of natural lithium with thickness of 3.7 mg/cm^2, sandwiched between two tantalum foils of different thickness. The front tantalum foil facing the proton beam has a thickness of 3.9 mg/cm^2, in which degradation of proton energy is only 30 keV. On the other hand the back tantalum foil has a thickness of 0.025 mm, which is sufficient to stop the proton beam. Behind the Ta-Li-Ta stack, the samples used for irradiation were placed.

The samples consist of natural U metal foil, wrapped with 0.025 mm thick super pure aluminum foil of purity 99.999%. The aluminum wrapper was used as a catcher to stop fission products recoiling out from the ^{238}U metal foil during irradiation. The size of ^{238}U metal foil was 1.0 cm^2 with thickness of 29.3 mg/cm^2. The Uranium sample wrapped with Al was mounted at zero degree with respect to the beam direction at a distance of 2.1 cm from the location of the Ta-Li-Ta stack. A schematic diagram of Ta-Li-Ta stack and sample is described in chapter two (Fig. 2.7). Different sets of Ta-Li-Ta stacks and uranium samples along with aluminum wrapper were used for different irradiations at various neutron energies.

The uranium sample along with aluminum wrapper was irradiated by the neutrons generated by impinging the proton beam on the lithium metal foil through the thin tantalum foil of the Ta-Li-Ta metal stack. In the first set, the irradiation time was 7 h for

neutron beam corresponding to the proton beam energy of 16 MeV. In the second set, the irradiation time was 6 h for neutron beam corresponding to the proton beam energy of 20 MeV. The proton current during the irradiations varied from 300-400 nA. For the proton energies of 16 and 20 MeV, the corresponding maximum neutron energies faced by Uranium sample targets were 13.5 and 17.28 MeV, respectively. After irradiation, the samples were cooled for sufficient time (6-24 h). Then the irradiated Uranium target along with aluminum wrapper were mounted on different Perspex plates and taken for γ-ray spectrometry.

The γ-ray counting of the irradiated uranium samples were done using energy and efficiency calibrated 80 cm^3 HPGe detector connected to a PC based 4K channel analyzer as mentioned before. The resolution of the detector system during counting was 2.0 keV at the 1332.0 keV of ^{60}Co. The γ-ray counting of the samples were done up to few months to check the half-life of the nuclides of interest. A typical γ- ray spectrum for irradiated ^{238}U sample for $^{238}U(n, \gamma)^{239}U$ and $^{238}U(n, 2n)^{237}U$ reactions are given in Fig. 3.2.

3.5.2 Calculation of Neutron Flux

Flux monitoring is important for the measurement of reaction cross section. Here the experimental flux has been reported at two different neutron energy ranges.

a. For the incident neutron energy less than 5 MeV

Production of radioactive nuclei is described by(Section 1.3)

The disintegration rate of produced radionuclide at the end of irradiation time (t_{irr}) is given by

$$A(t_{irr}) = N(t_{irr})\,\lambda = N_0 R\,[\,1 - \exp(-\lambda t_{irr})\,] \qquad (3.2)$$

This equation can be written in more simplified form as:

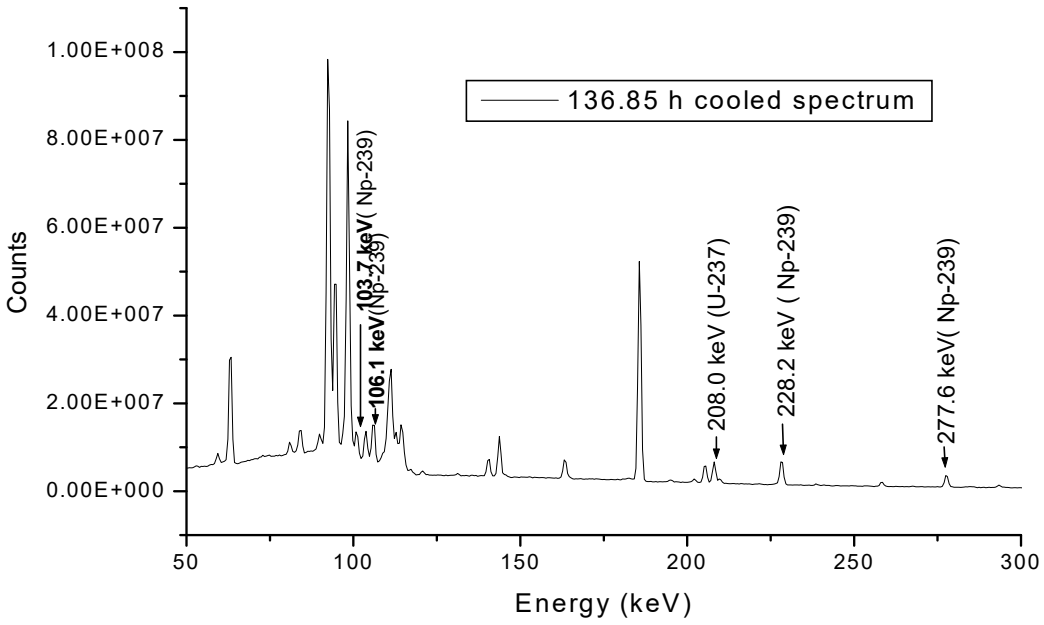

Fig. 3.2 Gamma Spectrum of for $^{238}U(n, \gamma)^{239}U$ and $^{238}U(n, 2n)^{237}U$ reactions

This equation can be written in more simplified form as:

$$A = N \sigma \varphi [\ 1 - \exp(-\lambda t_{irr})\ ] \qquad (3.3)$$

After a delay of time t_d

$$A = N \sigma \varphi [\ 1 - \exp(-\lambda t_{irr})\ ]\exp(-\lambda t_d) \qquad (3.4)$$

For a counting time of t_c

$$A = N \sigma \varphi [1 - \exp(-\lambda t_{irr})]\exp(-\lambda t_d)\ [1 - \exp(-\lambda t_c)] \qquad (3.5)$$

A = number of decays per second (Activity)

From the peak area, the number of detected γ-ray($A_{obs})_i$ at 336.2 keV γ-ray were obtained after subtracting the linear Compton background. The gamma line at 336.2 keV comes

out from the $^{115}In(n, n')^{115m}In$ reaction. The flux (Φ) is determination by the standard decay equation.

$$(A_{obs})_i = N\sigma \Phi a\varepsilon (1-e^{-\lambda t}) e^{-\lambda T} (1-e^{-\lambda \Delta T}) /\lambda \qquad (3.6)$$

Where N is the number of target atom, σ is the $^{115}In(n, n')$ cross section,' t', T and ΔT are irradiation, cooling and counting time respectively. 'a' is the abundance of γ-ray, 'ε' is efficiency of the γ-ray in the detector system.

The neutron flux at average neutron energy of 3.12 MeV was obtained to be (1.172 ±0.16) x 10^8 n cm^{-2} s^{-1}. This formula is used for E_n less than 5 MeV. For neutron energy less than 5MeV the neutrons generated in $^7Li(p,n)^7Be$ are mono energetic. The typical gamma ray spectrum for the irradiated Indium foil in shown in Fig. 3.3.

b. For neutron energy greater than 10 MeV

The neutron flux was calculated using the yield (Y) of fission products such as ^{97}Zr, extracted from the experimental yields of Refs. [102,104,110] assuming that the yields of asymmetric fission products in the fast neutron induced fission of ^{238}U does not change significantly with neutron energy. The neutron flux becomes,

$$\phi = \frac{A_{obs}\,(CL/LT)\,\lambda}{N\sigma_f Ya\varepsilon(1-e^{-\lambda t})(e^{-\lambda T})(1-e^{-\lambda CL})} \qquad (3.7)$$

Where, N = number of target atoms,

$\sigma_{f(E)}$ = fission cross-section as a function of neutron energy (E) of ^{232}Th / ^{238}U

a = branching intensity

ε = efficiency of the detector system for the γ-ray of the fission product.

Y = Yield of the fission product

φ = Neutron flux

λ = Decay Constant

t = irradiation time

T = cooling time

CL = clock time of counting

LT = Live time of counting

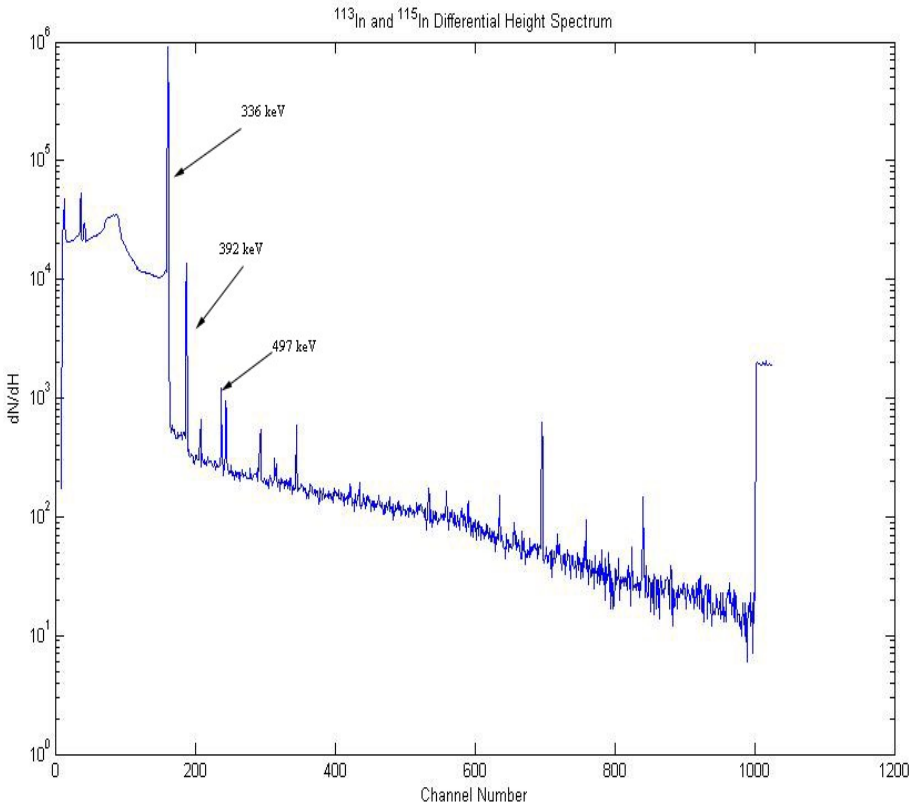

Fig. 3.3 Typical gamma-ray spectrum of irradiated indium foil

At average neutron energy of 13.5 and 17.28 MeV, the neutron flux calculated using Eq. (1) comes out to be (7.87± 0.12) x10^6 n cm^{-2} s^{-1} and (9.16±0.17) x10^7 n cm^{-2} s^{-1}, respectively. Folding the neutron spectrum of Fig. 3.4 and Fig. 3.5 [100,108] with ^{238}U(n, f) cross section [109] at different neutron energies gives average fission cross-

section. In ^{nat}U target, the percentage of ^{23}U is 0.7%. The fission cross-section of ^{235}U and ^{238}U at high neutron energy are comparable i.e. around 1-2 b. Based on these cross-sections, the contribution to $^{nat}U(n, f)$ from the $^{235}U(n, f)$ at higher neutron energy is around 1% and thus its effect is negligible.

3.6Calculation of average neutron energy (<E>)

In the present experiment, the incident proton energies used were 16 and 20 MeV. Neutrons are generated by the $^{7}Li(p, n)^{7}Be$ reaction. However, different reaction takes place when the proton beam hits the natural lithium target. Natural lithium consists of isotopes ^{6}Li and ^{7}Li with abundances 7.42 % and 92.58 % respectively. The degradation of the proton energy on the front thin tantalum foil of 3.9 mg/cm^2 thickness is only 30 keV. The Q-value for the $^{7}Li(p, n)^{7}Be$ reaction to the ground state is -1.644 MeV, where as for the first excited state is 0.431 MeV above the ground state leading to an average Q-value of -2.075 MeV. The ground state of ^{7}Be is having the threshold of 1.881 MeV, whereas the first excited state of ^{7}Be is having the threshold of 2.38 MeV. With ^{7}Li, a second neutron group at $E_P \geq 2.4$ MeV is produced due to the population of the first excited state of ^{7}Be. Thus for the proton energy of 16 and 20 MeV, the corresponding first group of (n_0) neutron energies are 14.12 and 18.12 MeV to the ground state of ^{7}Be. For the first excited state of ^{7}Be, the neutron energy of the second group of neutrons (n_1) will be 13.62 and 17.62 MeV, respectively. Fragmentation of $^{7}Li(p, \gamma)^{8}Be^{*} \rightarrow {}^{4}He+{}^{3}He+n$ (Q= -3.23 MeV) also occurs when the proton energy exceeds the value 4.5 MeV and the other reaction channels are open to give continuous neutron distribution besides n_0 and n_1 groups of neutrons.

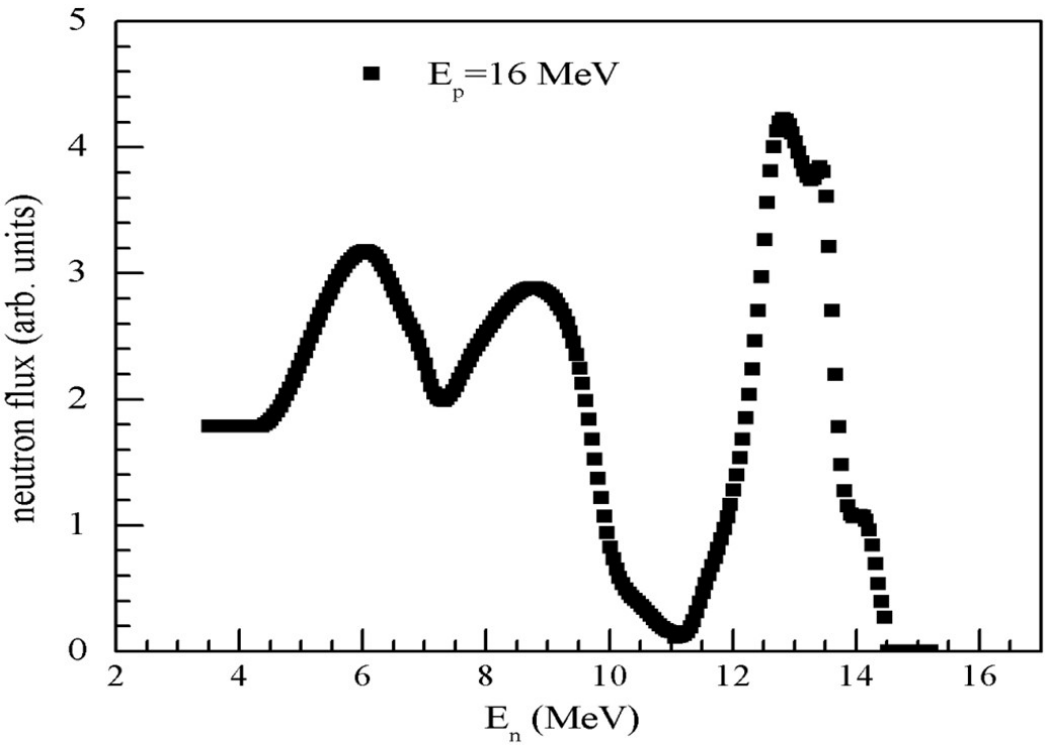

Fig. 3.4 Neutron spectrum from ^{7}Li(p, n) reaction at Ep=16.0 MeV calculated using the results of C.H. Poppe et al., and Meadows and Smith [97,100,108].

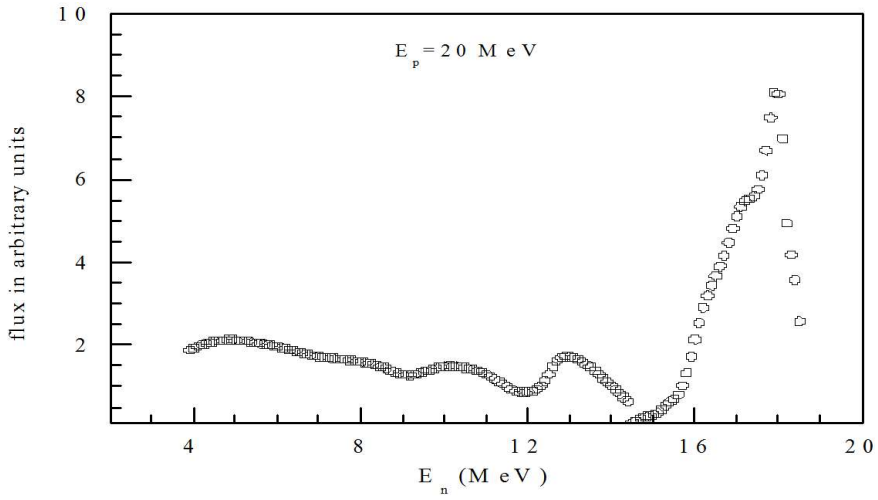

Fig. 3.5 Neutron spectrum from ^{7}Li(p, n) reaction at Ep=20.0 MeV calculated using the results of c. h. Poppe et al., and Meadows and Smith [97,100,108].

The branching ratio to the ground and first excited state of ^{7}Be up to proton energy of 7 MeV are given in the Refs. [110, 100], whereas for the proton energies from 4.2 MeV to 26 MeV are given in the Ref. [98]. For the proton energies of 16 and 20 MeV, the neutron energy spectra continue to lower energy one besides n_0 and n_1 group of neutrons. To observe the trend of continuous neutron spectrum, we have generated [Fig. 3.4, Fig. 3.5] by using the neutron energy distribution given in Refs. [97,100,108,110]. These distributions are obtained by shifting the peak by -0.5 MeV. So for the proton energies of 16 and 20 MeV the peak of the neutron energies distribution are around 14.12 and 18.12 MeV (this scaling has been done due to the fact that the maximum neutron energy from ^{7}Li(p, n) reaction cannot exceed (E_P -1.88) MeV). Based on the prescription given in refs.[97,100,108-110]for the proton energy of 16 MeV, the contribution to the n_0 and n_1 group of neutrons should be around 72% and 28% of flux under quasi monoenergtic peak respectively for a very thin ^{7}Li target, these flux distributions contain smearing in proton energy in thicker target and gives a continuous distribution instead of two separate peaks, which may not show sharp peaking at n0 and n1 groups. Therefore at proton energy of 16 MeV using the neutron distribution given in Fig.3.4, the average energy of these two n0 and n1 groups of neutrons (not considering the tailing distribution below) leads to an average neutron energy of 13.96 MeV MeV. Similarly for the proton energy of 20 MeV, the contributions to n_0 and n_1 group of neutrons are 73% and 27%, respectively, leads to an average neutron energy of 17.86 MeV. Thus after removing the tailing distribution, the average neutron energies (<E>) under the main peak region were obtained as 13.50 ± 0.35 and 17.28 ± 0.35 MeV for the proton energy of 16 and 20 MeV, respectively.

3.7 Determination of $^{238}U(n, \gamma)^{239}U$ and $^{238}U(n, 2n)^{237}U$ reaction cross-sections

The $^{238}U(n, \gamma)$ reaction cross-section (σ) was calculated from the 277.9 keV γ-rays activities (A_i) of the reaction product ^{239}Np ($T_{1/2}$ = 2.355 d) measured after sufficient cooling time.

Table 3.1 Nuclear spectroscopic data used for the cross sections and flux calculation

S.No	Nuclide	Half-life	γ-ray energy (keV)	γ-ray abundance (%) *
1	^{115m}In	4.49 h	**336.2**	**45.9**
2	^{239}U	23.54 m	74.7	52.2
3	^{237}U	6.75 Days	**208.0**	**21.2**
4	^{239}Np	2.355d	103.7	23.9
			106.1	22.7
			228.2	10.7
			277.9	**14.2**
5	Zr-97	16.9 h	**743.3**	**92.8**

*The photo-peak activities of the γ-ray energies marked in bold letters are used in the calculation.

This is because in the $^{238}U(n, \gamma)$ reaction, the half-life of ^{239}U (23.54 min.), which decays 99.6% to ^{239}Np within 3 h of cooling (Table 3.1). For the calculation of $^{238}U(n, \gamma)^{239}U$ and $^{238}U(n, 2n)^{237}U$ reactions cross-sections, the nuclear spectroscopic data used in the present work, are taken from the Refs. [105,111] and are given in Table 3.1. It can be seen from Table 3.1 that the reaction product ^{239}U has the half-life of 23.54 minutes within 3 hours, it decays 99.6% to its daughter product ^{239}Np having a half-life of 2.355 days. In the present experiment, since the cooling time of the irradiated samples were 6-24 hours, more than 99.6% of ^{239}U has decays to its daughter product ^{239}Np. Thus the $^{238}U(n, \gamma)^{239}U$ reaction cross-section (σ) can be calculated from the γ-ray activity of ^{239}Np

measured after sufficient cooling time (6-24 h). For the calculation of the $^{238}U(n, 2n)^{237}U$ reaction cross-section, the γ-ray activity of ^{237}U was used after 24-48 hours. In the calculation of $^{238}U(n, \gamma)^{239}U$ and $^{238}U(n, 2n)^{237}U$ reaction cross-sections, the self absorption of the γ-ray energy within the sample was taken care. The net area of the full energy photo-peak (A_{net}) for the γ-lines of ^{237}U and ^{239}Np are obtained by using PHAST [111] fitting program. The net photo-peak (A_{net}) for the γ-lines of ^{237}U and ^{239}Np is related to the cross-sections (σ) for the $^{238}U(n, \gamma)^{239}U$ and $^{238}U(n, 2n)^{237}U$ reactions with the following equation:

$$\sigma = \frac{A_{obs}\,(CL/LT)\,\lambda}{N\phi a\varepsilon(1-e^{-\lambda t})(e^{-\lambda T})(1-e^{-\lambda CL})} \quad (3.8)$$

All terms in Eq. (3.8) have the similar meaning as in the Eq. (3.7).

At average neutron energy of 13.5 MeV, the neutron flux (Φ) of (7.87±0.12) $x10^6$ and (6.69±0.14) $x10^6$ n cm^{-2} s^{-1} were used in Eq. (3.8) to calculate the $^{238}U(n, \gamma)^{239}U$ and $^{238}U(n, 2n)^{237}U$ reaction cross-sections, which are 1.992±0.08 and 1516.75±105.98 mb, respectively. Similarly, at average neutron energy of 17.28 MeV the neutron flux (Φ) of (9.16±0.17) $x10^7$ and (6.96±0.18) $x10^7$ n cm^{-2} s^{-1} were used for the calculation of $^{238}U(n, \gamma)^{239}U$ and $^{238}U(n, 2n)^{237}U$ reaction cross-sections, which are 1.276±0.07 mb and 1001.58±25.6 mb, respectively.

It can be seen from Fig.3.4 and Fig.3.5 that there is substantial contribution to the neutron flux from the tail region at the proton energy of 16 and 20 MeV, respectively.

Thus for $^{238}U(n, \gamma)^{239}U$ reaction, the low energy neutrons also contribute to the cross-section. In view of this the contribution from the tail region to $^{238}U(n, \gamma)^{239}U$ reaction has been estimated by using the evaluated nuclear data file ENDF/B-VII [10] and Japanese evaluated nuclear data library JENDL-4.0 [12] by folding the cross-sections with neutron flux distributions. The contribution to the cross-section of the $^{238}U(n, \gamma)^{239}U$ reaction due to the tail part of neutron spectrum at E_P = 16 MeV are 1.325 mb and 0.972 mb from the ENDF/B-VII [10] and JENDL-4.0 [12], respectively. Similarly, at E_P = 20 MeV, the contribution to the cross-section of the $^{238}U(n, \gamma)^{239}U$ reaction due to the tail part of neutron spectrum are 0.86 mb and 0.612 mb from ENDF/B-VII [10] and JENDL-4.0 [12], respectively. The actual value of $^{238}U(n, \gamma)^{239}U$ reaction-cross section due to the neutrons from the main peak of the n_0 and n_1 groups of the neutron spectrum is obtained after subtracting the average cross-section due to neutrons from tail region from the above mentioned experimental data. Thus the actual experimentally obtained $^{238}U(n, \gamma)^{239}U$ reaction cross-sections at average neutron energies of 13.5 and 17.28 MeV corresponding to proton energy of 16 MeV and 20 MeV are 0.844±0.08 mb and 0.546±0.07 mb, which are given in Table 3.2. In a similar way, the contribution to the $^{238}U(n, 2n)^{237}U$ reaction cross-section due to the tailing part of the neutron spectrum was evaluated. These are about 497.2 mb from ENDF/B-VII.0 [10] and 493.5 mb from JENDL-4.0 [12] for the average neutron energies of 13.5 corresponding to proton energy of 16 MeV. Similarly, at average neutron energy of 17.28 MeV corresponding to proton energy of 20 MeV, these are 558.43 mb from ENDF/B-VII.0 [10] and 531.2 mb from JENDL-4.0 [12], respectively. Thus the actual experimentally obtained $^{238}U(n, 2n)^{237}U$

reaction cross-section at average neutron energy of 13.5 and 17.28 MeV from present work are 1021.37± 106 and 456.78 ±25.6 mb, which are given in Table 3.2.

3.8 Uncertainties associated with the measurements

The uncertainties associated with the measured cross-sections come from the combination of two sets of errors, systematic error and statistical error. This overall uncertainty is the quadratic sum of both random and systematic errors. The random error in the observed activity is primarily due to counting statistics of γ-ray activities of reaction products ^{239}Np from ^{238}U(n, γ) reaction and ^{237}U from ^{238}U(n, 2n) reaction, which is estimated to be 10-15%. This can be determined by accumulating the data for an optimum time period that depends on the half-life of nuclides of interest. The systematic errors are due to uncertainties in neutron flux estimation (~4%), correction in the ^{238}U(n, γ)^{239}U and ^{238}U(n, 2n)^{237}U reaction cross-sections due to the tail part of the neutron (~4%) the irradiation time (~2%), the detection efficiency calibration (~3%), the half-life of the reaction/fission products and the γ-ray abundances (~2%) as reported in the literature [78-80]. Thus the total systematic error is about ~7%. The overall uncertainty is found to range between 12 to 17%, coming from the square root of quadratic sum of a statistical error of 10-15% and a systematic error of 7%.

3.9 Results and Discussion

The measured cross sections at incident neutron energy of 3.12 MeV is shown in Fig. 3.6 The ^{238}U(n, γ)^{239}U and ^{238}U(n, 2n)^{237}U reaction cross-sections at average neutron energies of 13.5 and 17.28 MeV of present work are determined using a neutron source from ^{7}Li(p, n) reaction. Since the average neutron energies of 13.5 and 17.28 MeV were obtained from ^{7}Li(p, n) reaction at proton energies of 16 and 20 MeV, the neutron

spectrum is tailing [Fig. 3.4 and Fig.3.5]. Thus the correction to the $^{238}U(n, \gamma)^{239}U$ and $^{238}U(n, 2n)^{237}U$ reaction cross-section due to the tail part of the neutron spectrum have been incorporated, details about the tailing correction is mentioned in section 3.6 in the present chapter. Same approach has been used in the earlier work [88] for the measurement of neutron induced reaction cross-section of ^{238}U at neutron energies of 3.7 and 9.85 MeV corresponding to the proton energies of 5.6 and 12 MeV, respectively.

In order to examine the validity of the present approach, the experimentally determined $^{238}U(n, \gamma)^{239}U$ and the $^{238}U(n, 2n)^{237}U$ reaction cross-sections were compared with the evaluated data from ENDF/B-VII.0 [10], JENDL 4.0 [12], Joint evaluation fission and fusion nuclear data library JEFF-3.1/A [11] and Chinese evaluated nuclear data library CENDL-3.1 [13].

These evaluated reaction cross-sections for $^{238}U(n, \gamma)^{239}U$ reaction from ENDF/B-VII.0 [10] and JENDL 4.0 [12] are quoted in Table 3.2 for the neutron energies of 13.5 and 17.28 MeV. Similarly for the $^{238}U(n, 2n)^{237}U$ reaction, the evaluated cross-sections from ENDF/B-VII.0 [10] and JENDL 4.0 [12] in Table 3. 2 are quoted for the neutron energies of 13.5 to 17.28 MeV. It can be seen from the Table 3.2 that the present experimental $^{238}U(n, \gamma)^{239}U$ and $^{238}U(n, 2n)^{237}U$ reaction cross-sections are within the range of evaluated data of ENDF/B-VII.0 [10] and JENDL 4.0 [12], showing consistency with our present approach and experimental results. The evaluated data from JEFF-3.1/A [11] are same as of ENDF/B-VII.0 [10] and thus not shown in Table 3.2. However, the evaluated data from CENDL-3 [13] are not in agreement with the present experimental values and thus are not quoted in Table 3. 2. In Fig.3 6, and Fig. 3.7, we present a detailed study comparing our results with various evaluations and available experimental data of

the $^{238}U(n, \gamma)^{239}U$ reaction cross-sections, and also discuss inconsistencies of the available data from literature [16-18, 69-88] given in EXFOR [112] in various neutron energy regions. From Fig. 3.7, it can be seen that the $^{238}U(n, \gamma)^{239}U$ reaction cross-section from present work at 13.5 MeV is in agreement with the value of Mc Daniels et al. [15]. However, the $^{238}U(n, \gamma)^{239}U$ reaction cross-section from present work at 17.28 MeV is lower than the value of Patikin et al., [17,18]. Besides this, it can be seen from Fig.3.7 that the $^{238}U(n, \gamma)^{239}U$ reaction cross-section decreases systematically from 100 keV to 7 MeV From Fig. 3.7, it can be seen that the $^{238}U(n, \gamma)^{239}U$ reaction cross-section from present work at 13.5 MeV is in agreement with the value of Mc Daniels et al. [15]. However, the $^{238}U(n, \gamma)^{239}U$ reaction cross-section from present work at 17.28 MeV is lower than the value of Panitkin et al., [17,18]. Besides this, it can be seen from Fig.3.7 that the $^{238}U(n, \gamma)^{239}U$ reaction cross-section decreases systematically from 100 keV to 7 MeV. However, at neutron energy of 7 MeV, the data of Mc Daniels et al., [15] is suddenly lower compared to the data of Leipunskiy et al., [82] and Patikin et al., [17,18]. From the neutron energy of 7 to 15 MeV, the data of Mc Daniels et al. [15] remains almost same. Beyond neutron energy of 17 MeV, the experimental data obtained by Patikin et al. [17,18] suddenly increases and then remains almost constant up to 20 MeV. For a comparison, the data of Ding et al. [19] based on neutron activation technique from the review article were shown in Fig.3.7. Further the evaluated $^{238}U(n, \gamma)^{239}U$ reaction cross-section data from ENDF/B-VII.0 [10], JENDL-4.0 [12], JEFF-3.1/A [11], CENDL [13]

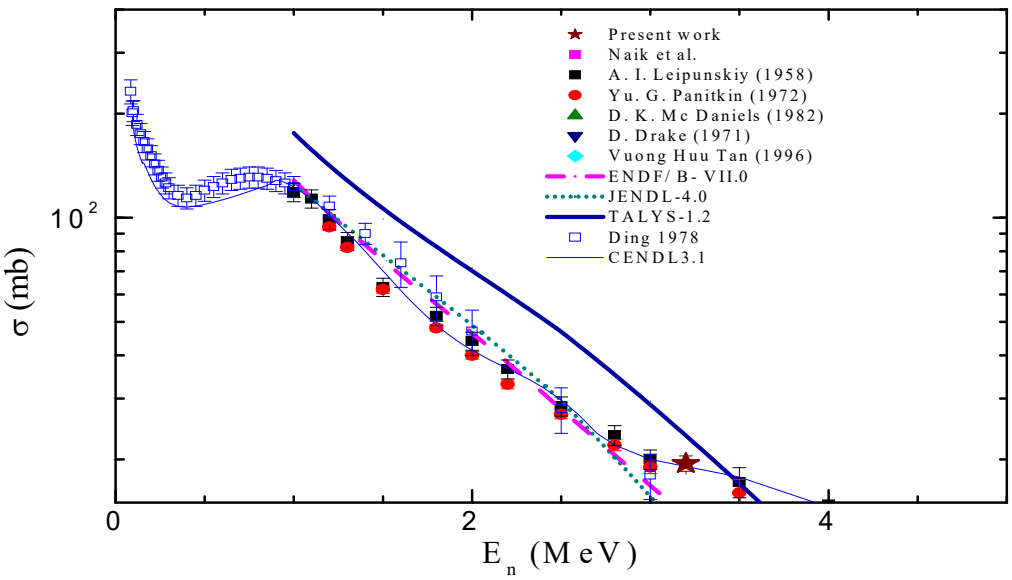

Fig. 3.6 Plot of experimental and evaluated $^{238}U(n, \gamma)^{239}U$ reaction cross-section as a function of neutron energy from 1 keV to 5MeV.Experimental value at 3.12 MeV is indicated

and INDC (VN)-8 [113] were also shown in Fig3. 7. From Fig.3 7, it can be seen that the evaluated data of CENDL [13] are in agreement with the earlier data from literature [1-7, 8, 9]. However, the evaluated data of CENDL [13] disagree with the present data and other evaluations. The trend of evaluated data from CENDL [13] is entirely different from the evaluated data from ENDF/B-VII.0 [10], JENDL-4.0 [12] and JEF-3.1/A [11]. Further, the data of Ding et al., [19] shows agreement with the present experimental data and evaluated data from ENDF/B-VII.0 [10], JENDL-4.0 [12] and JEF-3.1/A at lower energy only and significantly differ at higher energy. The experimental data of present work at 13.5 and 17.28 MeV as well as the data of Mc Daniels et al [15] at 7-15 MeV are

in good agreement with the evaluated data of ENDF-B-VII.0 [10], JENDL [12] and JEF-3.1/A [11].

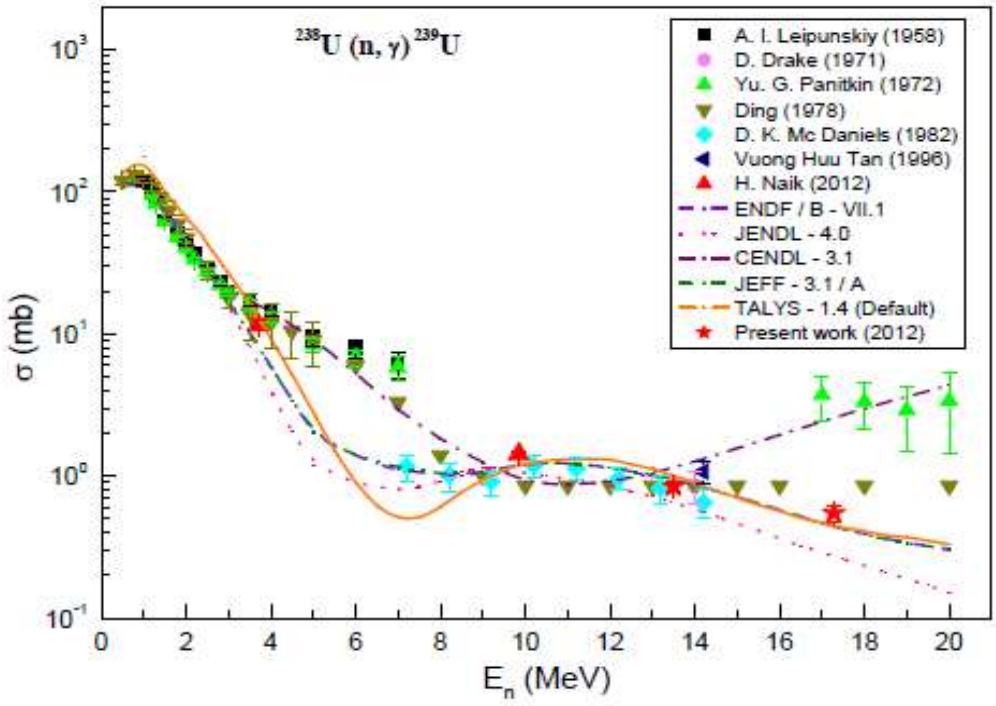

Fig. 3.7 Plot of experimental and evaluated ^{238}U(n, γ)^{239}U reaction cross-section as a function of neutron energy from 1 keV to 20 MeV. Experimental values from present work and from Refs. [16-18,72-88] are in different symbols, whereas the evaluated and theoretical values from TALYS (8,9)are in solid line of different color.

The experimental data of Leipunskiy et al. [82] and Patikin et al., [17,18] also shows a good agreement with the evaluated data [10-12] within neutron energy of 1-4 MeV. However, the experimental data of Leipunskiy et al. [82] and Panitkin et al. [17,18] at neutron energy of 5-7 MeV and of Panitkin et al., [17,18] at 17-20 MeV are higher then the evaluated data [10-12]. To examine this aspect, the ^{238}U(n, γ)^{239}U reaction cross-section within neutron energy of 1 keV to 20 MeV was also calculated theoretically using

computer code TALYS [8,9] as done earlier [88] and are shown in the Fig. 3. 7. From Fig. 3 7, it can be seen that the $^{238}U(n, \gamma)^{239}U$ reaction cross-section [10-13] obtained using TALYS computer code [8,9] reproduces the trend of evaluated data of ENDF/B-VII.0 [10], JENDL-4.0 [12] and JEF-3.1/A. However, within neutron energy of 1 keV to 3 MeV, the theoretical $^{238}U(n, \gamma)^{239}U$ reaction cross-section from TALYS are slightly higher than the experimental and evaluated values. This may be due to the use of default parameters in TALYS. However, the values from TALYS are agreeing with the value of our present work at 13.5 and 17.28 MeV as well as with the values of Mc Daniels et al., [15] at 7-14 MeV. On the other hand, the experimental values of Leipunskiy et al., [82] have a close agreement with Panitkin et al., [17,18] at neutron energy of 5-7 MeV. The measured values of Panitkin et al [17,18] at 17-20 MeV are higher than the theoretical value of TALYS code [8,9]. Higher experimental value at 5-7 MeV by Leipunskiy et al., [82] and Panitkin et al., [48] could be due to the contribution from the low energy scattered neutrons of the D+D neutron source. Similarly, the higher experimental value at 17-20 MeV by Panitkin et al., [17,18] may be due to the contribution from the low energy scattered neutron of the D+T neutron source. As also mentioned by Panitkin et al., [17,18] at low energy scatted neutrons contribute to the higher $^{238}U(n, \gamma)^{239}U$ reaction cross-section. Therefore, subtracting out the contribution (n, γ) cross section from low energy tailing neutrons is important to compare with TALYS calculations and other evaluations. In the present work we too found higher uncorrected cross-sections (Table 3.2) due to lower energy tail part in the neutron spectrum from $^{7}Li(p, n)$ reaction. Thus the contribution to the $^{238}U(n, \gamma)^{239}U$ reaction cross-section due to the low energy tail part of neutrons has been estimated and subtracted out, which has been mentioned earlier in

our calculation. As mentioned before, our experimental data agrees well with evaluations and TALYS results. Besides the above observations, the experimental [16-18, 72-88], evaluated [10-13] and the theoretical [8, 9] $^{238}U(n, \gamma)^{239}U$ reaction cross-section decreases from 100 keV to 7 MeV and predict a dip in around 6-8 MeV as shown in Fig. 3 7. The dip in the $^{238}U(n, \gamma)^{239}U$ reaction cross-section around neutron energy of 6-8 MeV indicates the opening of (n, 2n) reaction channel besides (n, nf) channel. Above 8 MeV, it increases and shows a bump up to the neutron energy of 14 MeV and then again decreases. This can be understood from the saturated $^{238}U(n, 2n)^{237}U$ reaction cross-section above 8 MeV. In order to illustrate this, $^{238}U(n, 2n)^{237}U$ reaction cross-section from the present work and literature [72-93] given in EXFOR [112] along with the evaluated data [10,12] were shown in Fig. 3.8. The $^{238}U(n, 2n)^{237}U$ reaction cross-sections at different neutron energy was also calculated theoretically using computer code TALYS [8,9] and plotted in Fig. 3.8. From Fig. 3. 8, it can be seen that the $^{238}U(n, 2n)^{237}U$ reaction cross-section from TALYS shows a close agreement with the experimental data within neutron energy of 8 MeV. Above 8 MeV, the TALYS results seem to over predict the experimental data. Further it can be seen from Fig. 3.8 that the experimental and theoretical $^{238}U(n, 2n)^{237}U$ reaction cross-sections show a sharp increasing trend from the neutron energy of 6.18 MeV to 8 MeV and there after remains constant up to 14 MeV. Thus the increasing trend of $^{238}U(n, \gamma)^{239}U$ reaction cross-section beyond 8 MeV up to14 MeV in Fig. 3.7 is due to near constant $^{238}U(n, 2n)^{237}U$ reaction cross-section observed in Fig. 3.8. It can be also observed from Fig. 3.7 and Fig. 3. 8 that the $^{238}U(n, \gamma)^{239}U$ reaction cross-section shows a dip, where the $^{238}U(n, 2n)^{237}U$ and $^{238}U(n, nf)$ reaction cross-sections show a sharp increasing trend. Similar trend of (n, γ)

and (n, 2n) reactions was seen in case of Similarly, above neutron energy of 14 MeV due to the opening of (n, 3n) and (n, 2nf) reaction channels, both $^{238}U(n, \gamma)^{239}U$ (Fig. 3.7) and $^{238}U(n, 2n)^{237}U$ (Fig. 3.8) reaction cross-sections show a decreasing trend.

3.10 Summary and conclusions

(i) The $^{238}U(n, \gamma)^{239}U$ and $^{238}U(n, 2n)^{237}U$ reaction cross-section at average neutron energies of 13.5 and 17.28 MeV are measured using a neutrons source from $^{7}Li(p, n)$ reaction. Since the neutrons are not mono-energetic, corrections in the cross sections are incorporated.

(ii) The $^{238}U(n, \gamma)^{239}U$ and $^{238}U(n, 2n)^{237}U$ reaction cross-section at average neutron energies of 13.5 and 17.28 MeV are in good agreement with the experimental data from literature and the evaluated data from ENDF/B-VII.0, JENDL-4.0 and JEFF-3.1/A but not with evaluated data from CENDL-3.

(iii) The $^{238}U(n, \gamma)^{239}U$ reaction cross-section decreases from neutron energy of 100 keV to 14 MeV with a dip at 6-8 MeV. The $^{238}U(n, 2n)^{237}U$ reaction increases sharply in the energy range from 6.18 MeV to 8.0 MeV and thereafter it remains constant up to the neutron energy of 14 MeV. Beyond neutron energy of 14 MeV both $^{238}U(n, \gamma)^{239}U$ and $^{238}U(n, 2n)^{237}U$ reaction cross-sections show decreasing trend due to opening of (n, 3n) and (n, 2nf) reaction channels.

Table 3.2 Neutron induced reaction cross section measured values for ^{238}U compared to ENDF/B-VII and JENDL-4.0

Neutron Energy	Neutron Flux n cm^{-2} s^{-1}	Cross Sections (mb)		
		Experimental	ENDF/B/VII.1	JENDL-4.0
$^{238}U(n, \gamma)\ ^{239}U$				
3.12	(1.17 ±0.16) x 10^8	19.7±0.10	16.8	15.05
13.5	(7.87±0.12) x 10^6	0.84±0.020	0.930	0.666
17.28	(9.16±0.17) x 10^6	0.54±0.070	0.460	0.277
$^{238}U(n,2n)\ ^{237}U$				
13.5	(6.06±0.14) x10^6	1021.37±0.1	1049.4	1248
17.28	(6.96±0.18) x10^6	456.78±25.6	331.43	327.9

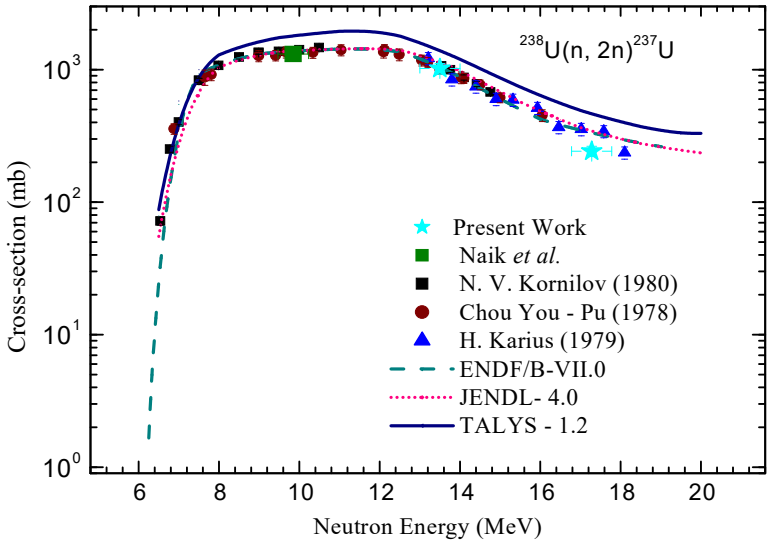

Fig. 3.8 Plot of experimental and evaluated ^{238}U(n, 2n)^{237}U reaction cross-section as a function of neutron energy for neutron energy 5 MeV to 25 MeV. Experimental values from present work and from Refs. [52-57/ 87-93] are in different symbols, whereas the evaluated and theoretical values from TALYS are in solid lines with different colors.

(iv) The ^{238}U(n, γ)^{239}U and ^{238}U(n, 2n)^{237}U reaction cross-sections were calculated theoretically using TALYS code. The TALYS results for ^{238}U(n, γ)^{239}U reaction cross-section over predict the experimental data within the neutron energy of 1 keV to 3 MeV and there after it is in agreement with the experimental data. However, the TALYS results for ^{238}U(n, 2n)^{237}U reaction cross-sections are in good agreement with the experimental data up to 8 MeV and thereafter over predict the experimental data.

CHAPTER 4

^{232}Th (n, γ) reaction cross-section at average neutron energies of 2.8, 3.12, 13.5, 15.5 and 17.28 MeV) and ^{232}Th (n, 2n) reaction cross-section at average neutron energy of 17.28 MeV

In this chapter results on ^{232}Th (n, γ) reaction cross-section measurements at average neutron energies of 2.8, 3.12 13.5, 15.5 and 17.28 MeV are reported. Neutrons were generated using ^{7}Li(p, n)^{7}Be reaction. These reaction cross sections in above energies have been determined for the first time using activation and off-line γ -ray spectrometric technique. The ^{232} Th(n, 2n) cross-section at 17.28 MeV neutron energy has also been determined using activation and off line gamma spectroscopic technique. The experimentally determined ^{232}Th(n, γ) and ^{232}Th(n, 2n) reaction cross-sections from the present work have been compared with the ENDF/BVII and JENDL-4.0 evaluated data and are found to be in good agreement. The present data, along with literature data in a wide range of neutron energies, were interpreted in terms of competition between different reaction channels of ^{232} Th(n, γ), (n, f), (n, n f) and (n, xn). The ^{232}Th(n, γ) and ^{232}Th(n, 2n) reaction cross-sections were also calculated theoretically using the TALYS computer code and were found to be in good agreement with the results obtained out of the present experiment but were slightly higher than the literature data at lower neutron energies.

4.1 Motivation behind the measurement of neutron induced reaction cross-section of ^{232}Th

The design of a hybrid reactor (ADSs) and even that of a demonstrator, as well as the study of the thorium cycle potentialities require the knowledge of a wide range of nuclear cross section data. Today, sufficient data are available for nuclei involved in the

uranium cycle, but for those involved in the thorium cycle and for high neutron energies the situation is not satisfactory. The experimental data are very scarce. Often discrepancies exist between evaluated data, and the data often fed by model predictions. For fission and capture cross sections of actinide nuclei, the variation is generally fairly small. For the (n, xn) reactions, the average discrepancy is relatively large. Due to the recent interest in ADS, a need has arisen for precise nuclear data of materials of the core, spallation target and structure materials of a hybrid system. These measurements should contribute to better evaluated data, but since all reactions cannot be measured, they should also provide adequate constraints on nuclear reaction models like the intra-nuclear cascade or the pre equilibrium model.

^{232}Th(n, xn) reactions which do not play a crucial role in classical reactors except for x=1 because of their high energy threshold, which increases with increasing x value, become more important in fast reactors and even more in hybrid systems. Indeed they participate to the neutron multiplication in the spallation target (Pb/Bi). Fast neutrons can also escape from the target, and reach the core and then interact with fuel materials by (n,xn) reactions. Their role is also important if we consider the thorium cycle. Indeed the ^{232}Th (n,2n) reaction produces ^{231}Th, which decays to ^{231}Pa that can dominate the radio-toxicity in some scenarios of fuel reprocessing. Another example concerns the ^{233}U(n,2n) reaction which leads to ^{232}U and which decays, after several α and β emissions, on the excited states in ^{208}Pb. This last nucleus decays by emitting a high energy (2.6 MeV) γ ray that makes the fuel fabrication more complicated. Nuclear reactors which will be using thorium as part of the fuel are, advanced heavy water reactors (AHWR) [4] and fast reactors [2] Recently, accelerator-driven sub-critical system (ADSS) [5,114-118] are

also of primary interest from the point of transmutation of long-lived fission products (^{93}Zr, ^{99}Tc, ^{107}Pd, ^{129}I and ^{135}Cs), and incineration of long-lived minor actinides(^{237}Np, ^{240}Pu, ^{241}Am, ^{243}Am and ^{244}Cm) to solve the problem of radioactive wastes. In AHWR, ^{232}Th–^{233}U is the primary fuel for power generation. The advantage of ^{232}Th–^{233}U fuel in AHWR [4] and ADSS [5, 114-118] over the present reactors based on uranium fuel is that it produces thousand times less radiotoxic wastes. Studies have shown that thorium-based fuels in fast spectrum systems can efficiently perform the task of reducing plutonium.

However, ^{232}Th–^{233}U fuel in combination with ADSS is another method for power generation besides for transmutation of long-lived fission products and incineration of long-lived minor actinides. an acceptable safety and control characteristics of the reactor system. Besides these, thorium in the Earth's crust is three times more abundant than uranium and thus can greatly extend the nuclear fuel resources. It is a fact that ^{232}Th is the only nucleus present in nature which give rise to an excess of fissile material ^{233}U in the presence of either thermal or fast neutrons, thus making it an excellent choice for nuclear fuel of the future. Furthermore, thorium based fuel is an attaractive option because no transuranics are produced compared to uranium based fuel, this reduces cost of fuel cycle. In the thorium-uranium fuel cycle the fissile nuclide ^{233}U is generated by the capture reaction ^{232}Th (n, γ) ^{233}Th followed by two beta decay A schematic diagram of the Th–U fuel cycle is given in Fig. 4.1.Thus, the production of the fissile nucleus ^{233}U depends on the ^{232}Th(n, γ) reaction cross-section, which is required with an accuracy of 1–2% for predicting the dynamical behavior of complex arrangements in fast reactors or ADSs [5,114-119]. In fusion–fission hybrid systems, a sensitivity study has shown that

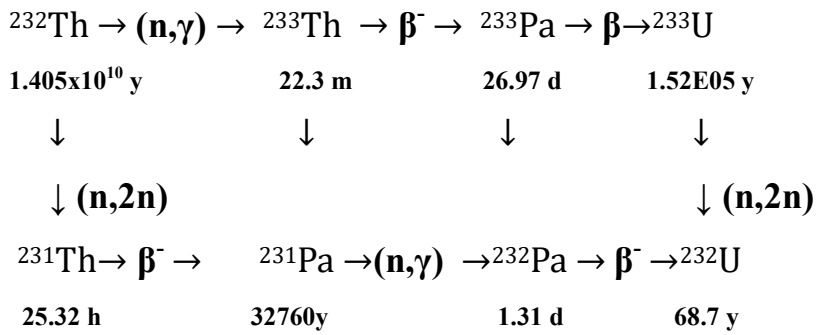

Fig. 4.1 A schematic diagram of (n, γ) and (n, 2n) reaction of ^{232}Th followed beta decay in the Th-U fuel cycle.

the production rate of ^{233}U can be predicted within 1%, provided the ^{232}Th(n, γ) cross-section is known within 2% [119,120]. Thus, the neutron interactions and fission cross-sections for ^{232}Th and ^{233}U in the low neutron energy are important for AHWR [4], whereas the neutron interactions and fission cross-sections in the higher energy range are important for ADSS [5,114-118] because they dominate the neutron transport and neutron regeneration. Thus, the ^{232}Th(n, γ) reaction cross-section at higher neutron energy has a strong impact on the performance and safety assessment for ADSS [5, 114-118]. In ADSS a 10% change in the ^{232}Th neutron capture cross section gives rise to a 30% change in the needed proton current of the accelerator if the system has to be operated at a sub-critical level of $K_{\text{eff}} \approx 0.97$ [121]. Thus, precise nuclear reaction cross-section data are important for the nuclear and shielding design of AHWR and ADSs. However, the database and experience of thorium fuels and the thorium fuel cycles are very limited compared to other conventional fuels. A careful look at the nuclear cross-section data, available in the existing cross-section libraries shows that, ^{232}Th(*n, γ*) reaction cross-section within neutron energies of thermal to 2.73 MeV which are based on physical measurements [115,122] and activation technique [123-133,134]. Beyond 2.73 MeV, the ^{232} Th(*n, γ*

)reaction cross-section data are available only at 3.7 and 9.85 MeV (Naik *et al* [136] and at 14.5 MeV (Perkin *et al* [133]) using the activation technique. From these data, it can be seen that the ^{232}Th(*n, γ*) reaction cross section decreases monotonically from 20 eV to 3.7 MeV. Beyond the neutron energy in the range of 6–7 MeV, ^{232}Th(*n, γ*) reaction cross-section increases and remains flat within 9.85–14.5 MeV [138,139]. It can also be seen from Refs. [133,136] that the ^{232}Th(*n, γ*) reaction cross-section at 14.5 MeV is higher than the expected trend. At neutron energy higher than 6.44 MeV, ^{232}Th(*n, 2n*) reaction begins and becomes the predominant mode besides fission and inelastic reaction channels, which are already significant above neutron energy of 1 MeV. In contrast to ^{232}Th (*n, γ*) reaction cross-section data, sufficient data on ^{232}Th(*n, 2n*) reaction are available from physical measurements [137] and from off-line activation methods [137–142]. However, the present literature data of ^{232}Th (*n, 2n*) reaction cross-sections [69-83,120] are within 11 MeV neutron energy. It can be seen from these data that the ^{232}Th (*n, 2n*) reaction cross-section increases from neutron energy of 6.44 MeV up to the neutron energy of 9.86 MeV and then remains constant up to 11 MeV. Keeping these facts in mind, it is important to measure the reaction cross-sections ^{232}Th(*n, γ*) and (*n, 2n*) besides the yields of fission products at higher neutron energy.

In the present work, we have determined the ^{232}Th(*n, γ*) reaction cross-section at average neutron energies of 2.81, 3.12 ,13.5, 15.5 and 17.28 MeV using the neutron beam from ^{7}Li(*p, n*) reaction and by activation followed by off-line *γ* -ray spectrometry. The reaction cross section ^{232}Th(*n, 2n*) ^{231}Th is also determined at an average neutron energy of 17.28 MeV using the same technique. The neutron interaction cross-sections in the energy range 14–18 MeV are of fundamental importance for fission and accelerator

driven reactors because they dominate the neutron transport and neutron regeneration. The present data along with literature data at different neutron energies, are interpreted from the point of view of (n, f), (n, nf), $(n, 2nf)$ and (n, xn) reaction thresholds.

4.2 Description of the experiment

The data concerning (n,xn) reactions are scarce because of the difficulty to measure their cross section. Though different techniques are available for the measurement but the most common among them is the activation method. The experiment was carried out at 14UD BARC-TIFR Pelletron Facility at Mumbai, India [64]. The experimental set up is similar to what is mentioned in chapter 2 and chapter 3. Thorium foil was wrapped with 0.025 mm thick super pure aluminum foil and mounted at zero degree with respect to the beam direction at a distance of 2.1 cm from the location of the Ta–Li–Ta stack.

The experimental arrangement is shown in figure 2.6. The isotopic abundance of ^{232}Th in natural thorium is 100%. Different sets were made for different irradiations at various neutron energies. For the measurements at the neutron energy of 2.18 MeV and 3.12 MeV Indium foils were also irradiated along with the thorium foils as flux monitors. For neutron energies greater than 10 MeV only thorium foils were irradiated because fission products are taken as the flux monitors. The samples were irradiated for 5–7 h depending on the proton beam energy. The proton beam energies were 5.8, 6.1,16,18 and 20 MeV and the proton current during the irradiation was within 300–400 nA. The maximum incident neutron energies on thorium targets were 2.8, 3.12, 14.1, 16.1 and 18.1 MeV respectively. After irradiation, the samples were cooled for few hours (6–24 h). Then the irradiated target of thorium along with Al wrapper were mounted on different Perspex plates and taken for γ -ray spectrometry. The γ -ray counting of reaction products

from the irradiated thorium was done using the same set up as shown in Fig. 2.6. The γ-rays of fission products from the irradiated ^{232}Th sample were counted in an energy and efficiency calibrated 80 cc. HPGe detector coupled to a PC-based 4K channel analyzer (set up mentioned in chapter 2 and chapter 3) . A typical γ -ray spectrum from the irradiated ^{232}Th sample for ^{232} Th(n, γ) and ^{232}Th(n, 2n) reactions are given in figures 4.1 and 4.2 respectively.

4.3 Data Analysis

4.3.1 Calculation of the neutron energy

The incident proton energies in the present experiment were 5.8, 6.1, 16, 18 and 20 MeV respectively. The maximum incident neutron energies on thorium targets were 2.8, 3.12,.13.5, 15.5, 17.28 respectively. Neutrons are generated by the ^{7}Li (p, n) reaction. The effective energies were calculated following the procedure mentioned in Chapter 3.

4.3.2 Estimation of the neutron flux

For higher mono-energetic neutrons up to 5 MeV, the photo peak activity of the 336.2 keV γ -line of ^{115m}In from the ^{115}In(n, n') reaction is used for flux determination. Because, neutron-induced fission cross-section of ^{232}Th [120] is a step function, where as the fission yields of fission products [121,122] at peak position of the mass-yield curve do not change significantly, the neutron flux [22] at neutron energies greater than 5 MeV were calculated using the yield (Y) of fission products as ^{131}I, ^{132}Te and ^{97}Zr, extracted from the experimental yields of Refs. [122,123] in the neutron induced fission of ^{232}Th. The neutron flux and the observed photo-peak activities (A_{obs}) for γ -lines of the respective nuclide are related by the equation 4.1.

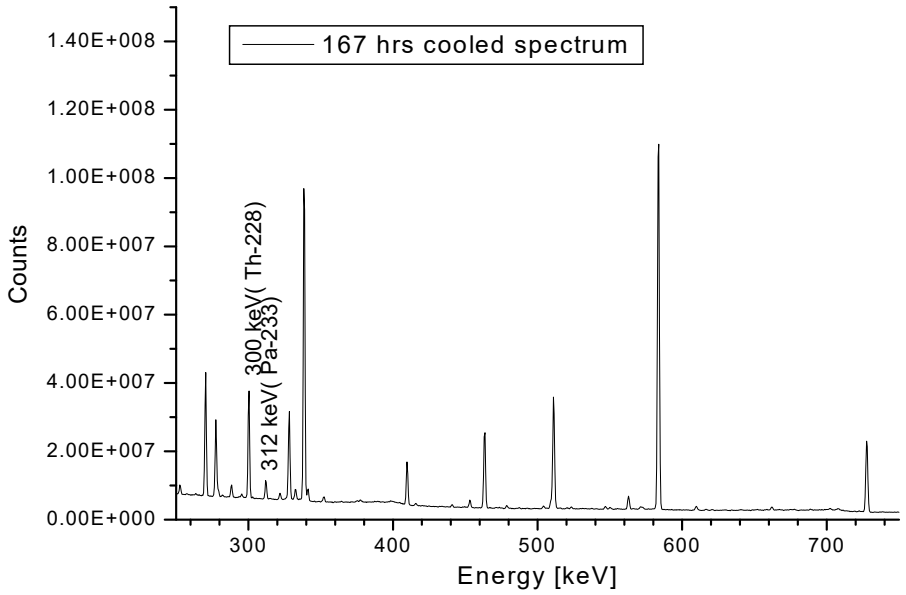

.

Fig .4.2 A typical γ -ray spectrum from the irradiated ^{232}Th sample.

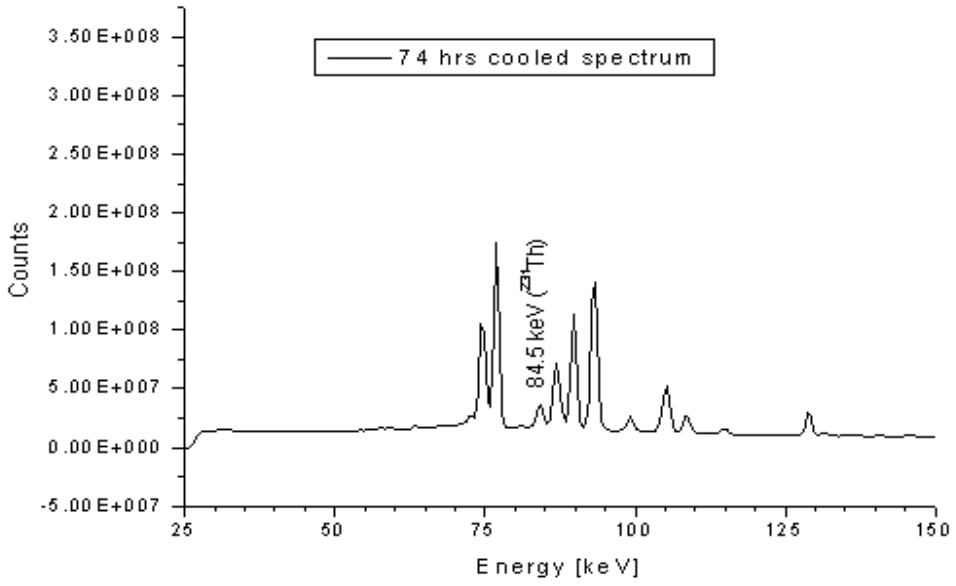

.

Fig. 4.3 A typical γ -ray spectrum from the irradiated ^{232}Th sample**.**

a. For the incident neutron energy less than 5 MeV

From the peak area,the number of detected γ-ray($A_{obs})_i$ at 336.2 keV γ-ray were obtained after substracting the linear Compton background. The gamma line at 336.2 keV comes out from the $^{115}In(n, n')^{115m}In$ reaction. The flux (Φ) is determination by the standard decay equation.

$$(A_{obs})_i = N\sigma \Phi a\varepsilon (1-e^{-\lambda t}) e^{-\lambda T} (1-e^{-\lambda \Delta T}) /\lambda \qquad \textbf{(4.1)}$$

where N is the number of target atom, σ is the $^{115}In(n, n')$ cross section , 't', T and ΔT are irradiation, cooling and counting time respectively. 'a' is the abundance of γ-ray, 'ε' is efficiency of the γ-ray in the detector system,

The neutron flux at average neutron energy of 3.12 MeV was obtained to be (1.172 ±0.16) x 10^8 n cm^{-2} s^{-1}. This formula is used for E_n less than 5 MeV. The typical gamma ray spectrum for the Indium foil in shown in Fig 3.2

b.For neutron energy greater than 10 MeV

The neutron flux was calculated using the yield (Y) of fission products such as ^{97}Zr, extracted from the experimental yields of Refs. [102, 104] assuming that the yields of asymmetric fission products in the fast neutron induced fission of ^{232}Th does not change significantly with neutron energy. The equation used for such calculation is as follows. The γ -ray energies and the nuclear spectroscopic data such as the half-lives and branching ratios of the reaction products are taken from Refs. [102,104] and given in Table-4.1

$$\phi = \frac{A_{obs}\,(CL/LT)\,\lambda}{N\sigma_f Ya\varepsilon(1-e^{-\lambda t})(e^{-\lambda T})(1-e^{-\lambda CL})} \qquad \textbf{(4.2)}$$

Where,

N= Number of target atoms,

Y= Yield of the fission product [102,104]

$\sigma_f(E)$ = Fission cross-section as a function of neutron energy (E) of $^{232}Th/^{238}U$ [102,104],

a = branching intensity and ε = efficiency of the detector system for the γ-ray of the fission product. [102,104]

φ = Neutron flux

λ= Decay Constant

t = irradiation time,

Tc = cooling time

CL = clock time of counting

LT = live time of counting.

4.4 Determination of ^{232}Th (n, γ) ^{233}Th and ^{232}Th(n, 2n) ^{231}Th reaction cross-sections

The radioactive products such as ^{233}Th and ^{233}Pa were produced from ^{232}Th(n, γ) reaction followed by beta decay. Similarly, the radioactive product ^{231}Th was produced from the ^{232}Th (n, 2n) reaction. For the calculation of ^{232}Th(n, γ) and ^{232}Th(n, 2n) reaction cross-sections, the decay data of ^{233}Th, ^{233}Pa and ^{231}Th are taken from refs [107-111] and are shown in Table 4.1. The radionuclide ^{233}Th($T_{1/2}$ = 21.83 m), which was produced by

the ^{232}Th(n, γ)^{233}Th reaction underwent β decays to ^{233}Pa($T_{1/2}$ = 26.975 days). In view of this, the ^{232}Th(n, γ) reaction cross-section was calculated from the observed photo-peak activity of ^{233}Pa in the γ -ray spectrum of the sample which has seen 7–15 days of cooling

Table 4.1 Nuclear Spectroscopic data used for ^{232}Th data analysis

S.No.	Nuclides	Half life	Gamma ray energy E_γ (KeV)	Abundances (%)
1	^{115}In	4.49 h	336.2	45.9
2	^{231}Th	25.52 h	84.2	6.6
3	^{233}Th	21.83 minute	86.5	27.0
4	^{233}Pa	26.97 days	311.9	38.4

So the ^{233}Pa radionuclide was identified through an analysis of the 311.9 keV characteristic γ -line. Similarly, the ^{232} Th(n, 2n) reaction cross-section was calculated from the observed photo-peak activity of the 84.2 keV γ -line of ^{231}Th in the γ -ray spectrum of a sample which has seen 12–25 hours of cooling. The number of detected γ -rays (A_{obs}) of the reaction products ^{233}Th and ^{231}Th was used to calculate the neutron-induced reaction cross-section of ^{232}Th using equation. (4.1) and is rewritten as:

$$\sigma = \frac{A_{obs}\,(CL/LT)\,\lambda}{N\phi a\varepsilon(1-e^{-\lambda t})(e^{-\lambda T})(1-e^{-\lambda CL})} \qquad \textbf{(4.3)}$$

All terms in equation (4.3) have the same meaning as in equation (4.1). In equation (4.2) the experimentally obtained neutron flux mentioned before was used to calculate the reaction cross sections ^{232}Th(n, γ) and^{232}Th(n, 2n) at different neutron energies. The ^{232}Th(n, γ) reaction cross-section for the average neutron energies of 2.8, 3.12, 13.5, 15.5 and 17.28 MeV were 28.59±0.40, 28.59±0.40, 2.49±0.15, 2.34±0.15 and 1.569±0.141 mb respectively. On the other hand, the ^{232}Th(n, 2n) reaction cross-section at neutron energy of 17.35±0.35 came out to be 6569±9 mb. The ^{232}Th(n, γ) cross section values were slightly higher because of the contribution from the low-energy neutron reaction cross-section. The contribution of the cross-section due to the tail region of the neutron spectrum for the ^{232}Th(n, γ) reaction has been estimated using the ENDF/B-VII [8] and JENDL-4.0 [10] by folding the cross-sections with neutron flux distributions of Refs [97,144]. At proton energies of 16, 18 and 20 MeV, the contribution of the cross-sections to the ^{232}Th(n, γ) reaction cross-section from ENDF/B-VII [10] was evaluated to be 1.402, 1.570 and 1.019 mb, respectively. On the other hand, the contribution of the cross-sections to the ^{232}Th(n, γ) reaction cross-section from JENDL-4.0 [12] for proton energies of 16, 18 and 20 MeV were 1.475, 1.709 and 1.113 mb, respectively. The actual experimentally obtained cross-sections for ^{232}Th(n,γ) reaction, after removing the contribution from the tail region, comes out to be 1.052±0.166, 0.701±0.171 and 0.501±0.141 mb for average neutron energies of 13.5±0.35, 15.5±0.5 and 17.28±0.35 MeV, which are given in Table 4.2.

4.5 Uncertainties in the measurements

The uncertainties associated with the measured cross-sections come from the combination of two sets of errors, systematic error and statistical error.. This overall

uncertainty is the quadratic sum of both statistical and systematic errors. The random error in the observed activity is primarily due to counting statistics, which is estimated to be 5–10%. This can be obtained by accumulating the data for an optimum time period that depends on the half-life of the nuclides of interest. The systematic errors are due to uncertainties in neutron flux estimation (~ 2%), the irradiation time (~0.5%), the detection efficiency calibration (~ 3%), the half-life of the reaction products and the γ - ray abundances about (~ 2%) as reported in [107-111]. Thus, the total systematic error is about ~ 4.2%. The overall uncertainty is found to range between 6.5 and 10.8%, coming from the combination of a statistical error of 5–10% and a systematic error of 4.2%.

4.6. Results and Discussions

The measured neutron capture ^{232}Th(n, γ) ^{233}Th cross sections at incident neutron energies of 2.8 MeV and 3.12 MeV are shown in Fig. 4.3.

The ^{232}Th (n, γ) reaction cross-section at average neutron energies of 13.35,15.5 and 17.28 MeV (Table 4. 2) as well as the ^{232}Th(n, 2n) reaction cross section at an average neutron energy of 17.28±0.35 MeV (Table 4.2) from the present work are determined for the first time. The experimentally obtained reaction cross-sections for the ^{232}Th(n, γ) and ^{232}Th(n, 2n) reactions are compared with the evaluated data from ENDF/B-VII [10] and JENDL-4.0 [12] and are given in Table 4.2. These evaluated reaction cross-sections given in Table 4.2 within the neutron energy range of 13–18 MeV for ^{232}Th(n, γ) reaction and 17–18 MeV for ^{232}Th(n, 2n) reaction are due to the finite width of the neutron energy under the main peak [97,144].

The experimentally obtained ^{232}Th(n, γ) reaction cross-sections at average neutron

energies of 13.5, 15.5 and 17.28 MeV as well as the ^{232} Th(n, 2n) reaction cross-section at a neutron energy of 17.28 MeV are within the range of the evaluated data (Table 4.2). To examine this aspect, experimental data from [21,101,144-157] in the neutron energies of 1 keV to 2.7 MeV are plotted in Fig. 4.4. The experimental data at neutron energies of 3.7 and 9.85 MeV from ref. [136] as well as at 14.5 MeV from ref. [137] are also shown in Fig. 4.4. In the same figure, the evaluated data from ENDF/B-VII [10] and JENDL-4.0 [12] are also plotted for comparison. It can be seen from Figure 4.4 that there are no data in the energy range of the present work except the data at 14.5 MeV [137]. The experimental data at 14.5 MeV are based on the neutron energy from D+T reaction and are significantly higher than the value of present work within neutron energy of 13.5–15.5 MeV. It can be seen from figure 4.4 that both experimental and evaluated ^{232}Th(n, γ) reaction cross-sections decrease up to a neutron energy of 6–7 MeV and thereafter increase up to 8 MeV and remain flat within neutron energy of 9–14 MeV. Lower value of ^{232}Th(n, γ) reaction cross-section around neutron energy of 6 MeV. In the present work, we have used neutron energies from 1 keV to 20 MeV for ^{232}Th target. In TALYS, the cross-section for reactions to all open channels is calculated. Several options are included for the choice of different parameters such as γ -strength functions, nuclear level densities, nuclear model parameters etc. All outgoing channels possible for the given ^{232}Th(n, γ) and ^{232}Th(n, 2n) cross-sections neutron energy, including inelastic and fission channels, were considered. However, the cross-sections for the (n, γ) and (n, 2n) reactions were specially looked for and collected.

Table 4.2 Neutron induced reaction cross section measured values for ^{232}Th Compared to ENDF/BVII and JENDL-4.0

Neutron Energy (MeV)	Neutron Flux n/cm^2 /sec	Cross Section (barns)		
		Experimental	Evaluated	
			ENDF-/B-VII.0	JENDL-4.0
^{232}Th(n, γ)^{233}Th				
2.80	(2.5 ±0.16) x 10^8	25.0±0.10	28.59±0.40	32.60±0.50
3.12	(1.17±0.16)x 10^8	19.7±0.10 mb,	24.61±0.20	24.39±0.20
13.5±0.35	(9.65±0.35) x10^6	1.052±0.166	1.212-1.147[a]	1.398-1.136 [a]
15.50±0.50	(3.09±0.25) x10^7	0.701±0.0.171	0.769-0.479[b]	0.962-0.773 [b]
17.28±0.35	(8.59±0.67) x10^7	0.503±0.141	0.350-0.262[c]	0.692 0.556 [c]
^{232}Th(n, 2n) ^{231}Th				
17.28±0.35	(7.02±0.55) x10^7	655±99[c]	436-354[c]	676-533[c]

[a]For ^{232}Th(n, γ) reaction, the neutron energy ranges are 13–14 MeV.

[b]For ^{232}Th(n, γ) reaction, the neutron energy ranges are 15–16 MeV.

[c]For ^{232}Th(n, γ) and (n, 2n) reaction, the neutron energy ranges are 17–18 MeV

Theoretically calculated ^{232}Th(n, γ) reaction cross-section using TALYS computer code is also plotted in Figure 4.4. and Figure 4.5 It can be seen from Figure 4.4 and Figure 4.5 that, the trend of the experimental and evaluated ^{232}Th(n, γ) reaction cross-

sections is well reproduced by the TALYS computer code. However, the ^{232}Th(n, γ) reaction cross-section calculated from TALYS are slightly higher than the experimental and evaluated data for neutron energies of 100 keV to 7.5 MeV but are comparable with the experimental values at neutron energies of 9.85 to 17.28 MeV. This is because in the TALYS the fission cross-section as a function of the neutron energy is quantitatively not well accounted, though the trend is reproduced. Similar to the evaluated data, the ^{232}Th (n, γ) reaction cross-section calculated using TALYS code shows a dip in 6–7 MeV neutron energy. The dip in the ^{232}Th(n, γ) reaction cross-section around 6–7 MeV neutron energy indicates the opening of the (n, 2n) reaction channel besides the(n, nf) channel. To verify this, ^{232}Th(n, 2n) reaction cross-sections from the present work and from [103-107,111] along with the calculated [8,9] and evaluated data [10,12] are plotted in figure 4.5. It can be seen from figure 4.4 that the experimental and calculated ^{232}Th(n, 2n) reaction cross-sections show a sharp increase from 6.6 MeV to 8.0 MeV neutron energy and thereafter remains constant up to 14 MeV. Thus, the increasing trend of ^{232}Th(n, γ) reaction cross-section beyond 8 MeV (Figure 4.5) is due to the constant ^{232}Th(n, 2n) reaction cross section (figure 4.6). Furthermore, it can be seen from figures 4.5 and figure 4.6 that the ^{232}Th(n, γ) reaction cross-section shows a dip, whereas the ^{232}Th(n, 2n) reaction cross-section shows a sharp increase. This is most probably due to the sharing of the excitation energy between ^{232}Th(n, γ) and (n, 2n) reaction channels in the neutron energy below 14 MeV.

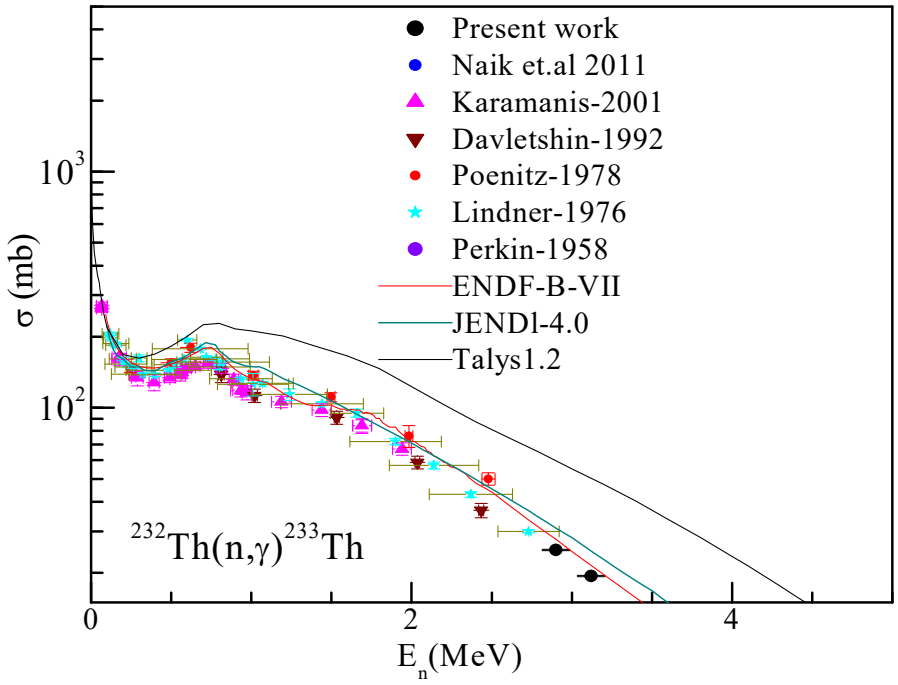

Fig 4.4 ^{232}Th(n,γ) ^{233}Th reaction cross sections at incident neutron energies of 2.8 MeV and 3.12 MeV.

4.7 Conclusions

(i) The ^{232}Th(n, γ)^{233}Th reaction cross-sections at average neutron energies of 2.8, 3.12 13.5 ±, 15.5 and 17.28 MeV as well as the ^{232}Th(n, 2n)^{231}Th reaction cross-section at 17.28±0.35 MeV neutron energy have been determined for the first time.

(ii) The ^{232}Th(n, γ) and ^{232}Th(n, 2n) reaction cross-sections at average neutron energies of 13.5, 15.5 and 17.28 MeV are in good agreement with the evaluated data from ENDF/B-VII and JENDL-4.0.

(iii) The ^{232}Th(n, γ) and ^{232}Th(n, 2n) reaction cross-sections were also calculated using the TALYS computer code and found to be in general agreement with the experimentally determined values.

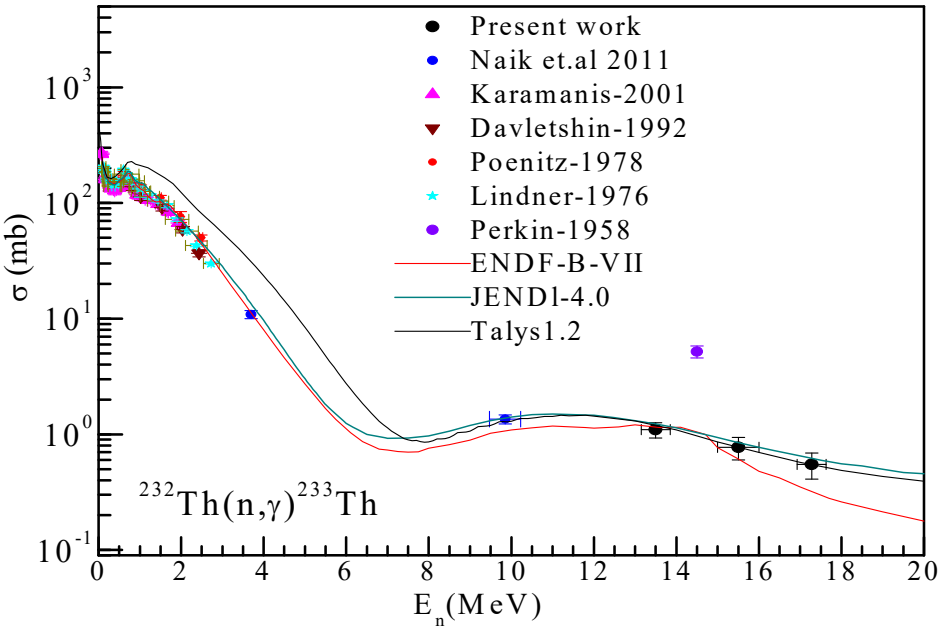

Fig 4.5 Variation of ^{232}Th(n,γ) ^{233}Th cross section as a function of neutron energy.

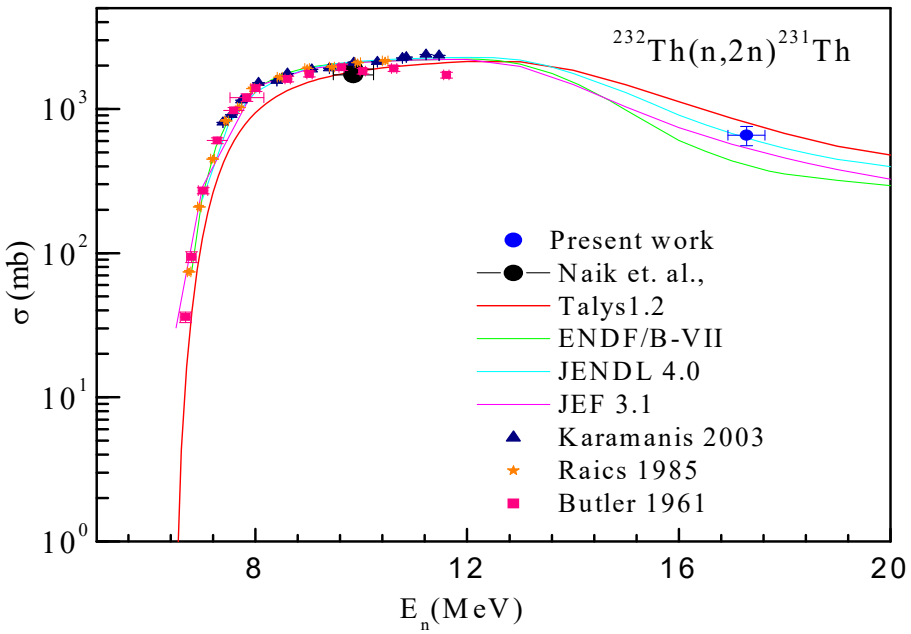

Fig. 4.6 Variation of ^{232}Th(n,2n) ^{231}Th cross section with neutron energy

Fission Studies

CHAPTER 5

Measurement of mass yield distribution of twelve fission products from neutron induced fission of ^{238}U at incident neutron energies of 9. 35 and 12.52 MeV

This chapter deals with measurement of mass distribution of twelve fission products, nuclides, from neutron induced fission of ^{238}U, at incident neutron energies of 9.35 and 12.52 MeV. It was felt highly desirable, to carry out a detailed comparative study on the mass-yield curves, for the neutron-induced fission of ^{238}U,as a function of incident neutron energy. These measurements have been carried out for the first time. Off line gamma ray spectroscopic technique was adopted for the measurement. For all the twelve fission products, which have been investigated in this thesis, yields are reported relative to reference i.e. ^{97}Zr (^{97}Zr fission yield has been taken as reference). The twelve fission products for which fission yield values are reported are, ^{91}Sr, ^{95}Zr, ^{92}Sr ^{97}Zr, ^{105}Ru, ^{115}Cd, ^{129}Sb, ^{133}I, ^{139}Ba, ^{132}Te, ^{1433}Ce, ^{147}Nd.

5.1 Outline of the present investigation

Measurement of fission product yields of in ^{238}U(n,f) at two different bombarding neutron energies (9.35 and 12.52 MeV) is reported. The measurements were carried out using activation and off line gamma ray spectroscopic techniques. The neutrons were generated using the ^{7}Li(p, n) reaction at BARC-TIFR Pelletron facility, Mumbai, Activated targets are counted in highly shielded HPGe detectors over a period of several weeks to identify decaying fission products The results obtained from present work have been compared with the similar data of mono-energetic neutrons of comparable energy from literature and are found to be in good agreement.

The term nuclear fission is the process in which a large nucleus splits into two smaller nuclei with the release of energy.. Nuclear reactor technology is based on neutron-induced fission which occupies a position of particular significance. Although a number of neutrons may be released at the instant of fission, the main fragments retain approximately the same neutron/proton ratio as the fissioning nucleus. Since this ratio is normally too high for stability, each primary fission product decays to a stable isobar by a series of beta decay in a chain of isobars (few of the fission product decay in chains are shown in Fig. 5.3). The wide number of fission product chains known is indicative of the variety of modes of fission which can occur. The position of a primary fission fragment in a decay chain is dependent on the nuclear charge distributions at the instant of fission. The fraction of fissions in which a given isobar is produced as an initial fragment is known as the independent yield of that isobar. Because of the rapid beta decay of many of these initial fragments independent yields are often difficult to measure experimentally. However for a limited number of' mass chains, measurements are possible in those cases where a given isobar is preceded by a much longer-lived or stable isobar and its yield in a short irradiation can clearly be attributed to its direct production.

The absolute fission yield of one nuclide (in the present experiment ^{97}Zr) has been chosen as reference, and its yield values are taken from reference [158]. For others fission product measured yields were found relative to ^{97}Zr. Absolute fission yields can also be determined by normalization of relative yields, i.e. by imposing the condition that the sum of all the yields should be 200%, since each fission results in the formation of two main fragments. This is the method which is frequently used to fix the absolute scale for

yields on the mass yield curves, which are drawn. Measurements of the yields of fission product nuclides are performed using the off line gamma spectroscopic technique.

5.2 Fission product mass yield distribution

Most isotopes in the fission products have extra neutrons, so they tend to decay to more stable isotopes through beta emission accompanied by gamma emission. Some isotopes in their metastable states could either decay to other isotopes through beta emission or release their extra energy through internal transitions. Neither of these types of decays changes the mass distribution of the fission products. Typically, the mass distribution curve of the fission products has a camel-type curve: two peaks and a valley at mass number of about 115. The initial yields of isotopes near the two peaks do not depend much on the materials fissioned or the energy of the neutrons that caused the fission. The yields of the isotopes at the valley, however, depend sharply on these variables. The decay chains of some isotopes are given in Fig5.3. The predominance of asymmetric fission is a common feature of fission of the heavier elements. It has been observed that product of neutron-induced fission of uranium were complementary light and heavy fragments rather than fragments of comparative mass. Two peaks with a deep trough between them, indicative of predominantly asymmetric fission. As the energy of' the fissioning nucleus is raised, the occurrence of symmetrical fission increases, resulting in the raising of the valley of the mass-yield curve and a splaying of the sides of the peaks. At very high energies symmetrical fission predominates, and the mass-yield curve takes the form of' a single broad hump.

Because of the use of ^{238}U, in fast reactor systems and ADSS thorough measurements of fission products yields i.e.,$^{238}U(n,f)$ is important for estimation of

safety parameters like delayed neutron fraction, spent fuel composition, decay heat etc. These measurements have become possible because of the availability of facilities like BARC-TIFR Pelletron accelerator and counting systems like HPGe detector. The most important characteristics of HPGe detectors is their excellent energy resolution. This quality of HPGe detector allows the separation of many closely spaced gamma lines, which is beneficial for measuring multi gamma emitting radioactive sources as in the case of fission products generated in the present experiments.

5.3 Utility of fission products yield measurement in nuclear energy

Fission product generation in the fission process is mainly quantified by fission products yield. Fission products have significance in design, safety and operations of the nuclear reactors. A number of reactor parameters are decided by fission products, i.e. delayed neutron fraction, isotopic composition of nuclear spent fuel, decay heat especially in the cooling time of 1 to 1000 seconds after loss of coolant accident. Many of the nuclides contributing to reactivity of the fuel are strong absorbers of neutron and are stable such as ^{147}Sm, ^{149}Sm, ^{151}Eu, ^{155}Gd. Some other sets of fission products such as ^{90}Sr, ^{137}Cs, ^{129}Sb, ^{90}Y, ^{99}Tc, ^{129}I, ^{135}Cs, ^{126}Sn contribute towards the radio-activity of the spent nuclear fuel. These fission products are unstable and highly radio-active. Few of the fission products such as ^{134}Cs, ^{147}Nd, and ^{137}Cs give an idea of the SNF(Spent Nuclear Fuel). burn-up. Some of the long lived fission products have high solubility in water and there is a risk of migration of these elements if groundwater is entering the repository. The long lived fission products like ^{135}Cs, ^{99}Tc, ^{129}I display high mobilities. Fission yield data, are available in sufficient detail to meet most of the nuclear data needs in the thermal neutron–induced fission based systems [159-163]. The data on the reactor fast

neutron–induced fission are, available in a limited way in the neutron induced fission of ^{238}U [164,165]. The development of ADSS systems and advanced reactor program requires significant amount of new and improved nuclear data [166]. Accurate nuclear data such as fission yields, neutron capture cross-sections, fission cross-sections and decay data including half-lives, decay energies, branching ratio, etc. are required for many advanced reactor calculations. Further, the advent and development of advanced reactors have highlighted the need for accurate determination of fission yields in the fission of actinides induced by neutrons. The potential benefits of advanced nuclear reactors are many and varied, including improved levels of efficiency in the use of fuel, a reduction in the amount of waste, and the ability to recycle at least part of the present reactor waste as energy-producing materials. In ADSS [5, 114-118], the energy of neutron goes up to 200 MeV. This is because in ADSS high energy (GeV) protons from an accelerator strike a heavy elements target like Pb and Bi yields a large number of high-energy neutrons by spallation reaction. Further, the yields of fission products are also needed for mass and charge distribution studies, which can provide valuable information for understanding the nuclear fission process. In order to get a mass yield distribution of the yields of various fission products in the neutron-induced fission of ^{238} U, we have determined the fission product mass yield using recoil catcher and off-line gamma-ray spectrometric technique with average energies of 9.35 and 12.52 MeV. The measured fission yield data from the present work have been compared with similar data from mono-energetic neutron induced fission of ^{238} U to examine the nuclear structure effect.

5.4 Description of the experimental setup

The experiment was carried out using the 14UD BARC-TIFR Pelletron facility at Mumbai, India. The neutron beam was obtained from the ^{7}Li(p, n) reaction [65] by using the proton beam main line at 6 m above the analysing magnet of the Pelletron facility to utilize the maximum proton current from the accelerator. The energy spread for proton at 6 m was maximum 50-90 keV. At this port, the terminal voltage was regulated by GVM mode using terminal potential stabilizer. Further, we used a collimator of 6 mm diameter before the target. The lithium foil was made up of natural lithium with thickness 3.7 mg/cm^2, sandwiched between two tantalum foils of different thickness. The front tantalum foil facing the proton beam was the thinnest one, with thickness of 3.9 mg/cm^2, in which degradation of proton energy was only 30 keV [24]. On the other hand, the back tantalum foil was the thickest (0.025 mm), which was sufficient to stop the proton beam. Behind the Ta-Li-Ta stack, the sample used for irradiation was natural ^{238}U metal foils, which was wrapped with 0.025 mm thick aluminium foil. The aluminium wrapper was used to stop and collect the fission products recoiling out from the surface. The size of ^{238}U metal foil was 1.0 cm^2 with thickness of 30.0 mg/cm^2. The ^{238}U metal foil wrapped with aluminium was mounted at zero degree with respect to the beam direction at a distance of 2.1 cm from the location of the Ta-Li-Ta stack. A schematic diagram of Ta-Li-Ta stack and ^{238} U metal foils is given in Fig.2.6. Different sets of samples were made for different irradiations at various neutron energies.

The Ta-Li-Ta and ^{238} U metal foil were irradiated at proton energies (E_p) of 16.0 and 20.0 MeV for a period of 15 and 5 h, respectively depending upon the energy of proton beam facing the tantalum target. The proton current during the irradiations varies from

100 nA to 400 nA. After irradiation, the samples were cooled for one hour. Then the irradiated target of ^{238}U along with Al wrapper was mounted on Perspex plate and taken for γ-ray spectrometry. The γ-rays of fission/reaction products from the irradiated ^{238}U sample were counted in energy and efficiency calibrated 80 c.c. HPGe detector coupled to a PC-based 4K channel analyzer. The counting dead time was kept always less than 5 % by placing the irradiated ^{238}U sample at a suitable distance from the detector to avoid pileup effects.

5.5 Calculation of effective average neutron energy

In the present experiment, the incident proton energies were 16.0 and 20.0 MeV. The degradation of the proton energy in the front thin tantalum foil was only 40-50 keV. The Q-value for the $^{7}Li(p, n)^{7}Be$ reaction to the ground state is -1.644 MeV, whereas the first excited state is at 0.431 MeV above the ground state leading to the Q-value -2.079 MeV. The ground state of ^{7}Be is having the threshold of 1.881 MeV, whereas the first excited state of ^{7}Be is having the threshold of 2.38 MeV With ^{7}Li, a second neutron group at $E_P \geq 2.4$ MeV is produced due to the population of the first excited state of ^{7}Be. Thus for the proton energy of 16 and 20 MeV, the corresponding first group of (n_0) neutron energies are 14.12 and 18.12 MeV to the ground state of ^{7}Be. For the first excited state of ^{7}Be, the neutron energy of the second group of neutrons (n_1) will be 13.62 and 17.62 MeV, respectively. Fragmentation of $^{8}Be^{*}$ to $^{4}He+^{3}He+n$ (Q= -3.23 MeV) also occurs when the proton energy exceeds the value 4.5 MeV and the other reaction channels are open to give continuous neutron distribution besides n_0 and n_1 groups of neutrons. The neutron spectra have been generated using the neutron energy distribution given by J.W. Meadows [100,108] et al., A typical neutron spectrum from ^{7}Li (p, n) reaction for proton

energy of 16 and 20 MeV is shown in Fig.5.1 and Fig.5.2, respectively. Based on the neutron spectrum, the flux weighted average neutron energy (<E>) has been calculated based on the entire spectrum shown in Figs.5.1 and 5.2 using the following equation.

$$<E> = \sum E_i \phi_i / \sum \phi_i) \qquad (5.1)$$

Where ϕ_i is the neutron flux for the neutron energy, E_i. The flux weighted neutron energies were obtained as 9.32 and 12.52 MeV for the proton energies of 16 and 20 MeV, respectively.

5.6 Calculation of fission product yields

The photo-peak areas of different γ-rays of interest were calculated by subtracting the linear background from their net peak areas. The number of γ-rays detected (A_{obs}) under the photo-peak of each individual fission products is related to the cumulative yield (Y_c) with the following relation,

$$A_{obs}(CL/LT) = N\sigma_f(E)I_\gamma \varepsilon Y_c(1 - \exp(-\lambda t))\exp(-\lambda T)(1 - \exp-\lambda LT) / \lambda \qquad (5.2)$$

Where,

N = number of target atoms,

$\sigma_f(E)$ = neutron-induced fission cross-section as a function of neutron energy (E)

I_γ = branching intensity for the γ-ray of the fission product,

ε = efficiency of γ line for the detector system,

t = irradiation time,

T_c = cooling time,

CL and LT = clock time and live time of counting respectively.

The nuclear spectroscopic data such as the γ-ray energy, branching intensity and half-life of the fission products are taken from Ref. [101,102]. The cumulative yields of the fission product relative to fission rate monitor ^{97}Zr were calculated using eq (5.2). The yield of fission rate monitor ^{97}Zr was chosen from the point of view of the near constant yield with change of neutron energy [158]. For neutron energies of 9.32 and 12.52 MeV, the fission yield data of ^{97}Zr in the neutron induced fission of ^{238} U with neutron energy of 9.32 and 12.52 MeV was taken from refs. [158].

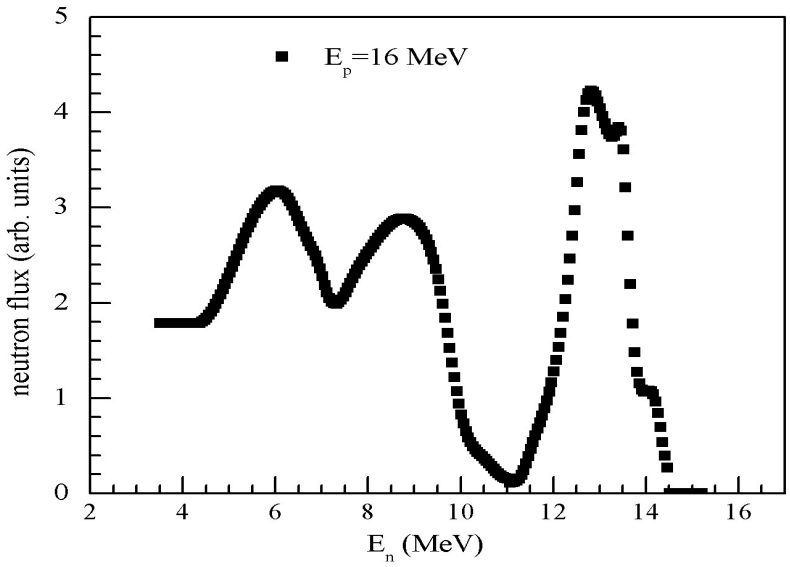

Fig. 5.1 Neutron spectrum from ^{7}Li(p, n) reaction at E_p= 16.0 MeV calculated using the results of C.H. Poppe et al., and Meadows and Smith[97,100,108].

5.7 Results and Discussions

The cumulative yields of various fission products relative to ^{97}Zr in the neutron-induced fission of ^{238}U at flux weighted average neutron energies of 9.35 and 12.52 MeV along with nuclear spectroscopic data are given in Table 5.1 and Table 5.2 respectively. The uncertainties associated to the measured cumulative yields come from the

combination of two experimental data sets. The overall uncertainty is the quadratic sum of both statistical and systematic errors. The random error in the observed activity is mainly due to counting statistics, is estimated to be 5-10 %. This can be reduced by accumulating the data for a longer time period(depending on the half-life of the nuclide of interest). The systematic errors are due to uncertainties in neutron flux estimation (~3 %), irradiation time (~1%), detector efficiency (~5 %), the half-life of fission products and gamma-ray abundances (~2%). The overall uncertainty is found to range between 8-12%, coming from the combination of statistical error of 5-10% and a systematic error of 6 %. The cumulative yields of different fission products of present work at incident neutron energies of 9.35 and 12.52 MeV for neutron-induced fission of ^{238}U were determined for the first time. The literature data [158] at the mono-energetic neutron at and are given in the Tables 5.1 and 5.2 respectively for comparison with the present data at average neutron energy of 9.35 and 12.52 MeV. The literature data for neutron induced fission of ^{238}U at 11.3MeV and 14.0 MeV are also indicated in Table literature [158] are shown in Table 5.2 with the data of the 13.81 MeV from present work. It can be seen from Table 5.1 and Table 5.2 that the cumulative fission yields determined from the present work at two different flux weighted neutron energies are in general agreement with the literature data [158] based on mono-energetic neutron-induced fission of ^{238}U. The yields of various fission products in the neutron energies of 9.35 and 12.95 MeV from present work and the fission product yield values for comparable neutron energy from literature [158] are plotted in Fig.5.4 and Fig.5.5.

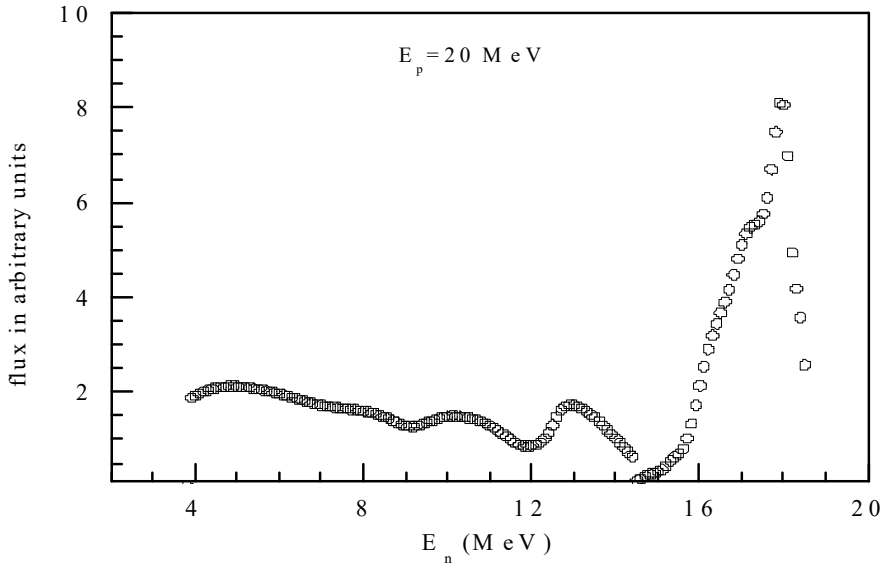

Fig.5.2 Neutron spectrum from ^{7}Li(p, n) reaction at E_p= 20.0 MeV calculated using the results of C.H.Poppe et al., and Meadows and Smith[97,100,108].

$$^{95}Zr \rightarrow \beta^- \rightarrow ^{95}Nb \rightarrow \beta^- \rightarrow ^{95}Mo$$
$$^{91}Rb \rightarrow \beta^- \rightarrow ^{91}Sr \rightarrow \beta^- \rightarrow ^{91}Y \rightarrow \beta^- \rightarrow ^{91}Zr$$
$$^{132}Te \rightarrow \beta^- \rightarrow ^{132}I \rightarrow \beta^- \rightarrow ^{132}Xe$$
$$^{92}Sr \rightarrow \beta^- \rightarrow ^{92}Y \rightarrow \beta^- \rightarrow ^{92}Zr$$
$$^{143}Ce \rightarrow \beta^- \rightarrow ^{143}Pr \rightarrow \beta^- \rightarrow ^{143}Nd$$
$$^{97}Zr \rightarrow \beta^- \rightarrow ^{97}Nb \rightarrow \beta^- \rightarrow ^{97}Mo$$
$$^{133}Sb \rightarrow \beta^- \rightarrow ^{133}Te \rightarrow \beta^- \rightarrow ^{133}I \rightarrow \beta^- \rightarrow ^{133}Xe \rightarrow \beta^- \rightarrow ^{133}Cs$$
$$^{139}Sb \rightarrow \beta^- \rightarrow ^{139}Te \rightarrow \beta^- \rightarrow ^{139}I \rightarrow \beta^- \rightarrow ^{139}Xe \rightarrow \beta^- \rightarrow ^{139}Cs \rightarrow \beta^- \rightarrow ^{139}Ba \rightarrow \beta^- \rightarrow ^{139}La$$
$$^{105}Mo \rightarrow \beta^- \rightarrow ^{105}Tc \rightarrow \beta^- \rightarrow ^{105}Ru \rightarrow \beta^- \rightarrow ^{105}Rh \rightarrow \beta^- \rightarrow ^{105}Pd$$
$$^{129}Sn \rightarrow \beta^- \rightarrow ^{129}Sb \rightarrow \beta^- \rightarrow ^{129}Te \rightarrow \beta^- \rightarrow ^{129}I \rightarrow \beta^- \rightarrow ^{129}Xe$$
$$^{115}Pd \rightarrow \beta^- \rightarrow ^{115}Ag \rightarrow \beta^- \rightarrow ^{115}Cd \rightarrow \beta^- \rightarrow ^{115}In \rightarrow \beta^- \rightarrow ^{115}Sn$$
$$^{147}Ce \rightarrow \beta^- \rightarrow ^{147}Pr \rightarrow \beta^- \rightarrow ^{147}Nd \rightarrow \beta^- \rightarrow ^{147}Pm \rightarrow \beta^- \rightarrow ^{147}Sm$$

Fig. 5.3 Decay schemes of ^{95}Zr, ^{91}Sr, ^{132}Te, ^{92}Sr, ^{143}Ce, ^{97}Zr, ^{133}I, ^{139}Ba, ^{105}Ru, ^{129}Sb, ^{115}Cd, ^{147}Nd

Table 5.1: Fission yields of fission products in ^{238}U Fission at E_n = 9.35 MeV relative to ^{97}Zr fission yield at E_n = 11.3 MeV as reference Taking ^{97}Zr as reference

Nuclide	Half-life	Gamma-ray energy (keV)	Gamma Abundance (%)	Fission yield (%)	
				Present Data	Z. Li, X.Wang, K. Jing, A. Cui, D Liu, S. Su, P. Tang, T. Chih, S. Zhang, J. Gao, Radiochim. Acta. **64**, 95 (1994)./ Joint Evaluated Fission and Fusion File, Incident neutron data,(JEFF/3.1A)***** , 2 October 2006
^{91}Sr	9.63 h	1024.3	33.0	3.831± 0.2	3.93 ± 0.15
^{92}Sr	2.710 h	1384.9	90.0	3.476± 0.4	4.18± 0.14
^{95}Zr	64.02 d	756.7	54.0	4.687±0.12	5.18 ± 0.18
^{97}Zr	16.91 h	743.4	93.0	5.206 ± 0.4	5.206 ± 0.046
^{105}Ru	4.44 h	724.0	47.0	3.346± 0.3	3.64 ± 0.18
^{115}Cd	53.46 h	336.2	45.9	0.54± 0.05	0.900 ± 0.025
^{129}Sb	4.32 h	812.4	43.0	0.94 ± 0.15	1.50 ± 0.09
^{132}Te	3.20 d	228.1	88.0	5.184 ± 0.4	5.36 ± 0.21
^{139}Ba	83.03 m	165.8	23.7	4.51 ± 0.4	5.10 ± 0.30
^{143}Ce	33.03 h	293.3	42.8	3.306± 0.35	4.28 ± 0.16
^{147}Nd	10.98 d	91.1	28.0	2.209± 0.10	2.39 ± 0.10

***** http://wwwnds.iaea.org/exfor/endf00.htm

Table 5.2: Fission yields of fission products in ^{238}U Fission at E_n = 12.35 MeV relative to ^{97}Zr fission yield at E_n=14 MeV.

Nuclide	Half-life	Gamma-ray energy (keV)	Gamma Abundance (%)	Fission yield (%)	
				Present Data	*****Joint Evaluated Fission and Fusion File, Incident neutron data,(JEFF/3.1A),2 October 2006
^{91}Sr	9.63 h	1024.3	33.0	3.56± 0.15	3.635 ± 0.084
^{92}Sr	2.710 h	1384.9	90.0	3.705± 0.35	3.820 ± 0.057
^{95}Zr	64.02 d	756.7	54.0	4.95± 0..12	4.594 ± 0.056
^{97}Zr	16.91 h	743.4	93.0	4.79 ± 0.40	5.206 ± 0.046
^{105}Ru	4.44 h	724.0	47.0	3.52± 0.40	3.109 ± 0.047
^{115}Cd	53.46 h	336.2	45.9	1.06±.0.05	0.900 ± 0.025
^{129}Sb	4.32 h	812.4	43.0	0.991± 0.2	1.66 ± 0.19
^{132}Te	3.20 d	228.1	88.0	4.5 ± 0.40	4.690 ± 0.066
^{133}I	20.80 h	529.9	87.0	5.05± 0.40	5.74 ± 0.17
^{139}Ba	83.03 m	165.8	23.7	4.70 ± 0.40	4.99 ± 0.21
^{143}Ce	33.03 h	293.3	42.8	3.11± 0.36	3.855 ± 0.058
^{147}Nd	10.98 d	91.1	28.0	2.39± 0.11	2.134 ± 0.041

*****http://wwwnds.iaea.org/exfor/endf00.htm,

5.8 Conclusion

In the present work, the yields of twelve, products in neutron induced fission of ^{238}U at average neutron energy of 9.35 and 12.52 MeV were determined using recoil catcher and off-line gamma ray spectrometric technique. The yields of fission products at average neutron energy of 9.35 MeV is determined for the first time this result has been compared with the evaluated values using JEFF.3.1/A[158] cross section libraries in the literature at incident neutron energy of 11.3 MeV. The present data at average neutron energy of 12.52 MeV are in general agreement with the neutron induced fission data of ^{238}U for mono-energetic neutron of 14 MeV [158].

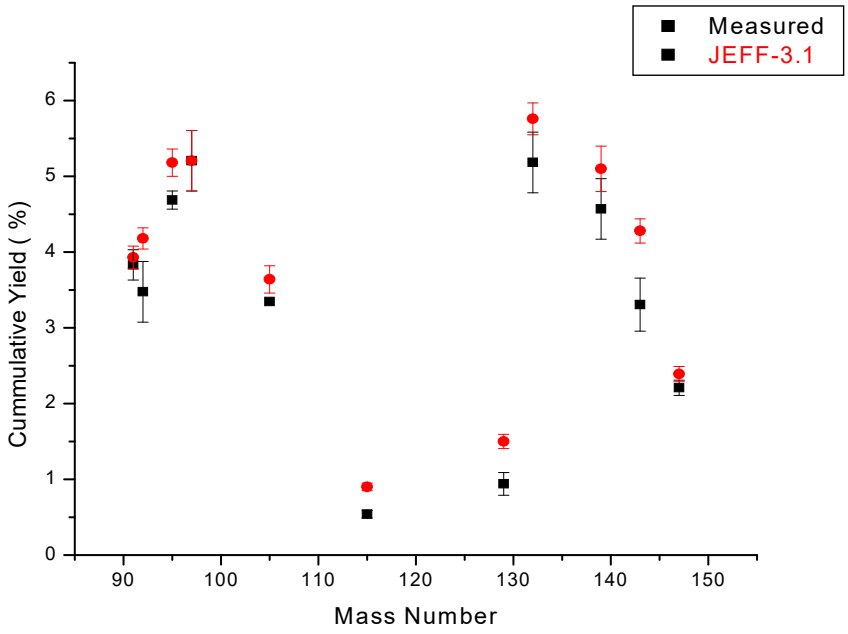

Fig. 5.4 Fission yield of fission products for En = 9.35 MeV compared to 11.3 MeV values taken from literature.

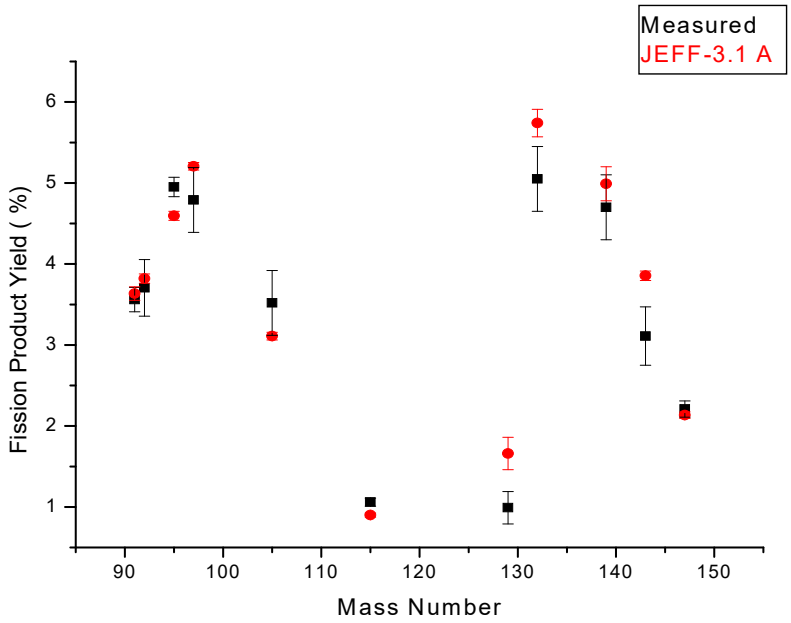

Fig. 5.5 Fission yield of fission products for $^{238}U(n,f)$ at E_n = 12.52 MeV compared to 14 1MeV values taken from literature.

CHAPTER 6

Measurement of mass yield distribution of twelve fission products from neutron induced fission of ^{232}Th at incident neutron energies of 9.35 and 12.52 MeV

This chapter is devoted to experimental studies of fission product mass distribution for ^{232}Th (n,f) fission at two different incident neutron energies, .i.e. 9.32 MeV and 12.52 MeV respectively. These studies have been carried out for the first time using off-line gamma spectroscopic technique. Very little measured nuclear data are available for neutron induced fission of thorium at intermediate and high energy, many basic nuclear data for ^{232}Th(n,f) reaction are still lacking or are not known well enough for a reactor development. Because thorium will be used in advanced systems like AHWR (Advanced Heavy Water Reactor), HTR (High Temperature Reactor), Molten salt reactor, and future ADSS systems, an accurate measurement of the fission product mass distribution is of significance.

In both applications in nuclear power and basic nuclear physics, the fission fragment mass distribution is one of the most important characteristics of the fission phenomenon. In nuclear energy applications, the composition of fission products must be known because they accumulate during the operation of nuclear reactor. The fission product composition influences the physical and chemical properties of nuclear fuel. For example, fission product may capture or emit neutrons and therefore change the neutron balance of the system; also, fission products decay and contribute to the heat released in the fission process. In spent nuclear fuel, fission product continues to generate heat due to radioactive decay. Typically, fission product dominates the decay heat for the first 50-80

yrs after extraction of spent nuclear fuel from reactor. Because very few measurements are available in the literature for thorium fission ^{232}Th (n, f)) at intermediate and high energy neutrons, fresh nuclear data measurement experimentation is important for thorium. The technology ^{232}Th-^{233}U cycle is more complex and more complicated than that of the uranium-plutonium cycle. From the point of view of waste handling Thorium based systems are superior compared to Uranium based systems (because of the better structural stability of Th fuels) and a much lower production of the long-lived transuranic elements as waste. Evaluated fission product yields data for the neutron induced fission of thorium ^{232}Th (n,f)) are available for the reactor calculations for thermal neutrons. However, the advent and development of advanced reactors such as fast reactors [2], advanced heavy water reactor (AHWR) [4] and accelerated driven sub-critical system (ADSS) [5,114,118] have highlighted the need for accurate determination of fission yields in the fast neutron fission of thorium ^{232}Th(n, f)).

The models available so far for interpretation of physics of nuclear fission are not been able to explain all the observed experimental facts about fission. It is by accumulating more experimental results all the observations related to fission process could be explained. As compared to uranium fission, in the case of thorium fission ^{232}Th(n, f)) in the region of symmetric fission a third peak is observed.The shape of the mass-yield distribution of thorium has been a long standing puzzle in fission observations. This is because of the presence of third peak in the mass yield distribution in the symmetric fission range. The observed fragment mass-yield curves for two different incident neutron energies of 9.32 and 12.52 MeV has been measured and presented here.

6.1 A brief description of few systems in which ^{232}Th-^{233}U fuel is the source for power production

6.1.1 AHWR (Advanced Heavy Water Reactor)

The AHWR reactor is similar to advanced CANDU reactor designs, with pressure tubes containing the reactor fuel and light water reactor coolant located inside of calandria tubes, surrounded by a low-pressure reactor vessel filled with heavy water that serves as both moderator and reflector, as shown in Fig. 6.1. Air fills the annulus between each pressure tube and calandria tube to provide thermal insulation between the hot pressure tube and the cooler external heavy water moderator. Use of light water for the coolant follows the approach used for advanced CANDU designs, although most existing CANDU reactors utilize heavy water for the reactor coolant as well as for the moderator. However, the AHWR is a boiling water reactor and uses vertical pressure tubes instead of horizontal pressure tubes. As a result, the AHWR refuels only from the top of the reactor. In addition, each pressure tube in the AHWR contains only one long fuel "cluster," as compared to the multiple shorter fuel bundles in a typical CANDU reactor pressure tube. Coolant flow through the reactor core is provided via natural circulation driven by coolant boiling (there are no primary coolant pumps. The AHWR operates in a closed fuel cycle with recycle of both ^{233}U and thorium back into the reactor. Overall, 60% of the power generated by the reactor comes from the ^{233}U created from thorium.

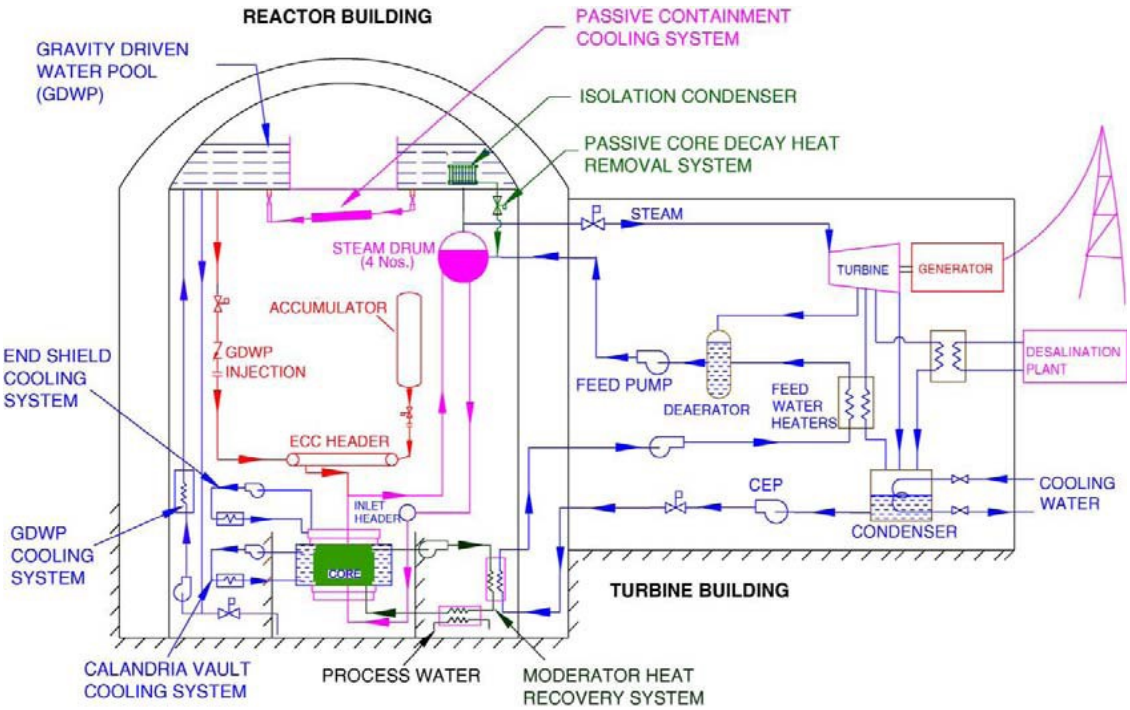

Fig. 6.1 Schematics of Advanced Heavy Water Reactor [4]

6.1.2 Molten Salt Reactor

In a molten salt reactor, the fuel is dissolved within a fluoride salt mixture (producing either Uranium Fluoride or Thorium Fluoride) and circulated around a graphite moderated core. While deliberately allowing a nuclear reactor's fuel to melt down might, from a safety point of view seem slightly counter intuitive, actually it does present certain advantages. Obviously a "melt down" accident is no longer a worry (its already melted down). UF_4 and TF_4 both have a negative temperature co-efficient, thus when the temperature drops, the reactivity increases, when it rises up, the reactivity decreases. Also, as the fuel requires slow neutrons to maintain chain reactions, removing the fuel from the core, should shut down the reactions. Many Molten Salt designs have a series of emergency dump tanks at the base (thus gravity fed) into which the fuel can be dumped in an emergency. As a further backup measure the valve controlling the tanks can

be a freeze plug of solid salt. If the temperature in the core exceeds some threshold level, or the cooling loop/blower maintain the freeze plug is turned off, the fuel escapes out of the core and into the dump tanks.

Thus a MSR type reactor offers several passive safety advantages over conventional reactor types. Another advantage is the ability to process the fuel as the reactor runs by passing it through a chemical plant, this removes the various isotopes that would otherwise "poison" the nuclear reactions and force a shutdown and fuel replacement (as is regularly the case in a conventional reactor). This would also reduce the nuclear waste volumes produced by these reactors. MSR's also operates at a low vapour pressure, which means they don't need the high pressure forged parts of other reactor types. In theory the core should also be relatively small and compact (indeed the initial attempts to build one were focused on the idea of a reactor that could be carried inside a plane, see ARE) which of course has numerous advantages. It may also be possible, as with many Generation IV reactors, to use MSR's to produce hydrogen via the Sulfur-Iodine process and utilize the more energy efficient Brayton cycle.

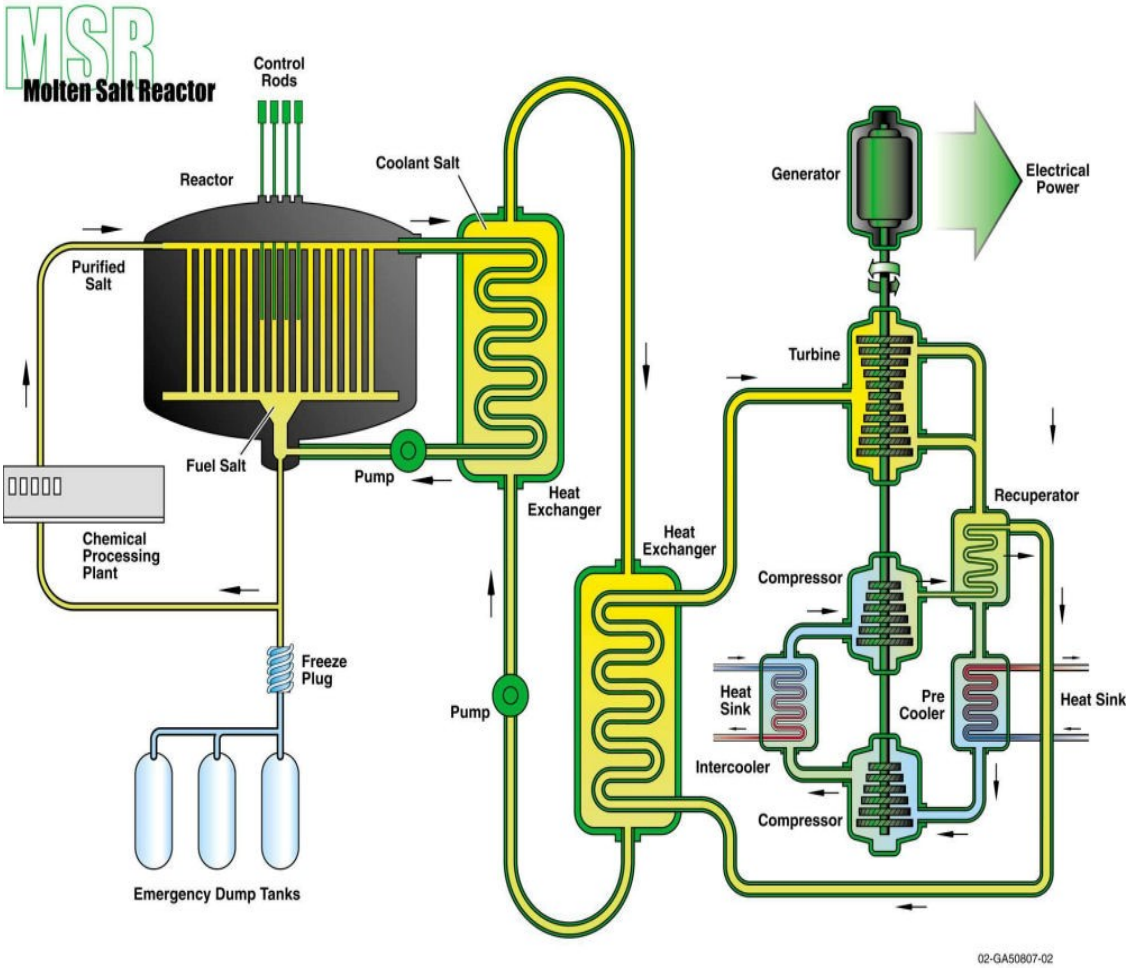

Fig. 6.2 Schematics of Molten Salt Reactor [168]**.**

6.1.3 Accelerator Driven Sub critical System(ADSs)

The core of such an ADSS is mainly thorium, located near the bottom of a 25 meter high tank. It is filled with some 8000 tones of molten lead or lead-bismuth at high temperature – the primary coolant, which circulates by convection around the core. Outside the main tank is an air gap to remove heat if needed. The accelerator supplies a beam of high-energy protons down a beam pipe to the spallation target inside the core, and the neutrons produced enter the fuel and transmute the thorium into protactinium,

which soon decays to U-233 which is fissile. The neutrons also cause fission in uranium, plutonium and possibly transuranics present, releasing energy. A 10 MW proton beam might thus produce 1500 MW of heat (and thus 600 MWe of electricity, some 30 MWe of which drives the accelerator). With a different, more sub-critical, core a 25 MW proton beam would be required for the same result. The major sub-systems of ADSS are:

(i) High power proton accelerator – 1 GeV, _10 mA current.

(ii) Spallation target – heavy element (Pb,W, U. . .), for _10 MW beam power.

(iii) Sub-critical core – fast neutron system, thermal neutron system or a combination of fast and thermal neutron system.

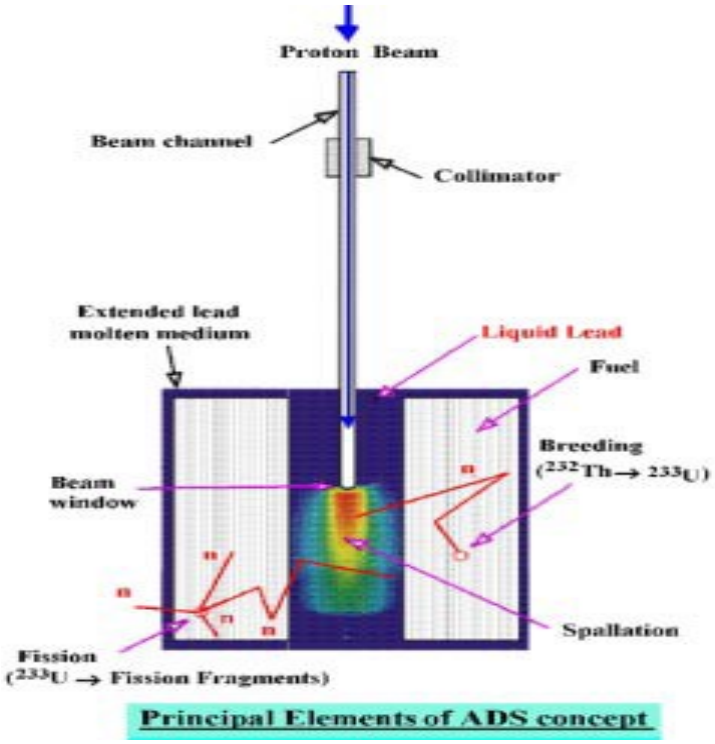

Fig. 6.3 ADS System Basic Concept [5,114-118].

6.2 Experimental setup for fission studies

Experimental setup is similar to what is mentioned in Chapter 5 for ^{238}U fission product mass distribution. Experiment was carried out using the 14UD BARC-TIFR Pelletron facility The neutron beam was obtained from the $^{7}Li(p, n)$ reaction [98,131,142] by using the proton beam main line at 6 m height above the analyzing magnet of the Pelletron facility to utilize the maximum proton current from the accelerator. The energy spread for proton at 6 m height was maximum 50-90 keV. At this port, the terminal voltage was regulated by GVM mode using terminal potential stabilizer. Further, we used a collimator of 6 mm diameter before the target. The lithium foil was made up of natural lithium with thickness 3.7 mg/cm^2, sandwiched between two tantalum foils of different thickness.

The front tantalum foil facing the proton beam was the thinnest one, with thickness of 3.9 mg/cm^2, in which degradation of proton energy was only 30 keV [24]. On the other hand, the back tantalum foil was the thickest (0.025 mm), which was sufficient to stop the proton beam. Behind the Ta-Li-Ta stack, the sample used for irradiation was natural ^{232}Th metal foils, which was wrapped with 0.025 mm thick aluminum foil. The aluminum wrapper was used to stop and collect the fission products recoiling out from the surface. The size of ^{232}Th metal foil was 1.0 cm^2 with thickness of 700.2 mg/cm^2. The ^{232}Th metal foil wrapped with aluminum was mounted at zero degree with respect to the beam direction at a distance of 2.1 cm from the location of the Ta-Li-Ta stack. A schematic diagram of Ta-Li-Ta stack and ^{232}Th metal foils is shown in Fig. 2.6. Different sets of samples were made for different irradiations at various neutron energies.

The fission cross section for thorium at energies specified in this thesis are less than half the values for uranium, so thorium samples were irradiated for longer time compared to uranium. The ^{232}Th metal foils were irradiated for a period of 10 and 5 h with the neutron beam generated by impinging proton beam of 16.0 and 20.0 MeV on Ta-Li-Ta stack. The proton current during the irradiations varies from 100 nA to 400 nA. After the irradiation, the samples were cooled for one hour. Then the irradiated target of ^{232}Th along with Al wrapper was mounted on Perspex plate and taken for γ-ray spectrometry.

The neutron energies are same as mentioned in Chapter 5 and the decay chains of the fission products are also mentioned in the same chapter. The flux and energy weighted effective neutron energies come out to be 9.32 MeV and 12.52 MeV respectively. The gamma rays used for analysis their abundances are shown in Table 6.1 and Table 6.2. Besides these natural thorium emits gamma lines. These natural thorium gamma lines require special precautions during gamma spectroscopy.

6.3 Data analysis and mass yield distribution calculation

The net photo-peak areas of different γ-rays of interest were calculated by subtracting the linear background from their gross peak areas. The number of γ-rays detected (A_{obs}) under the photo-peak of each individual fission products is related to the cumulative yield (Y_c) with the following relation,

$$A_{obs}(CL/LT) = N\sigma_f(E)I_\Upsilon\, \varepsilon Y_c\,(1 - \exp(-\lambda t))\exp(-\lambda T)\,(1 - \exp{-\lambda LT}) / \lambda \qquad (6.1)$$

Where, N= number of target atoms,

$\sigma_f(E)$ = neutron-induced fission cross-section as a function of neutron energy (E) of the target with average neutron flux (φ)

I_γ= branching intensity for the γ-ray of the fission product

ε= efficiency of the detector system

t = irradiation time, T_c= cooling time

CL and LT = clock time and live time of counting, respectively

The nuclear spectroscopic data such as the γ-ray energy, branching intensity and half-life of the fission products are taken from Refs. [101,102]. The cumulative yields of the fission product relative to fission rate monitor ^{97}Zr were calculated using Eq. (6.1). The yield of fission rate monitor ^{97}Zr was chosen from the point of view of the near constant yield with change of neutron energy [169]. For neutron energies of 9.32 and 12.52 MeV, the fission yield data of ^{97}Zr in the neutron induced fission of ^{232}Th with neutron energy of 14 MeV was taken from Ref. [169].

6.4 Results and Discussions

The results of the fission product mass yield measurements at incident neutron energy of 9.35 MeV are presented in Table 6.1 and depicted in Fig. 6.1 for comparison fission yield values taken from JENDL are also shown at incident neutron energy of 14 MeV. There are no data available in the literature close to 9.35MeV, so results were compared with 14MeV values.

It could be said that, in the relative fission yield measurement the total error in the measurements are less because no flux or fission cross sections will be required in the expression for relative yield calculations.Uncertainties in the fission yield values are obtained taking into account all sourced error including random and systematic error propagation. The results of the fission product mass yield measurements at incident neutron energy of 12.52 MeV are presented in Table 6.2 and depicted in Fig. 6.2 for comparison fission yield values taken from JENDL are also shown at incident neutron

energy of 14 MeV. Probability of increase of symmetric fission with increasing incident neutron energy has been observed in the present experiment. The increase in the symmetric fission component with the increase in the incident neutron energy is more prominent in the case of thorium compared to uranium. This fact could be seen from peak to vally ratio (P/V)

Thorium has its inbuilt gamma lines, because of these lines more care is required during gamma spectroscopy of thorium compared to uranium. The third peak in the mass distribution is observed in the present experiment. This is because of presence of second dip at the outer fission barrier called the thorium anomaly.

6.5 Uncertainties in the results.

The overall uncertainty is the quadratic sum of both statistical and systematic errors. The random error in the observed activity is particularly due to counting statistics, which is estimated to be 5-10 %. This can be obtained by accumulating the data for an optimum time period that depends on the half-life of the nuclide of interest. The systematic errors are due to uncertainties in neutron flux estimation (~3 %), irradiation time (~1%), detector efficiency (~5 %), the half-life of fission products and gamma-ray abundances (~2%). The overall uncertainty is found to range between 8-12%, coming from the combination of statistical error of 5-10% and a systematic error of 6 %

6.6 Conclusions

The observations made here are important from the ADSS point of view. In ADSS high energy neutrons contribute to fission. Since the probability of symmetric fission increases with increase in neutron energy, the mass of the fission products are expected to be near the symmetric split.

Table 6.1. Nuclear spectroscopic data and fission products yields in the neutron induced fission of ^{232}Th at average neutron energy of 9.35 MeV relative to ^{97}Zr fission yield at E_n = 14.0 MeV

Nuclide	Half-life	Gamma-ray energy (keV)	Gamma Abundance (%)	Fission yield (%)	
				JENDL-4.0 Fission Product Sub-library (J40-2010)FPY-2011	Present Data
^{91}Sr	9.63 h	1024.3	33.0	5.98±0.24	5.37±0.23
^{92}Sr	2.710 h	1384.9	90.0	5.74±0.40	5.26±0.37
^{95}Zr	64.02 d	756.7	54.0	4.77±0.30	4.59±0.40
^{97}Zr	16.91 h	743.4	93.0	3.41±0.15	3.41±0.15
^{105}Ru	4.44 h	724.0	47.0	1.28±0.07	1.13±0.09
^{115}Cd	53.46 h	336.2	45.9	1.11±0.07	1.10±0.07
^{129}Sb	4.32 h	812.4	43.0	1.24±0.12	1.41±0.16
^{132}Te	3.20 d	228.1	88.0	3.32±0.13	3.18±0.11
^{133}I	20.80 h	529.9	87.0	4.68±0.38	4.77±0.23
^{139}Ba	83.03 m	165.8	23.7	5.82±0.23	5.55±0.26
^{143}Ce	33.03 h	293.3	42.8	5.14±0.31	5.04±0.21
^{147}Nd	10.98 d	91.1	28.0	1.87±0.11	1.57±0.16

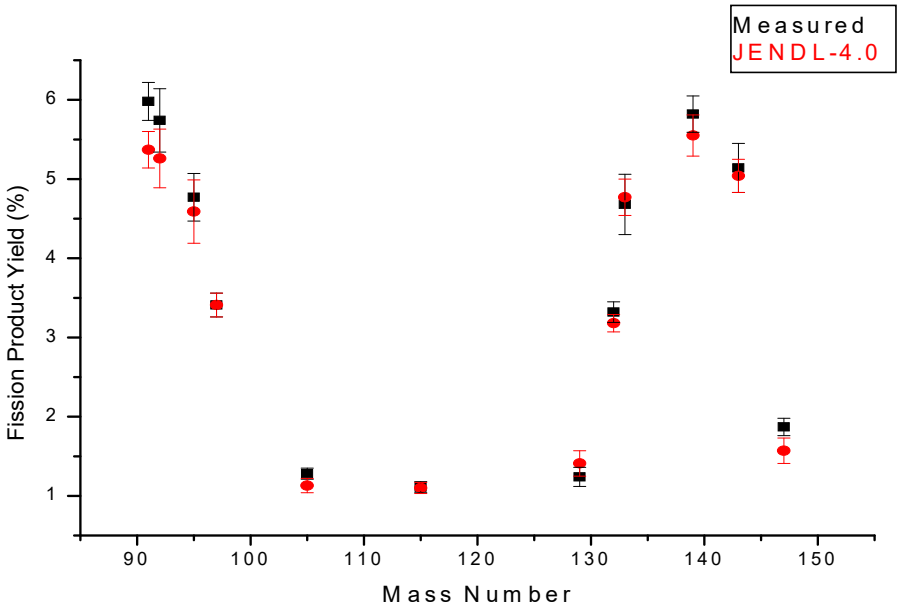

Fig 6.4 Fission Product Yield for ^{232}Th(n, f) fission at incident neutron energy of 9.32 MeV compared to the literature values at 14 MeV.

The increase in the symmetric fission component with the increase in the incident neutron energy is more prominent in the case of thorium compared to uranium. From Figs 6.1 and 6.2 it is observed that,the fission product mass distribution becomes more symmetric with increasing incident neutron energy. The probability of symmetric fission increases with increase in neutron energy. The increase in the symmetric fission component with the increase in the incident neutron energy is more prominent in the case of thorium compared to uranium.This fact could be seen from peak to vally ratio (P/V). Thorium has its inbuilt gamma lines. These require special care during gamma spectroscopy. In the case of thorium third peak in the mass distribution is observed. This is because of second dip at the outer fission barrier called the thorium anomaly. The yield

Table 6.2. Nuclear spectroscopic data and yields of fission products in the neutron induced fission of ^{232}Th at average neutron energy of 12.52 MeV relative to ^{97}Zr fission yield at E_n =14. 0 MeV

Nuclide	Half-life	Gamma-ray energy (keV)	Gamma Abundance (%)	Fission yield (%)	
				Present Data	JENDL-4.0 Fission Product Sub-library (J40-2010)FPY-2011
^{91}Sr	9.63 h	1024.3	33.0	**5.66±0.32**	**5.98±0.24**
^{92}Sr	2.710 h	1384.9	90.0	**5.89 ± 0.23**	**5.74±0.40**
^{95}Zr	64.02 d	756.7	54.0	**4.23 ± 0.21**	**4.77±0.38**
^{97}Zr	16.91 h	743.4	93.0	**3.41±0.15**	**3.41±0.15**
^{105}Ru	4.44 h	724.0	47.0	**1.12± 0.15**	**1.11±0.07**
^{115}Cd	53.46 h	336.2	45.9	1.21 ± 0.05	1.28±0.07
^{129}Sb	4.32 h	812.4	43.0	1.17±0.14	1.24±0.12
^{132}Te	3.20 d	228.1	88.0	3.44±0.19	3.32±0.13
^{133}I	20.80 h	529.9	87.0	5.20±0.05	5.10±0.31
^{139}Ba	83.03 m	165.8	23.7	5.56±0.26	5.82±0.23
^{143}Ce	33.03 h	293.3	42.8	5.17± 0.15	5.14±0.31
^{147}Nd	10.98 d	91.1	28.0	1.93±0.57	1.87±0.11

of fission products at mass numbers 133-135, 145-146 and their complementary parts are higher because of presence of 82n shells and deformed 88n shells at mass numbers 133-135 and 144-145 because of closure of shells. Higher yield at certain mass numbers are because of even-odd effect which indicates role of structural effect.

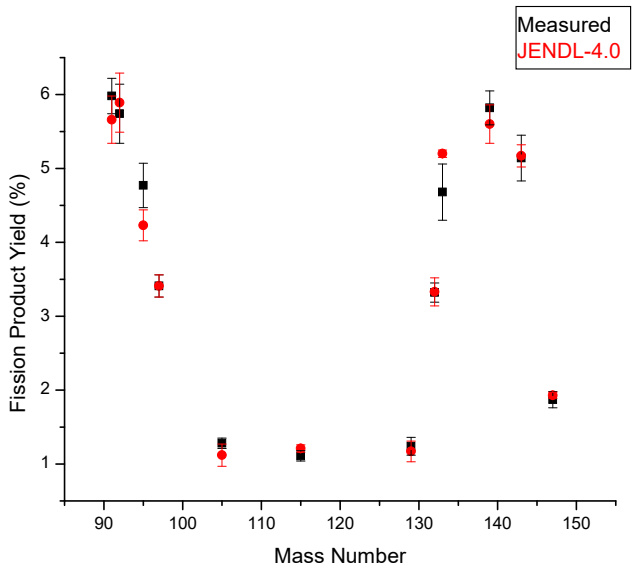

Fig. 6.5 Fission Product Yield for ^{232}Th(n, f) fission at incident neutron energy of 12.52 MeV compared to the literature values at 14 MeV.

CHAPTER 7

Summary and Conclusions

This dissertation describes our investigation on neutron induced cross section and fission yield measurements for thorium and uranium nuclei. Present results are first measurements of basic nuclear data i.e. reaction cross section and fission product mass distribution for ^{238}Uand ^{232}Th at specified energies using activation and off line gamma ray spectroscopy. It also includes the new possibilities opened up using the findings of this work.

7.1 Part – I Summary of Reaction cross section Measurements

The neutron capture cross section of (^{238}U(n, γ)^{239}U) were measured at incident neutron energies of 3.12 MeV, 13.5.MeV and 17.28 MeV respectively. Experimental results were compared with the evaluations obtained using different cross section libraries i.e. ENDF/B-VII.0, JENDL-4.0, JEFF-3.1/A and CENDL-3. It is observed that, all the evaluations match with the measured results at incident neutron energy of 3.12 MeV. For incident neutron energies of 13.5 MeV and 17.28 MeV ENDF/B-VII.0, JENDL-4.0, JEFF-3.1/A evaluations match with the measurements but CENDL-3 evaluations do not match with the measurements.

^{238}U(n,2n)^{237}U reaction cross sections were measured at incident neutron energies of 13.5.MeV and 17.28 MeV respectively. The results obtained from the present measurement were compared with the evaluated values of ENDF/B-VII.0, JENDL-4.0, JEFF-3.1/A. It is observed that, evaluations match with the experiments.

Experiments were carried out to measure ^{232}Th(n, γ)^{233}Th reaction cross sections at incident neutron energies of 2.18, 3.12, 13.5 and 17.28 MeV respectively. The results

obtained from the present experiment were compared with the evaluated results using different cross section libraries e.g. ENDF/B-VII.0, JENDL-4.0.The evaluations are matching with the measurements.

^{232}Th(n,2n)^{231}Th reaction cross sections were measured at incident neutron energy of 17.28 MeV. ^{232}Th(n,2n)^{231}Th cross sections were evaluated using different cross section libraries i.e. ENDF/B-VII.0, JENDL-4.0. It is seen that, the evaluations match with the experimental results.

For comparison with the present measurements, the detailed model calculations were performed using computer code TALYS. At incident neutron energies less than 8 MeV, the capture cross sections for Uranium and Thorium are less compared to the values obtained using TALYS. This could be due to default parameters in TALYS. This is opening up an opportunity for adjustment of input parameters in TALYS in the future. At incident neutron energies greater than 10 MeV the experimentally obtained cross sections match with TALYS.

7.2 Part – II Summary of Fission Studies

The second part of my thesis deals with the measurement of fission product mass distribution in ^{238}U(n,f) and ^{232}Th(n,f) fission at two different incident neutron energies i.e. 9.35 MeV and 12.52 MeV respectively. The following is concluded from the measurements.

In the present work, the yields of twelve, products in neutron induced fission of ^{238} U(n,f) at average neutron energy of 9.35 and 12.52 MeV were determined using recoil catcher and off-line gamma ray spectrometric technique. The yields of fission product in

^{238}U fission at average neutron energy of 9.35 MeV is measured for the first time. This experimentally obtained data is compared with the closest data available in literature at 11.3 MeV [158]. The results obtained in the present experiment present at average neutron energy of 12.52 MeV are compared with the neutron induced fission of ^{238} U for mono-energetic neutron of 14 MeV. The results are in general agreement.

The results of the fission yield measurements of ^{232}Th(n,f) at incident neutron energy of 9.35 are reported for the first time, the closest available literature values taken from evaluated results obtained using cross section data JENDL at incident neutron energy of 14 MeV[169]. The results of the fission yield measurements at incident neutron energy of 12.52 MeV mentioned here are compared with the evaluated values of JENDL[169] at incident neutron energy of 14 MeV.

The fission product mass distribution becomes more symmetric with increasing incident neutron energy. Means probability of symmetric fission increases with increase in neutron energy. The increase in the symmetric fission component with the increase in the incident neutron energy is more prominent in the case of thorium compared to uranium. This fact could be seen from peak to vally ratio (P/V). This is applied for ^{238}U(n,f) and ^{232} Th(n,f). In the case of Th(n,f) third peak in the mass distribution is observed. This is because of second dip at the outer fission barrier called the thorium anomaly.

The yield of fission products at mass numbers 133-135, 145-146 and their complementary parts are higher because of presence of 82n shells and deformed 88n shells at mass numbers 133-135 and 144-145 because of closure of shells. Higher yield at certain mass numbers are because of even-odd effect which indicates role of structural

effect.Many of the measured fission product yields behave qualitatively as would be expected from what is known about the changes in the mass yield distribution with increasing incident neutron energy. Measurements could be repeated in the future at finer energy intervals. Few more experiments would be needed to get better feeling of Th(n,f) reaction and its dependence on incident neutron energy.

References

1.0 T. Ethvignot, M. Devlin, H. Duarte, T. Granier, R. C. Haight, B. Morillon, R. O. Nelson,J. M. O'Donnell and D. Rochman Phys. Rev. Lett. 94 (2005) 052701

2.0 IAEA-TECDOC-1319

3.0 H. Nifenecker, O. Meplan and S. David, (Taylor and Francis, 2003).

4.0 R. K. Sinha and A. Kakodkar, Nucl. Eng. Des. 236 (2006) 683

5.0 C. Rubbia, J. A. Rubio, S Buono, F. Carminati, N. Fietier, J. Galvez, C. Geles, Y. Kad, R Klapisch, P. Mandrilion, J. P. Revol, and Ch. Roche, CERN/AT/95–44 (ET) 1995

6.0 E. T. Cheng and D. R. Mathews, Proc. Int. Conf. Nuclear Cross Sections for Technology, Knoxville, Tennessee, October 22-26, 1979 p. 834, NBS-SP 594, National Bureau of Standards.

7.0 T. K. Ghosh, Mark A. Prelas, ISBN: 978-90-481-2382-*7,*University of Missouri-Columbia Nuclear Science *2009928307* © Springer Science +Business Media B.V. 2009.

8.0 M. B. Chadwick *et al.*, "ENDF/B-VII.0: Nuclear Data Sheets, 107 (2006) 2931

9.0 A. J. Koning, *et al.*, Proceeding of the International Conference on Nuclear Data for Science and Technology, Nice, 2007.

10.0 K. Shibata *et al.*,J. Nucl. Sci. Tech., 48 (2011) 1.

11.0 China Evaluated Nuclear Data Library, CENDL-3.1, (2009)

12.0 S. M. Grimes Phys. Rev.C (88) (2013) 024613.

13.0 Jean-Louis Basdevant, James Rich, Michel Spiro: *Springer*;(2005)

14.0 Gregory et al.,ISBN-9780080515663, Ebook , Release Date: 20012.

15.0 D. K. Mc Daniels, P. Varghese, D.M. Drake, F. Arthur, A. Lindholm, I. Berquist, J. Krumlinde, Nucl. Phys. A, 88,384.(1982).

16.0 Vuong Tan, Nguyen Canh Hai, Nguyen Trong Hiep, INDC (VN)-8(1996).

17.0 Yu. G. Panitkin and V. A. Tolstikov, Atomnaya Energia, 33.(1972).825.

18.0 Yu. G. Panitkin and V. A. Tolstikov, Atomnaya Energia, 39 (1975).17.

19.0 Ding Da-Zhao, Guo Tai-Chang HSJ-77106, (1978)

20.0 American Institute of Physics Conference Proceedings,Las Vegas, Nevada, USA, 346 (1994)

21.0 G. Aerts *et al.*, Phys. Rev. C 73, 054610 (2006).

22.0 J.A. Miskel, K.V. Marsh, M. Lindner and R.J. Nagle, Phys. Rev.,128 (1962) 2717

23.0 H..M.J ain, S. Kailas, S. K. Gupta, V. S. Ramamurth, Annalas of Nuclear Energy 16.(1989).8

24.0 H. Naik, P. M. Prajapati, S.V. Surayanarayana, K. C .Jagadeesan, S.V.Thakare,D. Raj, V. K. Mulik, B. S. Sivashankar, B. K. Nayak, S.C. Sharma, S. Mukherjee,Sarbjit Singh, A. Goswami, S. Ganesan, V. K. Manchanda,Eur. Phys. J. A,47 (2011) 51.

25.0 J. L. Perkin, L. P. O'connor, R. F. Colemann, Proc. Phys. Soc. (London), 72, 505 (1958).

26.0 J. Gindler and J.R. Huizenga, “Nuclear Fission”, in Nuclear Chemistry, Vol II, L. Yaffe, ed. (Academic Press, New ... H.C. Britt in Actinides in Perspective, N.M. Edelstein, ed., (Pergamon, Oxford, 1982) p245. 9. G.T. Seaborg .

27.0 IAEA-EXFOR Database, at http://www-nds.iaea.org/exfor.

28.0 R.H. Iyer, C.K. Mathews, N. Ravindran, K. Rengan, D.V. Singh, M.V. Ramaniah, H.D. Sharma, J. Inorg. Nucl.Chem. 25 (1963) 465

29.0 H.N. Erten, A. Grutter, E. Rossler, H.R. von Gunten, Nucl. Sci. Eng. 79 (1981)

30.0 A. Turkevich, J.B. Nidday, Phys. Rev. 84 (1951) 52.

31.0 K. M. Broom, Phys. Rev. 126 (1962) 627.

32.0 G.P. Ford, R.B. Leachman, Phys. Rev. B 137(1965) 826.

33.0 R. Ganapathy, P.K. Kuroda, J. Inorg. Nucl.Chem. 28 (1966) 2071.

34.0 Tin Mo, M.N. Rao, J. Inorg. Nucl.Chem. 30 (1968) 345.

35.0 M. Thin, M.N. Rao, P.K. Kurdo, J. Inorg. Nucl.Chem. 30 (1968) 1145.

36.0 A.I. Sagachev, V.G. Vorobeieva, B.D. Kuzminov, V.B. Mikhaylov, Z. Tarsko,Sov. J. Nucl. Phys. 7 (1968) 475.

37.0 S.J. Lyle, J. Sellears, Radiochimica Acta 12 (1969) 43.

38.0 L.H. Gevaert, R.E. Jervis, H.D. Sharma, Can. J. Chem. 48 (1970) 641.

39.0 J. Blachot, L.C. Carraz, P. Cavallini, E. Monnand, F. Schusslor,J. RadioanalNucl. Chem. 7 (1971) 309.

40.0 D.L. Swindle, D.T. Moore, J.N. Beck, P.K. Kuroda,J. Inorg. Nucl. Chem. 33 (1971) 364

41.0 W. Holubarsch, L. Pfeiffer, F. Gonnenwein, Nucl. Phys.A 171 (1971) 631.

42.0 S.A. Rao, Phys. Rev. 5 (1972) 171.

43.0 J.P. Bocquet, R. Brissot, J. Crancon, A. Moussa, Nucl. Phys.A 189 (1972) 556.

44.0 S.M. Dubroviva, V.I. Nogorodtseva, L.N. Morozov, V.A. Pchevin, L.V. Chistyakov,V.A. Schigin, V.M. Shubko, YadornayaFizika, 17 (1973) 1470.

45.0 J. Trochon, H. A. Yehia, F. Brisard, and Y. Pranal, Nucl. Phys.A 318 (1979) 63.

46.0 L. E. Glendenin, J. E. Gindler, I. Ahmad, D. J. Henderson, and J. W. Meadows,Phys. Rev. C 22 (1980) 152.

47.0 S. T. Lam, L. L. Yu, H. W. Fielding, W. K. Dawson, and G. C. Neilson,Phys. Rev. C 28 (1983) 1212.

48.0 A.E. Richoortson, H.L. Wright, J.L. Meason, J.R. Smith, Nucl. Sci. Eng. 94 (1986) 413.

49.0 Li. Wenxin, S. Tongyu, S. Xiuhua, Fu Ming, D. Tianrong, High Energy Phys. and Nucl.Phys.11 (1887) 376.

50.0 S. Tongyu, Li Wenxin, D. Tianrong, Fu Ming, (Chineese)High Energy Phys. andNucl. Phys.12 (1888) 221.

51.0 V.D. Simutkin, I.V. Ryzhov, G.A. Tutin, L.A. Vaishnene, J. Blongren, S. Pomp,M. Oesterlung, P. Andersson, R. Bevilacqua, J.P. Menlders, R. Prieels,Conf. Proceeding by American Inst. Phys. USA No. 1175 (2010) 393.

52.0 P. M. Prajapati, H. Naik, S. Mukherjee, S. V. Suryanarayana, B.S. Shivashankar,R. Crasta, V. K. Mulik, K. C. Jagadeesan, S. V. Thakre and A. Goswami, Nucl. Sci. Eng. 176 (2014)

53.0 H. Naik, Rita Crasta, S.V. Suryanarayana, P.M. Prajapati, V.K. Mulik, B.S. Shivasankar,K.C. Jagadeesan, S.V. Thakare, S.C. Sharma and A. Goswami, Eur. Phys. J. A 50 (2014) 144

54.0 Gregory R. Choppin, Jan-Olov Liljenzin and J. Rydberg.ISBN: 978-0-7506-7463-8

55.0 S. Glasstone and A. Sesonske " Nuclear Reactor Engineering" 1994

56.0 J. M. Verbeke "Development of high-intensity DD and DT neutron sources and neutron filters for medical and industrial applications" Lawrence Berkeley National Laboratory, 2000

57.0 A. V. Tollestrup, W. A. Fowler, and C. C. Lauritsen,Phys. Rev. 76,428 (1949).

58.0 E J Axton and A G Bardell, Metrologia, 21 (1985), 59

59.0 James Sommers; Marcos Jimenez; Mary Adamic; Jeffrey Giglio; Kevin Carney ,Journal of Radio analytical and Nuclear Chemistry Journal ,282(2009).

60.0 A.Wattenberg, Argonne National Laboratory, Preliminary Report No. 6, 1949.

61.0 Martin . Stephen . " Bremsstrahlung and from and Tantalum "Review C. Volume: 2(1970).

62.0 A. Pizzuto,*et al.*, Nuclear Fusion,50(2010).

63.0 M. Gilberti, C. Pereira,M. Auxiliadora, F. Veloso and A. L. Costa, Science and Technology of Nuclear InstallationsVolume 2015(2015).

64.0 S.S. Kapoor, V.A. Hattangadi and M.S. Bhatia, Indian J. Pure and Appl.Phys. 27,623(1989).

65.0 V.Bhagwat, Indian Academy of Sciences,59,719.(2002).

66.0 G. R. Gilmore. “Practical Gamma-ray Spectrometry”, Second Edition,. ISBN 978-0- 470-86196-7. Published by Wiley-VCH Verlag, Wenheim, Germany, 2008

67.0 M. U. Khandaker,1,42(2011).

68.0 S. Harb, K. S. Din and A. Abbady,Proceedings of the 3Physics Conference, Aswan, Egypt, 19-23 Feb. 2008.

69.0 D. E. Bartine, Proc. Int. Conf. Nuclear Cross Sections for Technology, Knoxville, Tennessee, October 22-26, 1979, p. 119, NBS-SP 594, National Bureau of Standards.

70.0 S. Pelloni, G. Youinou and P. Wydler,Proc. Int. Conf. Nuclear data for Science and Technology, Trieste, Italy, May 19-24, 1997, PII,p.1172

71.0 J. L. Perkin, L P O’connor and R F Colemann, Proc. Phys. Soc. (London), 505 (1958)

72.0 R. Batchelor, W.B. Gilboy, J.H. Jowle, Nucl. Phys. 65,236(1965).

73.0 M. Asghar, C.M. Chaffey, M.C. Moxon, Nucl. Phys,85,305.(1966).

74.0 H.O. Menlok and W.P. Poenitz, Nucl. Sci. Eng. 33,24.(1968).

75.0 D. Drake, I. Bergqvist and D.K. McDaniels, Phys. Lett. B,36,557.(1971).

76.0 G.D. Saussure, E.G. Silver, R.B. Perez, R. Ingle, H. Weaver, Nucl. Sci Eng. 51,385 (1973).

77.0 W. P. Poenitz, Nucl. Sci. Eng. 57,300.(1975).

78.0 H.L. Liou and R.E. Chrien, Nucl. Sci. Eng. 62,463 .(1977).

79.0 K. Wisshak and F. Kappeler, Nucl. Sci. Eng. 66,363(1978).

80.0 R.B. Perez, G. de. Saussure, R.L. Macklin, J. Halperin, Phys. Rev. C, 20,528 (1979).

81.0 J. Voignier, S. Joly, G. Grenier, Nucl. Sci. Eng. 87,112(1992).

82.0 A. I. Leipunskiy, O. D. Kazachkovskiy, G. Ja. Artyukhov, A. I. Baryshnikov, T. S Belanova, V. I. Galkov, Yu. Ja. Stavisskiy, E. A. Stumbur, L. E. Sherman, Geneva, 15,50 (1958).

83.0 R.C. Hann and B. Rose, J. Nucl. Eng. 8,197.(1959)

84.0 M. Lindner, R.J. Nagle, J.H. Landrum, Nucl. Sci. Eng. 59,381.(1976).

85.0 W.P. Poenitz, L.R. Fawcell Jr., D.L. Smith, Nucl. Sci. Eng. 78,329 (1981).

86.0 N.N. Buleeva, A.N. Davletshin, O.A.Tipunkov, S.V. Tikhonov, V.A. Tolstokov,Atomnaya Energia, 65,348 (1988).

87.0 E. Quang and G.F. Knoll, Nucl. Sci. Eng. 110,282 (1991).

88.0 H. Naik, S.V. Suryanarayana, V.K. Mulik, P.M. Prajapati, V.S. Shivashankar, K.C. Jagadeesan, S.V. Thakare, D. Raj, S.C. Sharma, P.V. Bhagwat, S.D. Dhole, S. Ganesan, V.N. Bhoraskar, A. Goswami, J. Radianal. Nucl. Chem. 293,469.(2012).

89.0 J.H. Landrum, R.J. Nagle, M. Lindner, Phys. Rev. C 8,1938 (1973).

90.0 H. Kaius, A. Ackermann, W. Scobel, J. Phys. G. 5,715 (1979).

91.0 J. Frchaut, A. Bertin, R. Bois, Nucl. Sci. Eng. 74,29 (1980).

92.0 N. V. Kornilov, B. V. Zhuravlev, O. A. Sal'nikov, P. Raich, Sh. Nad', Sh. Darotsi, K.Sailr and I. Chiki , Atomnaya Energia,283 (1980).

93.0 G. Shani, Ann. Nucl. Energy,10,473 (1983).

94.0 X. Wang, S. Jiang, M. He, K. Dong, C. Xiao, Nucl. Ins. Meth. in Physics Research A 621,326 (2010).

95.0 S. Nagy, K.F. Flynn, J.E. Gindler, J.W. Meadows, L.E. Glendenin, Phys. Rev. C 17,163 (1978).

96.0 T.C. Chapman, G.A. Anzelon, G.C. Spitale, D.R. Nethaway, Phys. Rev. C17,1089 (1978).

97.0 C. H. Poppe, J. D. Anderson, J.C. Davis, S.M. Grimes, and C. Wong Phys. Rev. C 14,438(1976).

98.0 J. Blons, C. Mazur, and D. Paya, Phys. Rev. Lett.,35 ,1749(1975).

99.0 H. Liskien and A. Paulsen, "Neutron Production Cross Sections and Energies for the Reactions ^{7}(p,n)^{7}and ^{7}(p,n)^{7*}," At. Data Nucl. Data Tables,15,57 (1975).

100.0 J.W. Meadows, D.L. Smith, Neutrons from proton bombardment of natural lithium,Argonne National Laboratory Report ANL (7983) (1972).

101.0 E. Browne and R.B. Firestone, Table of Radioactive Isotopes, ed-ited by V.S. Shirley (Wiley,New York,1986); R.B. Firestone, L.P. Ekstrom, Table of Radioactive Isotopes, (2004).

102.0 J. Blachot and Ch. Fiche, Ann. Phys. Suppl. 6 (1981)3.

103.0 V. J. Tolstikov et al., Journal of Nuclear Engineering, A/ 1318, 599(1964)

104.0 E. Browne, Data Sheets, 93 (2001)763.

105.0 S. Nagy, K.F. Flynn, J.E. Gindler, J.W. Meadows, L.E. Glendenin, Phys. Rev. C **17** (1978) 163.

106.0 T.C. Chapman, G.A. Anzelon, G.C. Spitale, D.R. Nethaway, Phys. Rev. C **17** (1978) 1089.

107.0 Blachot,Nuclear Data Sheets, 104 , Pp 967-1110 (2005)

108.0 S.G. Mashnik, M.B. Chadwick, H.G. Hughes, R.C. Little, R.E. Macfarlane,L.S. Waters, P.G. Young, 7Li(p,n), Los Alamos National Laboratory, Los Alamos, NM 87545 USA (February 8,2008)

109.0 J. Blons, C. Mazur, and D. Paya, Phys. Rev. Lett. 35 (1975) 1749

110.0 B. Singh, J. K. Tuli, Data Sheets 105,109 (2005).

111.0 P. K. Mukhopadhyaya, Personal Communication (2001)

112.0 IAEAEXFOR Database, at http://www-nds.iaea.org/exfor

113.0 Vuong Tan, Nguyen Canh Hai, Nguyen Trong Hiep, INDC (VN)-8(1996).

114.0 F. Carminati, R. Klapisch, J.P. Revol, Ch. Roche, J.A. Rubio and C. Rubbia, CERN Report No. CERN/AT/93-47 (ET) 1993

115.0 American Institute of Physics Conference Proceedings, "The international conference on Accelerator-Driven Transmutation Technologies and Applications,Las Vegas, Nevada, USA, 346 (1994)

116.0 Accelerator Driven Systems: Energy Generation and Transmutation of nuclear waste, Status report: IAEA- TECDOC- 985 (1997).

117.0 C. D. Bowman, Ann. Rev. Nucl. Part. Sci 48,505 (1998).

118.0 S. Ganesan, Pramana J. Phys. 68,257 (2007).

119.0 K. Yamashita, K. Tokuhara and N. Fujimoto, Nucl. Science and Engg. 126,94 (1997).

120.0 The international Reactor Dosimetry File:IRDF-2002 (Nuclear Data Section, International Atomic Energy Agency, 2002)

121.0 E. T. Cheng and D. R. Mathews, Proc. Int. Conf. Nuclear Cross Sections for Technology, Knoxville, Tennessee, October 22-26, 1979, p. 834, NBS-SP 594, National Bureau of Standards.

122.0 .M. Salvatores, Nuclear Data for Science and Technology (Proc. Int. Con. Trieste, 1997), Vol. 59, part I (G. Reffo, A. Ventura, and C. Grandi, Eds.), Italian Physical Society, Bologna ,3(1997).

123.0 R. L. Macklin, N. H. Lazar and W. S. Lyon, Phys. Rev. 107,504 (1957).

124.0 J.A. Miskel, K.V. Marsh, M. Lindner and R.J. Nagle, Phys. Rev.128,2717 (1962).

125.0 D. C. Stupegia, B. Smith and K. Hamm, J. Inorg. Nucl. Chem. 25,627 (1963).

126.0 M. C. Muxon, TRDWP/P-8, U.K. Atomic Energy Authority, Harwell (1963).

127.0 L. Forman, A.D. Schelberg, J.H. Warren and N.W. Glass, Phys. Rev. Lett. 27, 117(1971).

128.0 V.B. Chelnokov et al. USSR Obninsk Report Jaderno Fizicheskii Issledovanija-13 P. 16 (Oct. 1972).

129.0 M. Lindner, R. J. Nagle and J. H. Landrum, Nucl. Sci. Eng. 59,381 (1976).

130.0 R. E. Chrien, H. I. Liou, M. J. Kenny and M. L. Stelts, Nucl. Sci. Eng. 72,202 (1979).

131.0 G.T. Baldwin and G.F. Knoll, Nucl. Sci. Eng. 88,123 (1984).

132.0 R. T. Jones, J. S. Merritt and A. Okazaki, Nucl. Sci. Eng. 93,171 (1986).

133.0 J. L. Perkin, L. P. O'connor, R. F. Colemann, Proc. Phys. Soc. (London), 72, 505 (1958).

134.0 D. Karamanis, M. Petit, S. Andriamonje, G. Barreau, M. Bercion, A. Billebaud, B. Blank, S. Czajkowski, R. Del Moral, J. Giovinazzo, V. Lacoste, C. Marchand,L. Perrot, M. Pravikoff and J.C. Thomas, Nucl. Sci. Eng. 139,282 (2001).

135.0 P.Anand, H .M.J ain, S. Kailas, S. K. Gupta, V. S. Ramamurth ,Annalas of Nuclear Energy 16,87.(1989).

136.0 H. Naik, P. M. Prajapati, S.V. Surayanarayana, K. C .Jagadeesan, S.V.Thakare,D. Raj, V. K. Mulik, B. S. Sivashankar, B. K. Nayak, S.C. Sharma, S. Mukherjee,Sarbjit Singh, A. Goswami, S. Ganesan, V. K. Manchanda,Eur. Phys. J. A,47,51 (2011).

137.0 J.P. Butler and D. C. Santry, Can J. Chem., 39,689.(1961).

138.0 M. Bormann, Nucl. Phys. 65,257 (1965).

139.0 H. Karius, A. Ackermann and W. Scobel, J. Phys (G), 5,715 (1979).

140.0 H. Chatani, Nucl. Inst. Methods.205,5.01 (1983).

141.0 P. Raics, S. Daroczy, J. Csikai, N.V. Kornilov, V. Ya. Baryba and O.A. Salnikov,Phys. Rev. C, 32,87 (1985)

142.0 E. Browne, R.B. FirestoL E Glendenin, J E Gindler, I Ahmad, D J Henderson and J. W. Meadows, Phys. Rev. C22, 15(1980)

143.0 E A C Crouch, At. Data. Nucl. Data Tables 19, 419 (1977)

144.0 J. Adam, A. R. Balabekyan, V. S. Barashenkov, R. Brandt, V. M. Golovatiouk,V.G. Kalinnikov, K. Katovosky, M. I. Krivopustov, V. Kumar, H. Kumawat,R. Odoj, V. S. Pronskikh, A. A. Solnyshkin, V.I. Stegailov, V. M. Tsoupko-Sitnikov, W.Westmeier, Eur. Phys. J. A, 23 (2005) 61

145.0 R. L. Macklin, N. H. Lazar and W. S. Lyon, Phys. Rev. 107,504 (1957).

146.0 J.A. Miskel, K.V. Marsh, M. Lindner and R.J. Nagle, Phys. Rev.128,2717 (1962).

147.0 D. C. Stupegia, B. Smith and K. Hamm, J. Inorg. Nucl. Chem. 25,627 (1963).

148.0 M. C. Muxon, TRDWP/P-8, U.K. Atomic Energy Authority, Harwell (1963).

149.0 L. Forman, A.D. Schelberg, J.H. Warren and N.W. Glass, Phys. Rev. Lett. 27, 117(1971).

150.0 V.B. Chelnokov et al. USSR Obninsk Report Jaderno Fizicheskii Issledovanija-13 P. 16 (Oct. 1972).

151.0 M. Lindner, R. J. Nagle and J. H. Landrum, Nucl. Sci. Eng. 59,381 (1976).

152.0 R. E. Chrien, H. I. Liou, M. J. Kenny and M. L. Stelts, Nucl. Sci. Eng. 72,202 (1979).

153.0 G.T. Baldwin and G.F. Knoll, Nucl. Sci. Eng. 88,123 (1984).

154.0 R. T. Jones, J. S. Merritt and A. Okazaki, Nucl. Sci. Eng. 93,171 (1986).

155.0 K. Wisshak, F. Voss and F. Kappeler, Nucl. Sci. Eng., 137,183 (2001).

156.0 D. Karamanis, M. Petit, S. Andriamonje, G. Barreau, M. Bercion, A. Billebaud, B. Blank, S. Czajkowski, R. Del Moral, J. Giovinazzo, V. Lacoste, C. Marchand,L. Perrot, M. Pravikoff and J.C. Thomas, Nucl. Sci. Eng. 139,282 (2001).

157.0 R. C. Little, R. C. Block, D. R. Harris, R. E. Slovacek and O. N. Carlson,Nucl. Sci. Eng.. 79,175 (1981).

158.0 Joint Evaluated Fission and Fusion File ,Incident neutron data,http://wwwnds.iaea.org/exfor/endf00.htm, 2 October 2006

159.0 R. Konecny and D. J. Doren, Surf. Sci. 417 (1998) 169.

160.0 S. S. Kapoor, V. A. Hattangadi and M. S. Bhatia, Indian J. Pure and Appl.Phys,.27 (1989) 623.

161.0 H. Naik *et al.*, Eur. . J. A , 51(2011).

162.0 D.J. Gorman and R.H. Tomilson, Can. J. Chem. 46 (1968) 1663.

163.0 H. Naik, P.M. Prajapati, S.V. Suryanarayana, K.C. Jagadeesan, S.V. Thakare,D.Raj,V.K. Mulik, B.S. Shivashankar, B.K. Nayak, S.C. Sharma, S. Mukherjee, Sarbjit Singh, A. Goswami, S. Ganesan, V.K. Manchanda, Eur. Phys. J. A 47 (2011) 51.

164.0 S. Daroczy, P. Baics, S. Nagy, in Proceedings of the Panel on Fission ProductNuclear Data,3 (1990) 281.

165.0 A.J. Koning, S. Hilaire, M.C. Duijvestijn, Proceedings of the International Conference on Nuclear Data for Science and Technology, ND 2004, Santa Fe, 2004, Edited by R.C.Haight, M. B. Chadwick, T. Kawano, P. Talou, AIP Conf. Proc. 769(2005) 1154.

166.0 S. Mukerji, H. Naik, S. V. Suryanarayana, S. Chachara, B. S. Shivashankar, V. K. Mulik, S. Samanta., A. Goswami and P. D. Krishnani, J. Basic and App.Phys.2(2013)104.

167.0 D. Gorodisskiy, K. Kovalchuk, S. Mulgin, A. Rusanov, and S. Zhdanov, Ann. Nucl. Energ., vol. 35, no. 2, pp. 238– 245,2008.

168.0 D. F. Williams, Stephen , Application under Solicitation No. LAB NE 2002-Nuclear Energy Research Initiative 18 February 2010.JENDL-4.0 Fission Product Sub-library (J40-2010)FPY-2011).